2809

Dissertation
on

STUDIES IN UPPER ATMOSPHERE

"MEASUREMENT OF NEUTRAL ATMOSPHERE WINDS ABOVE 80 KM"

Presented
by

K. RAMANUJA RAO

for the degree of
DOCTOR OF PHILOSOPHY
of the
Gujarat University

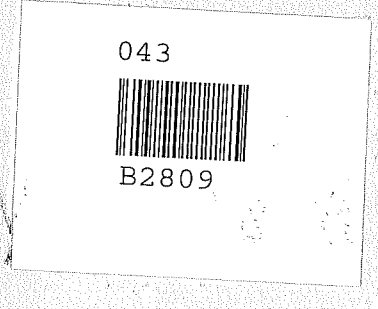

October 1966

Physical Research Laboratory
AHMEDABAD.

S T A T E M E N T

The work presented in the thesis was carried out by the author, at the Physical Research Laboratory, Ahmedabad, under the guidance of Professor P.D. Bhavsar, and is a part of an extensive research programme for the study of the equatorial upper atmosphere sponsored by the Indian National Committee for Space Research (INCOSPAR).

Till 1956 upper atmosphere winds were studied only by observing natural phenomena, like meteor trails, not under human control. After a suggestion by Dr. D.R. Bates, a technique developed, in which chemicals like sodium, are released at high altitudes with the help of rockets and the vapour cloud thus generated is used as a marker for studying the winds. So far such experiments were conducted at middle and high latitudes only. The equatorial upper atmospheric motions were not known. The present study has revealed for the first time the wind field in the upper atmosphere between 100 to 180 km, near the equator and therefore, the results presented are new findings.

The Thumba Equatorial Rocket Launching Station (TERLS) from where these experiments were conducted, is also situated on the magnetic equator. The upper atmosphere, in the ionospheric region at the magnetic equator, is characterised

by the presence of a large electric current called the equatorial electrojet. So far the driving forces responsible for this current are not well understood. As a first step to understand the properties and the dynamics of this region of the atmosphere, the present study has been undertaken, and thus the results obtained have great significance.

Present study also provides valuable first results near the equatorial region, which, when combined with results at other latitudes will lead to the better understanding of the global circulation in the upper atmosphere.

In Chapter I, the author has reviewed the existing knowledge in his field of study. In Chapter II, the experimental technique is described. In Chapter III the results are presented and discussed and the conclusions drawn. In Chapter IV a short summary and the important conclusions arrived at, are listed. The author has included at the end of the thesis a list of references to original papers published in different parts of the world. The thesis mentions the specific information derived from each of them.

P.D. Bhavsar

(PRAFUL D. BHAVSAR)

K. Ramanuja Rao

(K. RAMANUJA RAO)

ACKNOWLEDGEMENTS

The author is deeply indebted to Professor Praful D. Bhavsar for the guidance and encouragement he gave throughout the period of the work and in the preparation of the thesis.

The author records his sincere gratitude to Professor Vikram A. Sarabhai, Chairman, Indian National Committee for Space Research, and Director, Physical Research Laboratory, who took keen interest in the progress of the work.

The author is very grateful to Prof.K.R.Ramanathan and Dr.R.Raghava Rao for the helpful discussions and comments during the interpretation of the results and preparation of the thesis.

The author expresses his sincere thanks to Mr.M.G.S. Murthy, Test Director, TERLS, and his staff, who carried out all the rocket launchings with great skill at the desired time and made the experiments successful.

The author is very thankful to the Indian Posts and Telegraph Department, for helping in establishing quick and reliable communication arrangements between the rocket launching site and the camera sites; and to the Kerala State Tourist Department, for helping in establishing the camera stations in their guest houses. The help received from the Principal, St.Xavier's College, Palayamkottai in establishing one camera station at the College is gratefully acknowledged.

The author gratefully acknowledges the help received from Mr.K.G.Vernekar and other colleagues, the technical staff working on the Project and the volunteers in establishing and maintaining the camera stations successfully, and from Mr. S.N. Thakore, Head of the Computing Centre, Physical Research Laboratory, and his staff in preparing the computer programme for data analysis.

The author is thankful to Professor R.G.Rastogi and his colleagues for making available the ionospheric drift results.

The author is also thankful to Mr.V.J.Parikh and Mr.Jacob Mathews for their help in preparing the diagrams and typing the thesis.

The whole programme was jointly supported by the National Aeronautics and Space Administration (NASA) of the U.S. of America who supplied the rockets, and Centre National d'Etudes Spatiales (CNES) of France who supplied the payloads for the present work. Financial support for the work was provided by the Department of Atomic Energy, Government of India and the Physical Research Laboratory. In the initial stages the author was a recipient of a Government of India Scholarship.

(K. RAMANUJA RAO)

C O N T E N T S

CHAPTER I INTRODUCTION ... 1

1.1. Structure of the upper atmosphere ... 4

1.2. Sources of energy supply to the upper atmosphere ... 10

1.2.1. Thermal energy from the sun ... 10

1.2.2. The tidal forces ... 14

1.2.3. Internal atmospheric gravity waves ... 18

1.2.4. Particle bombardment and solar wind ... 20

1.2.5. Other sources of energy in the upper atmosphere ... 21

1.3. Winds in the upper atmosphere ... 22

1.3.1. Neutral atmosphere motions ... 22

1.3.2. Ionospheric motions ... 26

1.3.3. Interaction between the neutral and ionized components of the upper atmosphere ... 31

1.3.4. Relation between the neutral winds and the ionosphere ... 36

1.4. Methods employed for observing neutral upper atmosphere winds. ... 43

1.4.1. Observation of noctilucent clouds ... 44

1.4.2. Meteor trails ...

1.4.3. Rocket released sodium vapour clouds

1.4.4. Grenades

1.4.5. Chemiluminescent trails

1.5. Neutral wind measurement at high latitu

1.6. Neutral wind measurement at middle lat

1.7. Models of the general circulation in neutral upper atmosphere

1.7.1. Models based on the experimental results ... 68

1.7.2. Models based on theoretical considerations ... 74

1.8. Necessity for the present study ... 76

1.9. Statement of the problem ... 79

CHAPTER II EXPERIMENTAL TECHNIQUE ... 81

2.1. Rockets ... 82

2.2. Rocket payload for the release of sodium vapour trail ... 82

2.2.1. Sodium vaporiser ... 86

2.2.2. Electronic timer ... 87

2.3. Photography of the vapour trail ... 91

2.3.1. The time of experiment ... 91

2.3.2. Camera for the photography of vapour trail ... 95

2.3.3. Selection of films and filter for the sodium vapour trail photography ... 100

2.3.4. Camera adjustments and preparations for the vapour trail photography at twilight 104

2.3.5. Exposure sequence ... 106

2.4. The camera sites ... 111

2.4.1. Selection of a camera site ... 111

2.4.2. Position of camera sites in relation to launch site ... 117

2.5. Data reduction ... 121

2.5.1. Determination of distances between the camera sites ... 123

2.5.2. Determination of the direction of the camera axis ... 126

2.5.3. Determination of the focal length of the camera lens ... 132

2.5.4. Camera tilt ... 134

2.5.5. Determination of the elevation and the azimuth of the vapour cloud point ... 139

2.5.6. Determination of the space coordinates of points on a vapour cloud 142

2.6. Errors in determining heights and the wind velocity ... 152

2.6.1. Systematic errors ... 153

2.6.2. Accidental errors ... 155

2.6.3. Estimation of error in height determination ... 157

2.6.4. Estimation of error in wind velocity .. 158

CHAPTER III EXPERIMENTAL RESULTS AND DISCUSSIONS ... 163

3.1. Experimental results ... 163

3.2. Discussion of results ... 177

3.2.1. Meridional component of winds ... 177

3.2.2. Zonal component of winds ... 194

3.2.3. Variation of wind speed with height ... 198

3.2.4. Diurnal variation of the winds ... 201

3.2.5. Rotation of the wind vector with change in the altitude ... 210

3.2.6. Hines method of determining diurnal component ... 215

3.2.7. Prevailing wind and semi-diurnal tide.. 219

3.2.8. Internal atmospheric gravity waves ... 221

3.2.9. Comparison of our results with the ionospheric winds derived from S_q variation ... 228

3.2.10. Comparison of neutral upper atmosphere winds and drift measurements at TERLS ... 229

CHAPTER IV SUMMARY AND CONCLUSIONS ... 236

Appendix I

References

CHAPTER - I

INTRODUCTION

Man has tried to understand the atmospheric phenomena from the early ages. In the early stages, his interest was confined to the lower strata of the atmosphere, as it was easily approachable and of more direct concern to him. The meteorologist studied the winds, temperature, humidity and the allied problems, close to the earth's surface, where direct measurements could be made with ease. With the balloons coming into use, this region was extended to 30 km, and in present times it is possible to go up to 40 to 45 km with the help of balloons.

The indirect study of the upper atmosphere* started when Marconi sent the radio waves across Atlantic in 1901, and Kennelly and Heaviside explained this phenomenon as due to the reflection of the radio waves from ionized regions present at great heights. These regions, extending above about 60 km, were extensively studied using the radio waves since then. The radio waves, sent from the ground in the upward direction, come back after reflection from these ionized regions and bring with them valuable information about these regions. Among other parameters, drift of the ionized component of the atmosphere above 80 km is studied by this method. The movement of the ions depend not only on the general circulation of the

---

* For the present work the upper atmosphere is defined as the atmospheric region above 80 km .

atmosphere but also on the magnetic field of the earth and electric fields present at these heights, and therefore, the information about their motions cannot be considered as a complete information about the neutral atmosphere at these heights.

The interest in the neutral atmosphere winds in higher regions has increased in recent times. The earliest studies started with the observation of the noctilucent clouds[32], and the meteor trails[83] which provided some data, above 80 km, regarding winds in the neutral upper atmosphere. The noctilucent clouds appear around 80 km altitude and are mostly observed at high latitudes. The meteor trails which appear between 80 and 120 km altitude, have been studied extensively at only two places, Jodrell Bank in England (latitude 51° N) and Adelaide, Australia (latitude 35° S). The information available from the above two techniques is limited and so very little was known about the dynamics of the neutral atmosphere above 80 km before the start of investigations with sounding rockets. The release of artificial vapour clouds with the help of rockets, and studying optically their movements has proved to be a strong technique for the study of wind motions in this high atmosphere region from 80 - 200 km .

With an ultimate aim of understanding the general circulation of the atmosphere at these heights, the vapour cloud experiments are being carried out at different places on the earth. Such places of observation are still very few and

isolated in geographical distribution. The experiments are also not always conducted at the same time, or on the same day, from all the places. With such a meager data from four places, Kochanski[1], for the first time, tried to understand the upper atmosphere general circulation in the middle latitudes.

The author presents in this thesis the results of such vapour cloud experiments conducted near the equator from Thumba Equatorial Rocket Launching Station (TERLS), India. These results are the first of their kind as no vapour cloud experiments have been conducted at the equator before. These results give the preliminary information about the circulation of the neutral atmosphere above 100 km near the equator.

Attempts have been made on three occasions to conduct simultaneous experiments of this kind from more than one place on the earth. Three launchings, whose results are presented in this thesis, form a part of such a synoptic attempt.

Before an experimental study of the upper atmosphere dynamics is undertaken, it is necessary to review the present state of knowledge about the characteristics and structure of the region concerned (the height range 80 to 200 km), the sources of energy available and the studies made elsewhere to understand the upper atmosphere dynamics. These are briefly reviewed in the following sections of this chapter. Section 1.1 deals with the physical structure of the height range 80 to 200 km. Section 1.2 gives the sources of energy which may affect the general circulation. Section 1.3 deals with the

neutral and ionospheric motions and the possible interaction between these two motions. Section 1.4 briefly summarises the different methods used to determine the upper atmosphere motions. Sections 1.6 and 1.6 review the available information for the neutral upper atmosphere wind fields at high and middle latitudes respectively. In section 1.7, the experimental and theoretical models of the general circulation of upper atmosphere, proposed by different authors, are briefly reviewed. In section 1.8 the necessity of the present study is stressed and finally in section 1.9 the problem for the present study is stated.

1.1. STRUCTURE OF THE UPPER ATMOSPHERE

The region between 80 and 200 km is called lower thermosphere or lower ionosphere. Fig.1 to Fig.3 give the main physical features of this region of the atmosphere. Fig.1 gives the variation of temperature and mean molecular weight with height, Fig. 2 gives the variation with height of number density of neutral particles and electrons and Fig. 3 gives collision frequencies at different heights. Fig. 1 shows that after a temperature minimum around 80 km, the temperature increases rapidly with height. The temperature distribution from ground up to about 90 km is fairly known from balloons and small meteorological rocket experiments[2], but above these heights, in the thermosphere, the temperatures are mainly derived indirectly, and thus not yet accurately known. A few direct measurements from the Doppler broadening of sodium-D lines emitted by the sodium vapour released by rockets, and

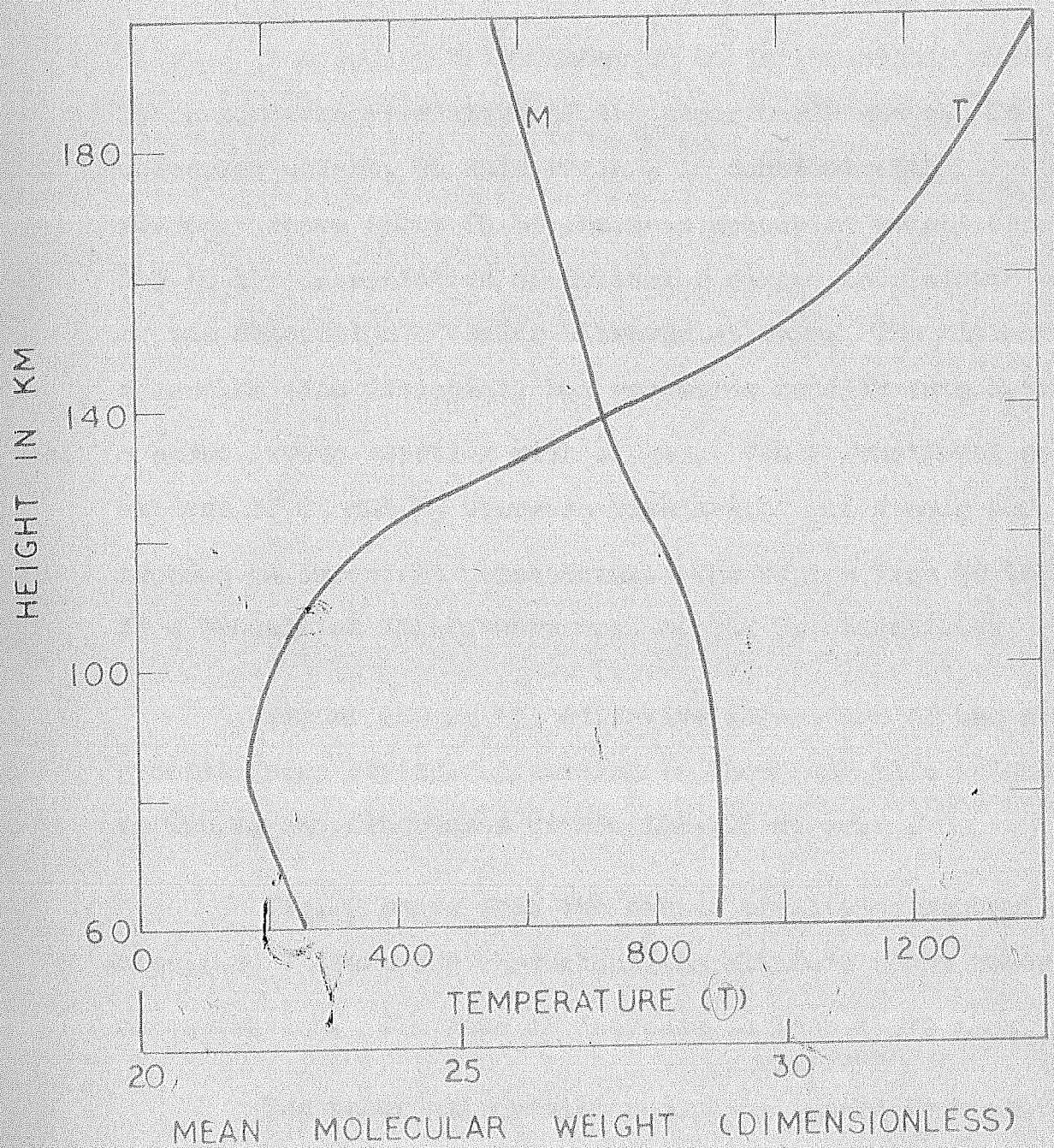

FIG. 1

VARIATION OF TEMPERATURE (T) AND MEAN MOLECULAR WEIGHT (M) WITH HEIGHT IN THE EARTH'S ATMOSPHERE.

the spectroscopic observations of aurora, substantiate these indirect observations.

The region below about 90 km is thoroughly mixed and has a homogeneous mixture of the atmospheric gases. The mean molecular weight, in this region, is constant with height being 28.966. Above about 90 km the mean molecular weight decreases due to the dissociation of molecular oxygen into atomic oxygen, by the absorption of solar ultraviolet rays. The nitrogen molecules also dissociate but recombine rapidly into N_2 through a short living reaction with oxygen. Hence fractional contributions of O_2 and N_2 decrease with height and atomic oxygen becomes an important constituent. The region from 90 to 120 km is a transition layer where most of the O_2 dissociates.

Around 120 km the diffusive separation of the atmospheric gases begins. According to Champion[3] this height is variable, and fluctuates within 105-120 km range.

Fig. 2 shows that the number density of neutral particles (n_n) decreases throughout the altitude range under consideration. The rate of decrease is less above about 110 km.

The solar ultraviolet radiation, apart from photodissociating molecular oxygen, causes ionization at these altitudes. The observed electron densities (n_e) at various levels are given in Fig. 2. The region from 60 to 90 km is called the D layer of the ionosphere, with maximum electron density of about 10^3 cm^{-3} around 80 km. The region from 90 to 160 km

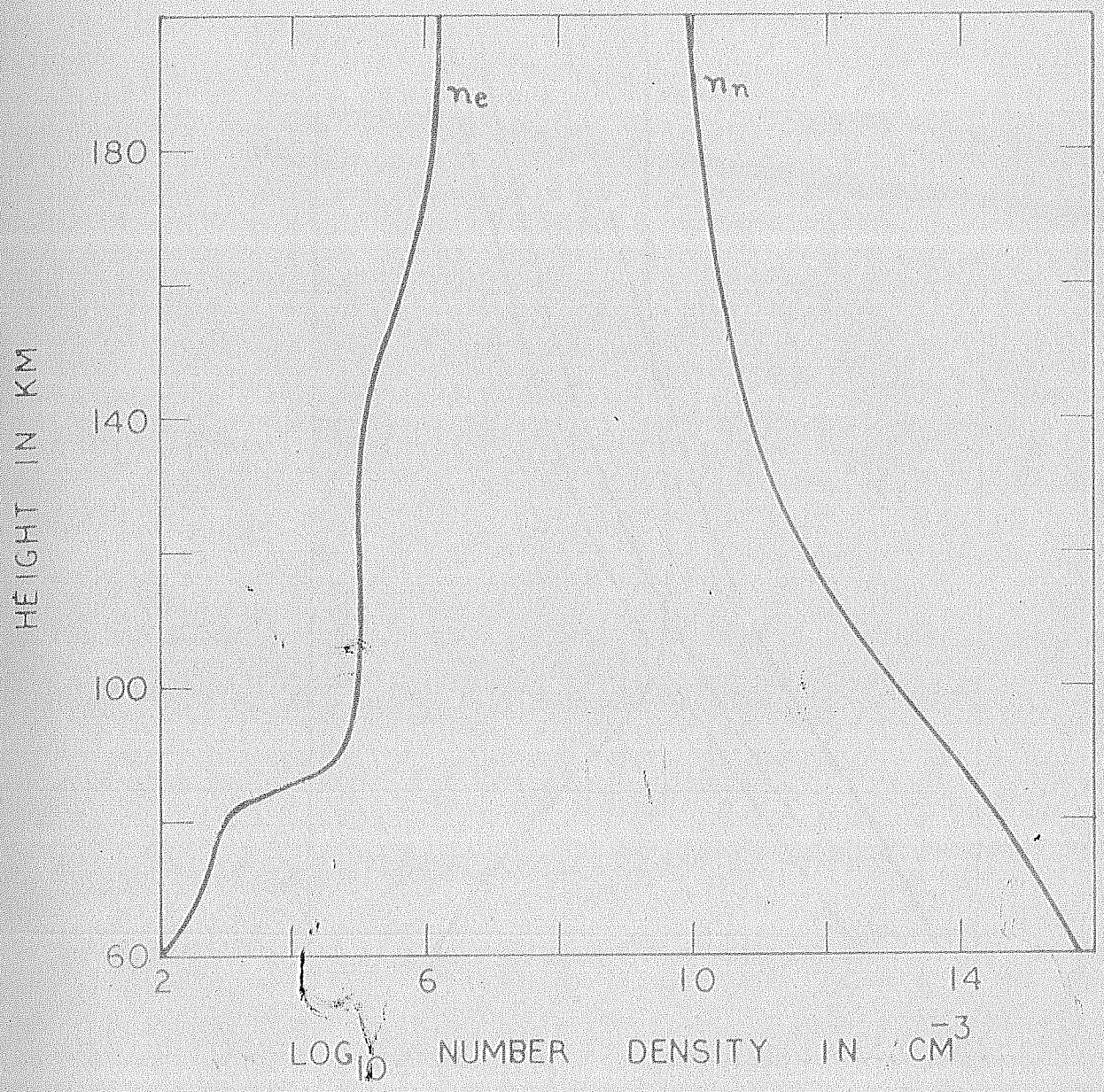

FIG. 2

VARIATION OF NUMBER DENSITIES OF NEUTRAL PARTICLES (n_n) AND ELECTRONS (n_e) WITH HEIGHT IN THE EARTH'S ATMOSPHERE

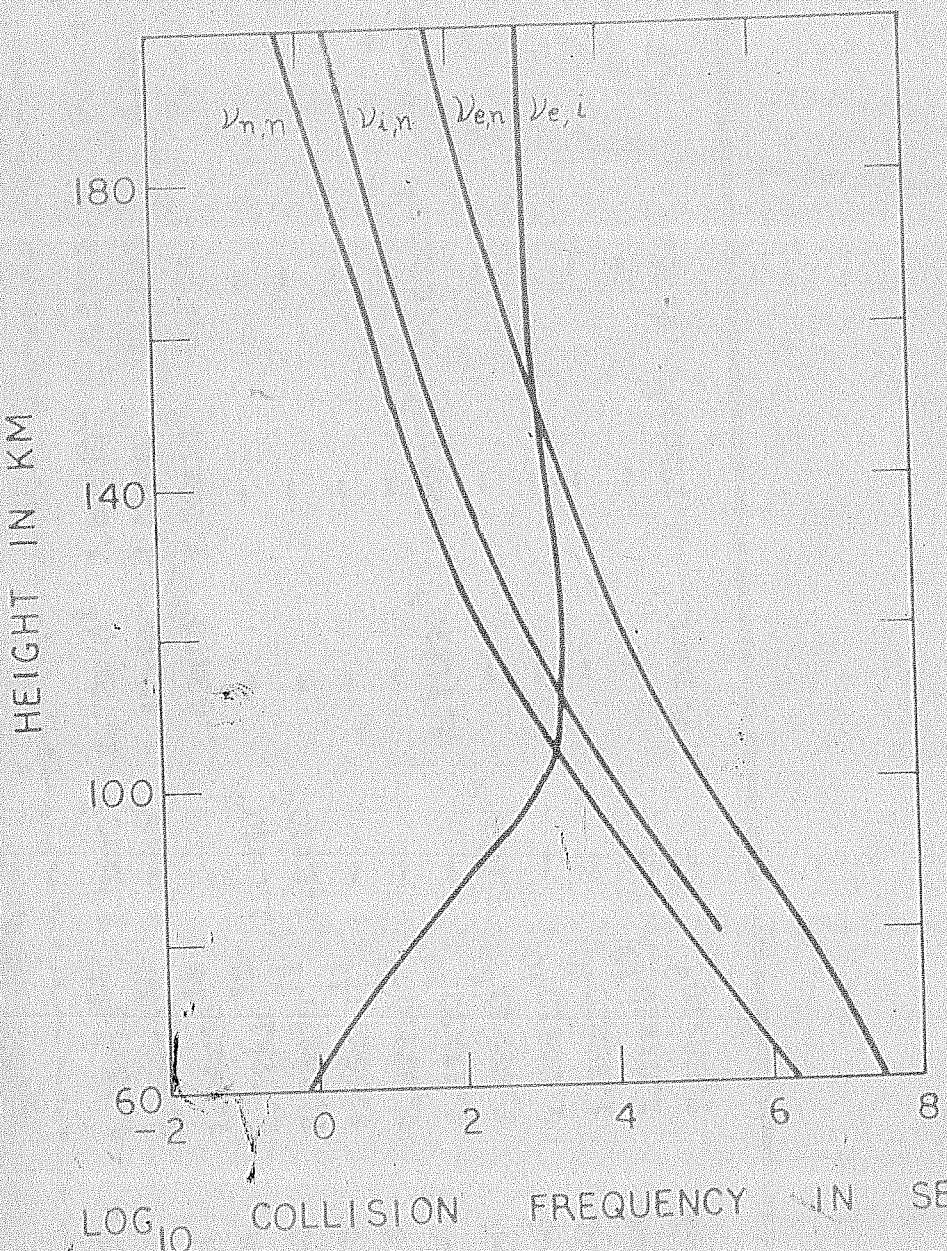

FIG. 3

VARIATION OF COLLISION FREQUENCIES WITH HEIGHT IN THE EARTH'S ATMOSPHERE. $\nu_{e,n}$ IS THE COLLISION FREQUENCY OF ELECTRONS WITH NEUTRAL PARTICLES; $\nu_{e,i}$ IS THE COLLISION FREQUENCY OF ELECTRONS WITH IONS; $\nu_{i,n}$ IS THE COLLISION FREQUENCY OF IONS WITH NEUTRAL PARTICLES AND $\nu_{n,n}$ IS THE COLLISION FREQUENCY OF NEUTRALS WITH OTHER NEUTRAL PARTICLES.

Table 1.

Physical properties of the earth's atmosphere in the height range 60-200 km.

Height km.	Temperature[4] θ_K	Pressure[6] mb.	Number Density[6] n_n cm^{-3}	Electron Density[6] n_e cm^{-3}	Collision Frequency[5] e,i	e,n	i,n	n,n	Molecular weight.[6]
60	181	1.04×10^{-2}	4.16×10^{14}	1.0×10^{3}	1.72×10^{1}	3.39×10^{6}	2.11×10^{5}	9.0×10^{4}	28.966
90	181	1.64×10^{-3}	~~6.59×10^{13}~~	5.0×10^{4}	1.43×10^{2}	6.83×10^{5}	4.12×10^{4}	1.6×10^{4}	28.966
100	211	3.01×10^{-4}	1.04×10^{13}	-	1.09×10^{3}	1.56×10^{5}	8.64×10^{3}	2.9×10^{3}	28.888
110	261	7.35×10^{-5}	2.07×10^{12}	1.0×10^{5}	-	-	-	-	28.56
120	360	2.52×10^{-5}	5.23×10^{11}	1.0×10^{5}	-	-	-	-	28.07
130	560	1.22×10^{-5}	1.66×10^{11}	-	-	-	-	-	27.58
140	760	7.41×10^{-6}	7.52×10^{10}	-	-	-	-	-	27.20
150	960	5.06×10^{-6}	4.11×10^{10}	-	1.11×10^{3}	1.05×10^{3}	5.07×10^{1}	1.6×10^{1}	26.92
160	1110	3.69×10^{-6}	2.62×10^{10}	4.0×10^{5}	-	-	-	-	26.66
170	1210	2.79×10^{-6}	1.83×10^{10}	-	-	-	-	-	26.40
180	1280	2.15×10^{-6}	1.35×10^{10}	-	-	-	-	-	26.15
190	1350	1.68×10^{-6}	1.01×10^{10}	-	-	-	-	-	25.85
200	1400	1.33×10^{-6}	7.62×10^{9}	-	7.16×10^{2}	5.17×10^{1}	2.26x	5.0	25.55

is called the E layer with a maximum electron density of about 10^6 cm^{-3} around 110 km. The region between 160 and 200 km is the F_1 layer and that above 200 km is the F_2 layer. The electron density increases from 10^5 cm^{-3} in the E layer to about 10^6 cm^{-3} in the F layer. Even at these levels the electron density is very much less compared to the neutral particle density, as can be seen from Fig. 2.

Fig. 3 gives the collision frequencies of electrons with neutral particles ($\nu_{e,n}$), electrons with ions ($\nu_{e,i}$), ions with neutral particles ($\nu_{i,n}$) and neutral particles with other neutral particles ($\nu_{n,n}$). It is seen that up to about 100 km, $\nu_{e,i}$ is very much less than the collision frequencies $\nu_{e,n}$, $\nu_{i,n}$ and $\nu_{n,n}$. Table 1 gives the main physical features of the upper atmosphere between height range 80 to 200 km. The values of temperature are taken from the revised 1962 United States Standard Atmosphere[4], and the collision frequencies $\nu_{e,i}$, $\nu_{e,n}$ and $\nu_{i,n}$ from Chapman[5] and other values from Murgatroyd[6].

1.2. SOURCES OF ENERGY SUPPLY TO THE UPPER ATMOSPHERE

1.2.1. Thermal energy from the sun.

The main external source of energy on the earth is the sun, and the upper atmosphere also derives large amount of energy from the solar radiations. The incoming electromagnetic radiation, in different wavelength regions, is absorbed by different constituents of the atmosphere at various heights. This absorption is essentially confined to two wavelength regions, the long

wavelength region from 10^8 Å to 7000 Å and the short wavelength region with $\lambda \leq 3500$ Å. The character of the absorption and its effect on the atmosphere differ considerably in the two regions. In the long wavelength region, absorption takes place in bands of discrete spectral lines which are seen against the background of the solar spectrum. This absorption is mainly due to minor atmospheric constituents, namely CO, CO_2, N_2O, C H_4 and water vapour, which are present in lower atmosphere near tropopause and stratosphere. This infrared absorption becomes an important factor again between 60 and 80 km[7].

In the short-wavelength region, the absorption is continuous, and leads to a complete cut-off at the ground level of the solar radiation for wavelengths $\lambda < 2900$ Å. The absorption of ultraviolet radiation in the wavelength region $\lambda \simeq 3000$ Å to 2000 Å, takes place mainly in the ozone layer between 30 and 60 km. Between $\lambda \simeq 2400$ Å and 2000 Å, the absorption due to diatomic oxygen, O_2, is weak and so does not prevent the radiation to enter lower altitudes to about 60 km.

Except for the important Lyman α radiation at $\lambda = 1215$ Å and some other lines between $\lambda \simeq 1300$ Å and 1100 Å, which reach 60-90 km, the solar radiation between wavelengths $\lambda \simeq 2000$ Å to 1000 Å is absorbed by the atmospheric constituents, mainly the diatomic oxygen, O_2, lying above 90 km altitude. Due to this absorption O_2 becomes dissociated, thereby releasing large amount of energy in the form of heat. The solar radiation having

wavelengths $\lambda \simeq 1000$ Å to 200 Å, is mostly absorbed before reaching an altitude of about 150 km, mainly by N_2, N and O. These atmospheric constituents undergo photoionisation, in the process of absorption of the solar far ultraviolet radiation, and release heat and thus constitute energy sources in the upper atmosphere. The solar radiation in the wavelength region $\lambda \simeq 200$ Å to 100 Å is probably absorbed before reaching 130-160 km region and X-rays having wavelengths $\lambda < 100$ Å reach levels of about 60 to 120 km. Fig. 4 gives the vertical distribution of the absorption of solar radiation in three spectral regions $\lambda \simeq 1800$ Å to 1300 Å, $\lambda \simeq 1000$ Å to 220 Å and X-rays, as estimated by Johnson[8].

The energy absorbed in the thermosphere from the solar radiation with wavelength $\lambda < 2000$ Å (except some narrow windows which allow the radiation to penetrate to lower altitudes), is of the order of 30 erg cm^{-2} sec^{-1} at normal incidence of the radiation. The altitude of this absorbed energy depends on vertical distribution of O_2, the important constituent absorbing this radiation. In comparison to this, the energy absorbed in the mesosphere, between 50 and 80 km, is of the order of 10^{-2} erg cm^{-2} sec^{-1} for each $(cm)^2$ column in the direction of the solar beam, and the energy absorbed by ozone layer between 20 and 50 km is of the order of 1.8×10^{-4} erg cm^{-2} sec^{-1} for each $(cm)^2$ column in the direction of the solar beam between these height limits.

Part of the energy absorbed by the atmospheric constituents is reradiated in the form of thermal energy. In the

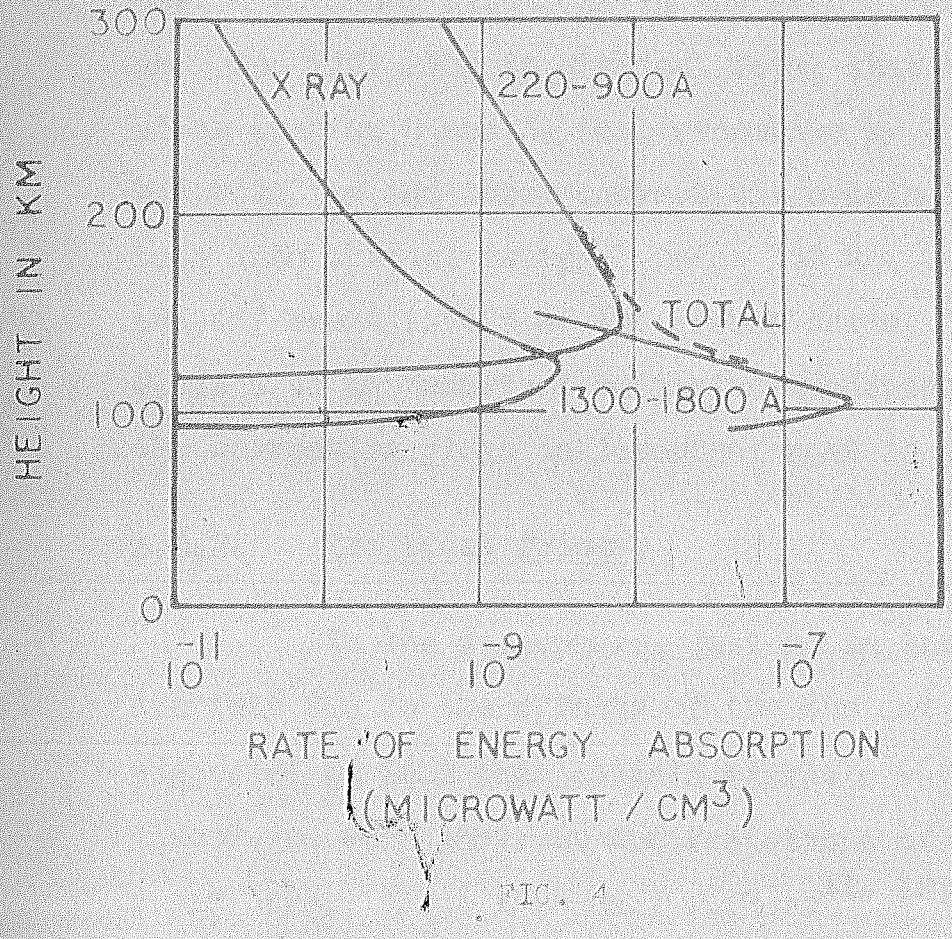

FIG. 4

RATE OF ABSORPTION OF SOLAR ENERGY IN THE EARTH'S ATMOSPHERE PER UNIT VOLUME IN THREE DIFFERENT WAVELENGTH REGIONS OF THE SOLAR SPECTRUM, (i) 1300 TO 1800 Å, (ii) 220 TO 900 Å AND (iii) X-RAYS (JOHNSON[8]).

thermosphere, the height at which the radiation is absorbed and the height at which it is converted to thermal energy are not, in general, same. Above about 130 km, the transfer of energy is mainly due to downward conduction of heat gained by the absorption of extreme ultraviolet radiation in the spectral range $\lambda \simeq 1000$ Å to 200 Å. Some fraction of this energy is transported to lower altitudes in the form of molecular conduction and also diffusion in chemical form, that is, in the form of atoms such as O and N_2 that recombine by three body collision below 130 km, and there convert the original energy of dissociation into thermal energy. Below 130 km, the transitions between the different levels of the ground terms, ^3P, of atomic oxygen, O, is also an important radiative mechanism. In this region, the convection plays an important part in transporting the energy.

1.2.2. The tidal forces.

In the atmosphere, just as in the oceans, tidal forces are felt due to the effects of the sun and the moon. Stewart[10] suggested in 1882 that certain magnetic variations which had been discovered were indirect manifestations of tidal motions in the atmosphere. Since then many workers[11, 12, 13, 14, 15, 16] have developed the theory of atmospheric tides. On the ground, the tidal effects are clearly seen in barometric reading of the pressure variations. Since the sun and the moon both exert tidal influence, the semi-diurnal wave should have components of both solar and lunar periods. While solar semi-diurnal component is easily recognizable in barometric records, the lunar semi-diurnal

component is very weak. It has an amplitude which is only one-sixteenth of the solar tide. This is contrary to the tidal theory. The tide generating force of the disturbing body varies as $\frac{M}{D^3}$ where M is the mass and D the distance of the disturbing body from the earth. The moon, due to its proximity to the earth, exerts a tide generating force which is nearly 2.5 times as powerful as that of the sun, and so the lunar component of the atmospheric tide should be larger than the solar component. But actually the solar semi-diurnal oscillation at the ground is observed to be about 100 times larger than what it ought to be. To explain this, Laplace had suggested that the solar tide might be caused by the thermal rather than the gravitational action of the sun on the atmosphere. The daily variation of the atmospheric temperature has a 12-hourly harmonic and other higher harmonics in addition to 24-hourly harmonic. The amplitude of the diurnal component of the temperature curve is considerably larger than that of semi-diurnal component while reverse is the case in the pressure curve. To overcome this difficulty Lord Kelvin[17] put forward the resonance theory in which it is assumed that the earth's atmosphere has a natural period of free oscillation of about 12 hours, due to which, the oscillations produced by the feeble tidal forces of the sun are magnified very much. Later workers[13,14] further developed this theory. In this theory, the maximum tidal energy is supplied to the atmosphere at the lowest levels. The diurnal component propagates upwards as a modified pressure wave, until it reaches regions of high viscosity around 120 km where it is damped out.

The semi-diurnal component, having larger frequency, propagates similarly but is strongly reflected at lower heights (60-90 km) by a region of diminishing low temperature. The reflected disturbance returns to the ground and suffers further reflection. Thus these oscillations are effectively trapped within the lowest 60 or 70 km of the atmosphere, and this region acts as a resonance cavity for this component. Standing waves are established, whose amplitudes depend on the relative phases at successive reflections, and a resonant response is achieved under suitable circumstances. Such a response takes place in the case of solar semi-diurnal variation, and it is accordingly magnified greatly in comparison with the other solar components and the lunar semi-diurnal component.

The first objection to this theory was put forward when the effects of the Krakatoa eruption of 1883 and great Siberian meteor of 1908 were studied. When the free period of the atmosphere was computed from the phase velocities of long air waves generated by the above disturbances, a free period of about 10.6 hours was obtained instead of 12 hours. However, Pekeris[14] suggested that the atmosphere has two resonant periods, one at 10.6 hours and one at 12 hours. But the recent reports of pressure waves from the atomic blasts and the large USSR explosion in 1961 do not give evidence for these two resonant periods[15].

According to Mac Donald[16], the terms proportional to the horizontal component of the Coriolis force included in the

equations of motion in the resonance theory give rise to mathematical difficulties. He also points out that the mixed character of the differential equations, which arises due to the inclusion of these terms were not considered fully. One of the assumptions in the theory, that the atmosphere is an oscillating system about a stable mean is not valid, because the large temperature gradients existing between the poles and the equator show that the atmosphere is far from a stable equilibrium state.

These difficulties arose because the resonance theory was formulated from the inadequate data available at that time. Pekeris assumed a maximum temperature of about 350°K near the mesopause whereas the measured values are much less, being about 275°K. Again, the earlier calculations were based on a driving force derived from gravitation, whereas, a thermal source appears to be more important. With the present day knowledge of the temperature distribution, the magnification of solar semi-diurnal amplitude becomes only about three-or four-fold, and it is also found that there is no pronounced resonance peak at 12 hours[19]. Siebert[20], and Sen and White[21] pointed out that in the earlier resonance theory, only the part of the diurnal heat wave, which is propagated by eddy conductivity from the ground upward, to about 600 m, was considered. If the daily variation of the air temperature at higher levels due to the absorption of radiation by water vapour[20] and Ozone[22] is considered, a much smaller magnification would be required than assumed earlier. The present

day calculations indicate that resonance is far less effective in determining the relative magnitudes than is the degree of matching that exists between the vertical profile of heat input and the vertical structure of the resultant tidal wave[23].

The atmospheric tides carry significant energy to higher levels and when they dissipate at higher altitudes, they form an energy source at these altitudes. Hines[24] estimated a semi-diurnal tidal flux of about 10^{-3} watt/m^2 in the E region with an energy density of about 6 x 10^{-3} joule/m^3 at 90 km altitude. Theoretical or experimental assessment of the contribution of tidal energy at higher altitudes is still not made.

1.2.3. Internal atmospheric gravity waves.

Superimposed on the prevailing and tidal winds at meteor heights, that is, between 80 and 120 km, there are periodic components of magnitude comparable to the tides but with time scale of the order of one or two hours[25]. Observations have shown that these periodic winds vary randomly with height. These changing winds were previously attributed to turbulence in the upper atmosphere[26]. Hines[27] attributed them to internal atmospheric gravity waves. These waves are physically similar to the tidal and planetary waves, in that the effects of gravity play an important role in determining their properties. They are low frequency compliments of the family of high-frequency acoustic waves[28]. According to Hines, for these waves, the group velocity propagates almost vertically upwards, while the phase

velocity propagates downwards, and the individual air particle motions are nearly horizontal. The small vertical component of the particle motion is sufficient for gravity to provide the restoring force for the wave motion. Hines[23] showed that a number of observable properties of upper atmosphere motions like the wind shears, the eddy mixing, the occurrence of sporadic-E and the travelling ionospheric disturbances can be explained qualitatively as well as quantitatively on the basis of these waves.

The internal atmospheric gravity waves are believed to originate in the troposphere, either near the earth's surface or near the jet stream[29], and propagate upwards through mesosphere to ionospheric heights. Theoretically a wide spectrum of gravity waves is allowed at any altitude above 50 km. But at higher levels, the wave energy is decreased partly due to partial reflection of some modes, and partly due to viscous dissipation of the wave energy. Much of the energy due to this dissipation goes to heat the atmosphere. Hines[24] estimated, that the energy loss of these waves, at 95 km height, is about 10^{-1} watt/kg, which gave a heating rate of the order 10^{0} k/day. Around 106-110 km, the energy loss becomes 4×10^{-1} watt/kg, or a heating rate of about 30^{0} K/day, and around 140 km, the energy loss becomes 1 watt/kg yielding a heating rate of about 100^{0} K/day. It thus appears that the viscous dissipation of the internal atmospheric gravity waves contributes largely to the very rapid rise of temperature found in the E region.

1.2.4. Particle bombardment and solar wind.

It is known that the energetic particles, right from thermal energies to cosmic ray energies, constantly bombard the upper atmosphere, and loose their energy in the atmosphere. Part of this energy appears as the heat energy. This phenomenon is very much pronounced at higher latitudes, in the auroral zones and near the poles, where even very low energy particles are able to enter the atmosphere. At lower latitudes very few high energy particles are allowed by the earth's magnetic field and their contribution to the atmospheric energy is negligible. The heat generated due to the energetic particles can be obtained by the relation

$$Q = F \sigma E n$$

Where Q is the heat energy in $cal/cm^3/sec$, F is the flux of energetic electrons, σ the cross section for inelastic collisions, E the energy transferred per collision and n the number density of atmospheric particles. Various estimates have been made for the heat generated by these energetic particles. Jastrow[30] estimated from the data of Sputnik III that a heat energy $Q \simeq 4 \times 10^{-16}$ $cal/cm^3/sec$ is generated at a height of 200 km and a heat energy of about 10^{-14} $cal/cm^3/sec$ around 100 km. Apart from these auroral particles, during magnetically disturbed periods, the plasma clouds ejected by the sun during solar disturbances enter the atmosphere at all latitudes. This plasma, having very high temperature, can impart the heat to the upper atmosphere by conduction, and thus act as heating agent. Contribution of

heat from the above discussed phenomena are not yet well studied and hence their contribution to the energy supply to the general circulation at high altitudes is not yet understood.

1.2.6. Other sources of energy in the upper atmosphere.

Apart from the sources of energy discussed in the earlier sections, which affect the general dynamics of the upper atmosphere considerably, the energy is also obtained from the planetary waves, with periods of days, in the troposphere. These planetary waves carry a large dynamic energy, a part of which leaks to higher levels through mesosphere[28]. The dissipation of these waves, again gives rise to thermal energy.

Up to about 100 km altitude, the turbulence, in the form of eddy diffusion, is an important factor, which imparts a fraction of energy to the atmosphere. Greenhow[31] deduced a turbulence power of 7×10^{-3} watts/Kg (70 ergs g^{-1} sec^{-1}) at meteor heights, that is, at about 90 km, from the transitional growth of meteor trails.

Some energy is also imparted to the upper atmosphere by the rotation of the earth around its axis. Due to the viscosity, the atmosphere is dragged along with the surface of the earth in its rotation. The motions of the atmospheric constituents, both neutral and ionised, due to this rotation, give rise to kinetic energy at these heights which cannot be neglected in the consideration of dynamical processes.

1.3 WINDS IN THE UPPER ATMOSPHERE.

From the systematic studies of meteor trails Jesse[32], in 1896, established the existance of winds in the upper atmosphere. In the atmosphere, unbalance between the resultant heating rates at different latitudes supply the primary driving force for the atmospheric circulation. However, this general circulation is modified to a great extent by other forces. An attempt is made in section 1.3.1 to understand the effects of various forces on the general circulation of the neutral upper atmosphere.

The winds in the neutral atmosphere are controlled by hydrodynamic forces, which are modified at higher altitudes due to the presence of ionization. The motion of the ionised particles, which also experience the hydrodynamic forces, are largely controlled by electrostatic and magnetic fields, and by the collisional interactions with the neutral particles.

In section 1.3.2 the motion of ionized component is studied, and in section 1.3.3 the possible interaction between the neutral and ionised component of the upper atmosphere is briefly studied. In section 1.3.4 the formation of sporadic E, due to the neutral wind shear, is briefly discussed.

1.3.1. Neutral atmosphere motions.

The unequal latitudinal and geographic heating, of the earth's surface and the atmosphere, gives rise to pressure gradients which are directed, in general, along the temperature

gradients. The pressure gradient acts as a force to drive the atmosphere and causes wind. The wind motion, thus generated in the atmosphere, is affected by the rotation of the earth. If the pressure gradient is such that wind would blow from south to north in the northern hemisphere on a non-rotating earth, in reality it would blow towards north-east because of the earth's rotation. Similarly wind towards east would blow towards south-east, south wind towards south-west and west wind towards north-west. In the southern hemisphere the conditions are just the reverse. This effect is maximum near the poles and decreases towards the equator, with no effect at the equator.

This force due to the rotation of the earth, which deflects the winds caused by the pressure gradient is called Coriolis force, and is given by

$$F_x = 2\omega v_y \sin\phi$$

and $$F_y = 2\omega v_x \sin\phi$$

where v_x and v_y are the wind velocities in x and y directions, pointing towards east and north respectively. The z-axis points vertically upwards. ω is the angular velocity of the earth, and ϕ is the latitude of observation.

At lower altitudes, the Coriolis force due to the rotation of the earth, and the force due to the pressure gradient balance each other, and a steady wind called geostrophic wind is obtained. The geostrophic wind, which approximates the true wind observed, is given by

$$v_x = - \frac{1}{\rho f} \frac{\partial p}{\partial y}$$

$$v_y = \frac{1}{\rho f} \frac{\partial p}{\partial x}$$

where v_x and v_y are zonal and meridional components of motion directed towards east and north respectively. ρ is the density, p the pressure and $f = 2\omega \sin\phi$ is the coriolis term. The direction of the geostrophic wind is approximately parallel to the isobars, with low pressure to the left of the line of motion in the northern hemisphere, and to the right in the southern hemisphere.

The pressure distribution with height for a given temperature profile is given by the relations

$$p = p_o \exp \left(- \frac{mg}{k} \int_{z_o}^{z} \frac{dz}{T} \right)$$

where T, the temperature, is a function of z, p is pressure at altitude z and p_o is the pressure at some datum level z_o. m, g and k are constants being mean molecular weight, acceleration due to gravity and Boltzmann constant respectively. In a case where temperature changes with height with a gradient α, that is, when $T = T_o + \alpha z$, T_o being the temperature at the datum level, we have

$$\frac{p}{p_o} = \left(\frac{T_o + \alpha z}{T_o} \right)^{- \frac{mg}{k\alpha}}$$

This shows that when α is positive, that is, when the temperature increases with height, the pressure decreases slowly with height,

and when α is negative, the pressure decreases more rapidly with height. When the temperature fields having different gradients at two places are considered, the isobars become inclined to the horizontal due to the above effect. This gives rise to a shear vector in the horizontal wind with height. The relation between the controlling temperature gradients and the resultant horizontal flow and shear is called the thermal wind equation, which has the components

$$v_x = v_{x_o} \frac{T}{T_o} - \frac{gT}{f} \int_{z_o}^{z} \frac{1}{T^2} \frac{\partial T}{\partial y} \, dz$$

$$v_y = v_{y_o} \frac{T}{T_o} - \frac{gT}{f} \int_{z_o}^{z} \frac{1}{T^2} \frac{\partial T}{\partial x} \, dz$$

where v_{x_o} and v_{y_o} are the horizontal components of geostrophic wind and T_o the temperature at the level z_o and v_x and v_y the geostrophic wind components and T the temperature at a higher level z. Thus it is seen, that the geostrophic wind at a higher level has a component depending on the horizontal temperature gradient, and is known as the thermal wind component. The thermal wind has a direction parallel to the isotherms of the mean temperature of a layer of thickness z, with high temperature to the right in the northern hemisphere. It has a magnitude proportional to the horizontal gradient of this mean temperature. The above equation for v_x representing the zonal wind may be written in a simpler form as

$$\frac{\partial T}{\partial y} = - \frac{f T^2}{g} \frac{\partial}{\partial z} \left(\frac{v_x}{T} \right)$$

This equation indicates that the ratio $\frac{v_x}{T}$ should increase with height, in any region, where the temperature is increasing towards the equator. Thus if the temperature distribution with height and latitude are known, the zonal wind at each height can be obtained from the above equation. Conversely, from the known values of zonal winds, the temperature distribution can be obtained. Murgatroyd[33] used this method to compute the temperature distribution with latitude up to about 100 km.

Superimposed on the geostrophic wind and thermal wind, which constitute the prevailing winds, the winds caused by the tidal oscillations of the atmosphere are present which are more important at higher altitudes. The solar semi-diurnal oscillation is the most important oscillation of the atmosphere as discussed in section 1.2.2, though the diurnal component as well as higher harmonics are present. The variation of amplitudes and phase at different heights, for different modes of these oscillations, can be computed[34]. The observation of winds, by meteor trails[35], has shown that with height the amplitude of the semi-diurnal oscillation increases and the phase advances. The tidal wind vector rotates clockwise (as seen from above) in the northern hemisphere and anticlockwise in southern hemisphere, in accordance with the theory.

As discussed in section 1.2.3, the internal atmospheric gravity waves are superimposed on the dominant tidal motions and the prevailing winds around 80 km altitude. These waves act as irregular winds and distort the wind field randomly at vertical intervals that grow with height. These intervals are of the order of 6 km in the 70 to 120 km region and of 16 km around 140 km. The amplitude of these waves also increases with height. Due to dissipative effects introduced by viscosity, and conversion to thermal energy, the smaller scale modes disappear at higher altitudes. Thus the effect of these internal atmospheric gravity waves is predominantly observed in the height range 70 to 120 km, above which height, the removal of small scale modes and the lengthening of the dominant scale render them unimportant.

Up to about 100 km altitude, the atmospheric turbulence is important and must be considered in studying the wind field. Up to this height level, eddy diffusion takes place and the wind is not steady. At a height of about 100-110 km the turbulence stops abruptly. According to Mamont and de Jager[36], the termination of turbulence is due to the decrease of Reynold's number below some critical value. Near the height of the termination of turbulence, a transition from a chemically mixed state of atmosphere to a state of diffusive equilibrium occurs. Above about 110 km, due to the molecular diffusion, the wind flow becomes laminar.

1.3.2. Ionospheric motions.

In the ionosphere above 70 km, the plasma, consisting of electrons and positive ions in equal number, is immersed in neutral air, such that, the ratio of the number density of neutral molecules or atoms to the number density of the electrons is about 10^9 in the D region, 10^7 in the E region and 10^4-10^3 in the F region. The processes discussed in section 1.3.1 which cause the neutral wind motion, also drive the ions and electrons of these regions. The drift of the uniform layer of ionization cannot be detected in general. The majority of methods, of measuring ionospheric drifts, take advantage of the existance of irregularities in the region. The measurements of the irregularities in the ionosphere can be studied from the ground using different methods. The most general method is by studying the amplitude fluctuations of pulsed radio wave, reflected from the ionospheric irregularities, as received at three receiving antennas kept at suitable distances[37]. This method using spaced receivers gives the movement of diffraction pattern over the ground and so is not a direct measurement of the movement or drift of the irregularities in the ionosphere. It is not obvious that such irregularities will move in the same way as the background ionization or with the neutral air, if there is a wind[38]. Some results of Rosenberg et al[39] have revealed drift measurements in the same direction as, but appreciably exceeding, the corresponding wind measurements. This may show that the drifts are not indicative of irregularities borne by the local wind[40]. Another disadvantage with this

method of measuring ionospheric drifts using spaced receivers is that the height at which the movements are measured is not accurately known by this technique. In the lower ionosphere, where the winds are known to vary rapidly with height, the height determination is very important.

At many places in middle latitudes the drift measurement of ionospheric irregularities are being carried out since many years. Near the magnetic equator only a few stations are located. In January 1964, an ionospheric drift recorder was started at Thumba which is only 30 km south of magnetic equator. The results from this station are quite interesting in that, the direction of the drift in E region is predominantly towards west throughout the year[41]. The percentage occurrence of westward drift is highest being 75% during equinoxes, 68% during winter and 46% during summer. The eastward drift direction occurs only on about 5% of occasions, during winter and summer, around 0700 hours and 1800 hours and is almost absent during equinoxes. The north-south component of the drift velocity is almost negligible. The average values of drift speeds are 136 m/sec during winter, 138 m/sec during equinoxes and 128 m/sec during summer. The individual values vary from about 40 m/sec to about 400 m/sec. During winter, the morning maximum is at 0800 hr, and the afternoon maximum is flat between 1200 to 1500 hr. During equinoxes and summer, the morning maximum is shifted towards noon by about one hour, and the afternoon minimum is shifted to about 1700 hr.

Table 2.

Summary of ionospheric drift measurements at middle and low latitudes.

Author and Technique:	Place	Height	Velocity	Direction	Season	Time	Reference.
1. Briggs et. al. (Spaced receiver)	Cambridge U.K. 51°N	E and F region	10-200 m/sec (average 70 m/sec)	towards east	summer	noon	45
			20-250 m/sec (average 100 m/sec)	towards west	winter	noon	
2. Mitra (Spaced receiver)	Cambridge U.K. 51°N	80 km	0 m/sec	N-S component	all seasons		37
			-	towards south-west		00-12 hours	
				towards north-east		12-24 hours	
3. Salzberg and Greenstone (Spaced receiver)	Washington U.S.A.	E region	50-100 m/sec (average 70 m/sec)	towards west	summer	night	43
				towards east	summer	mid-day	
4. Chapman (Spaced receiver)	Ottawa Canada	E region	80 m/sec	towards SE and NE	-	day time	44
5. Deshpande (Spaced receiver)	Thumba India 8.5°N	E region	40-300 m/sec (average 130 m/sec)	towards west	all seasons	day time	41
6. Koster	Tamale Ghana 0-5°S	E region	mean 67 m/sec maximum 115 m/sec	towards west	-	day time	46
7. Kelleher and Niall	Nairobi	E region	-	towards NW	-	day time	47
				towards SE	-	night time	
8. Norris and Lyon	Ibadan 6°S	E region	mean 43 m/sec	towards east	-	day time	48
			mean 55 m/sec	towards west	-	night time	

Table 2 gives some of the results of drift measurements obtained in middle and low latitudes.

Sometimes horizontal movement of large scale travelling disturbances extending over hundreds of kilometers are observed in F region. Munro[49] found that these disturbances occur on the average about six times during any one day, but hardly ever at night, and the movement is predominantly towards the north-east in winter and south-east in summer, with an average velocity of about 120 m/sec. These disturbances can extend over distances as great as 100 km and can travel distances of 3000 km. Martyn assumes that these disturbances are either caused by the atmospheric wind associated with cellular wave[50], or by ionisation drift induced by an electric field[51]. Hines[27] treats these as due to the internal atmospheric gravity waves.

1.3.3. Interaction between the neutral and ionized components of the upper atmosphere.

Due to the presence of the earth's magnetic field, the movement of ions and electrons, in the upper atmosphere, gives rise to the electrodynamic forces in these regions. These electrodynamic forces have a direct influence on the charged particles, while their influence on the motion of the neutral particles, if any, is only felt through the collisions of the neutrals with the charged particles, collisions with heavy ions being more important than those with the electrons. The

collision frequency of neutral particles with heavy ions is believed to be roughly independent of temperature and to have a value of about $10^{-9}n$ collisions/sec, where n is the number density of heavy ions[52]. Ratcliff[38] has shown, that in D region, the electromagnetic force will not have any effect even on the movement of electrons and ions, and they are carried along with the neutral particles in their motion. The energy transferred during collisions, by the charged particles to neutral particles, is negligible compared to the energy transferred by the neutral particles to charged particles, due to the large number density of neutral particles compared to ions. Hines[26] shows that the drift of ions with neutral air takes place till $\nu_{i,n}$, the ion-neutral collision frequency, is greater than ω_i, the ion gyrofrequency; this height being about 120 km. Above 120 km, the electrodynamic forces and the neutral air are roughly equally efficient in producing the ion movement. Cowling[53] suggested that above about 160 km, the collisions between the drifting ions and the neutral air would set the latter into motion. This motion is called the ion-drag. Rishbeth et al[54] show that above 140 km the neutral air does not take up the ion drift velocity at night, but by day the air does move with the ions. This difference arises principally from the very large day-night changes of ion density in the lower F region. Thus it is seen that the electrodynamic forces acting above about 110 km may alter the geostrophic and thermal winds considerably.

The equations for zonal and meridional winds above 110 km can be written as[66]

$$v_x = - \frac{M \frac{\partial p}{\partial x} + L \frac{\partial p}{\partial y}}{\rho (M^2 + L^2)}$$

$$v_y = - \frac{M \frac{\partial p}{\partial y} - L \frac{\partial p}{\partial x}}{\rho (M^2 + L^2)}$$

where $M = \frac{\sigma_1 H_z^2}{\rho c^2}$

$$L = \frac{f + \sigma_2 H_o H_z}{\rho c^2}$$

with H_o = earth's magnetic field, total intensity,

H_z = vertical component of geomagnetic field,

σ_1 = conductivity across the lines of magnetic force,

σ_2 = Hall conductivity,

c = electric charge.

Up to about 130 km $M < L$ and hence, the above equations become

$$v_x = - \frac{c^2}{(\rho f c^2 + \sigma_2 H_o H_z)} \frac{\partial p}{\partial y}$$

$$v_y = - \frac{c^2}{(\rho f c^2 + \sigma_2 H_o H_z)} \frac{\partial p}{\partial x}$$

Above about 145 km where $M > L$, the equations become

$$v_x = - \frac{e^2}{\sigma_1 H_z^2} \frac{\partial p}{\partial x}$$

$$v_y = - \frac{e^2}{\sigma_1 H_z^2} \frac{\partial p}{\partial y}$$

At higher altitudes the viscosity cannot be neglected. As the density decreases with height the kinematic viscosity given by $\eta = \frac{\mu}{\rho}$ increases where μ is molecular viscosity. The kinematic viscosity whose value is 1.97 1.97×10^2 cm^2/sec at 80 km becomes about 1.30×10^9 cm^2/sec at 200 km. The effect of this viscosity is to reduce the velocity of the atmospheric gas.

The tidal effects observed by the meteor study in the height range 80 to 110 km, appear to lose much of their importance in the E region of ionosphere because of the loss of energy due to the dissipative effects, such as inductive viscosity, brought in by the intense polarisation fields established by the E region currents[56].

The electric polarisation fields, associated with main electric currents flowing at about 110 km, are communicated to the higher ionospheric regions along the highly conducting magnetic field lines. Consequently the viscous drag, associated with collisions between neutral particles and charged particles, becomes sufficiently important in the higher region. Thus the forces acting on the neutral air at these heights include

its partial pressure gradient, gravity, drag due to viscosity and collisions with ions and electrons. The equation of motion for neutral air becomes

$$\frac{d\vec{U}}{dt} = -\frac{1}{\rho}\nabla p + \vec{g} + \eta\nabla^2\vec{U} + \frac{Nm_i\nu_i}{N_n m_n}(\vec{U_i} - \vec{U})$$

where $\vec{U} = (U, V, W)$ is the hydrodynamic velocity,

p = pressure,

$\rho = N_n m_n$ = mass density of neutral particles,

η = Kinematic viscosity,

$\vec{g}$ = acceleration due to gravity,

and $\vec{U_i}$ = velocity of ions.

Rishbeth et al[64] find that the relative motion of the air at any two heights h_1 and h_2, is strongly influenced by viscosity if $h_1 - h_2 \ll H_v$, a scale distance, given by

$$H_v = \left(\frac{\eta}{\rho_i \nu_i}\right)^{\frac{1}{2}}$$

in this case, viscosity provides a strong coupling between these velocities and diminishes rapidly any difference between the horizontal velocities at h_1 and h_2. But if $h_1 - h_2 \gg H_v$, the viscous coupling is weak and is ineffective in removing differences between the horizontal air velocities at the two heights. These conditions hold good only if H_v is independent of height.

Above 140 km, where the ion-neutral collision

frequency $\nu_{i,n}$ is equal to the ion gyrofrequency ω_i, the ions move freely under the influence of an electric field. Below this level the ion velocity $\vec{U}_i$ decreases rapidly downwards and is directed more nearly parallel to $\vec{E}$ and the air is not set into motion by ion-drag. Above 250 km, the scale distances H_v are so large as to suggest that the neutral air in the F_2 layer moves bodily with little vertical variation of $\vec{U}$. Hence, between 140 and 250 km the values of H_v determine whether the neutral air is free to move with the ions.

During intense solar activity, the number of charged particles increase considerably in the ionosphere. Therefore during the great solar and magnetic storms, due to the ion-drag, the neutral particles above about 140 km may be carried over by the charged particles, which may have large velocities along the magnetic lines of force.

1.3.4. Relation between the neutral winds and the ionosphere.

Radio soundings of the ionosphere, at vertical incidence, show certain irregular echoes from heights near and above 100 km, which do not fit into the regular pattern expected for the E layer. These echoes are believed to be reflections of the radio waves from patches of dense concentrations of ionisation, having critical frequency well above that of the normal E layer. Such a layer of ion-electron clouds, normally observed at heights intermediate between the E and the F_1 layers of the ionosphere, is called sporadic E

or E_s . The formation of sporadic E is a world wide phenomenn, but it appears that the mechanism of the formation is different at different latitudes. The probability of occurrence of sporadic E at different latitudes depends on the time of the day. In low latitudes sporadic E occurs frequently during the five or six hours centred around noon. The sporadic E near the magnetic equator is called q type E_s and is connected with the equatorial electrojet. It is quite a regular phenomenon, but certainly it is an abnormality for the E region. In the auroral zone and polar cap, the sporadic E occurs most prominently around midnight. For these two types of sporadic E seasonal variations are secondary compared to diurnal and other variations. In the middle latitudes, as the latitude increases, the seasonal variation becomes more and more pronounced. The sporadic E is formed both during day time as well as by night.

The following properties of sporadic E layers appear to be well established:

(a) The thickness of a typical sporadic E layer is between 500 and 5000 metres.

(b) The profile of a typical sporadic E layer has very steep sides. Typical gradients are 10^5 to 10^6 electrons/cm^3/km.

(c) Sporadic E layers are superimposed on an apparently unperturbed background.

(d) Although these layers of enhanced ionization are nearly uniform in thickness, the ratio N_{max}/N, where N_{max} is maximum electron density and N is the equilibrium value of electron

density, varies over a wide range (1 to 100) from one layer to the other.

Dungey[52] put forward the wind-shear theory to explain the formation of the sporadic E. According to this theory, the neutral air moving in opposite directions at two neighbouring layers, tries to carry the ionized gas with it in its motion; but the magnetic field resists the motion of ionized gas across the lines of force. In Fig.5, let the sloping lines indicate the direction of magnetic field, the horizontal arrows represent

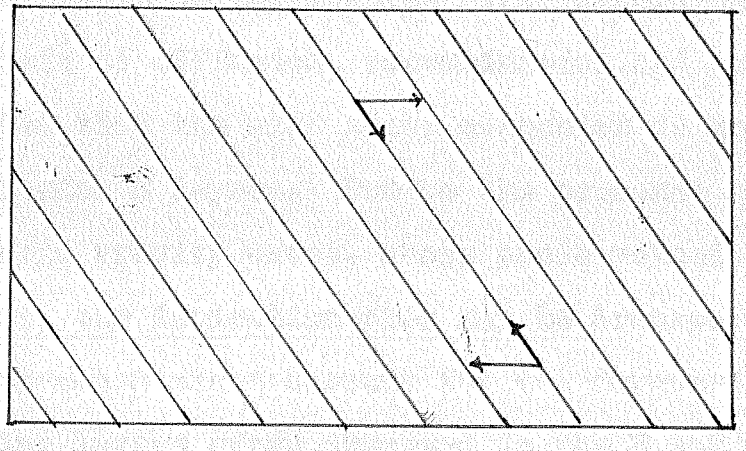

Fig.5

the velocity of neutral molecules and the arrows along the lines of force represent the velocity of charged particles. The velocity component of the charged particles parallel to the lines of force is equal to the velocity component of neutral particles in this direction, but the velocity component of charged particles in the direction of movement of neutral particles is less than that of neutral particles. Consequently the ionized gas is compressed locally, and large variations in the density of the charged particles result from this type of

motion, in which the density of neutral particles change very little. Thus the ionization piles up at the point where the neutral wind velocity is zero until its partial pressure gradient balances the force exerted by the neutral particles. This means thin but dense layers of ionization are produced in the ionosphere as a result of shearing motions of the neutral gas in which the ionized gas is imbedded.

Axford[57] extended this theory to include the effects of internal atmospheric gravity waves which may give rise to the wind shears in the neutral air. Axford also considered the effects of diffusion, recombination and photoionization and showed that the wind shear mechanism is most efficient in mid-latitude E layers. Due to the presence of internal atmospheric gravity waves, whose phase velocity is directed downwards, the ionization also may be transported downwards. This phenomenon might account for the downward moving radio reflecting layers often observed in the E and lower F regions and called 'sequential sporadic E'. An extension of this theory[58] which takes into account more than one species of ions shows that a sporadic E layer is formed in the region of positive ion convergence and that this layer will consist principally of the more slowly recombining ion. If substantial number of negative ions are present, a layer of ionization develops by wind shear in a region where the ion convergence is negative.

This theory of wind shear by Dungey and Axford fails

near the geomagnetic equator, the width of the zone where it fails being of the order of 2^{0} to 4^{0} and probably extending to 6^{0}[58]. This is because the magnetic lines of force in this zone are horizontal and the ionized gas cannot be transported vertically. The neutral air also is incapable of moving the ionized gas in vertical direction. Again, a vertical polarisation electric field is built up which opposes the vertical movement of charged particles. Heisler and Whitehead[59] have noted, that the fraction of time the critical frequency of the sporadic E layer exceeded 5 Mc/sec depended on the horizontal component of the earth's magnetic field for stations in the middle latitudes. On this basis Whitehead[60] proposed that the vertical velocity of ions depends particularly on a term

$$\frac{\nu_i \, \omega_i \, \cos I}{\nu_i^2 + \omega_i^2}$$

where ν_i and ω_i are respectively collision frequency with neutral particles and gyrofrequency of the ions, and I is the dip angle. The ion vertical velocity also depends on a function involving the horizontal velocity of the neutral air. The probability of the formation of sporadic E is more when the electron and ion concentration is more. Thus the day time in summer season is more suitable time for the sporadic E to be formed near E layer maximum. In the above expression $\omega_i \cos I$ is proportional to the horizontal component of the earth's magnetic field and will not vanish at magnetic equator also. Though this modification of wind shear theory was propounded

for temperate zone, this may explain the formation of sporadic E near geomagnetic equator also. Many other workers, notably Kato[61], Layzer[62,63], Tsuda et al[64] and Hines[40] have given explanations for the formation of sporadic E in temperate zone. No satisfactory theory has been proposed to explain the formation of sporadic E near the geomagnetic equator. A very intense sporadic E layer is found in the day time in a narrow zone centered near the magnetic equator surrounding the earth[65]. The sporadic E at night is not so intense. Due to this abnormality of sporadic E in day time, Matsushita[66] suggested that there is some relationship between the sporadic E formation and the eastward intense electric current flow in the atmosphere that produces the daily magnetic variation.

Whitehead[67] suggested that wind shear may not be the sole cause of temperate zone sporadic E but meteor ionization and turbulence may also play an important part. As these phenomena are not affected by earth's magnetic field, these may be of some importance at the magnetic equator also.

As the wind-shear theory shows, the east-west component of the horizontal neutral wind is most effective in producing the sporadic E layers. The sense of shear most suitable for the formation of sporadic E layer is provided by an underlying wind directed towards east along with an overlying wind directed towards west[40]. If a large number of negative ions are present, the north-south rather than the east-west component of the neutral wind becomes most effective to produce sporadic E. Above

about 120 km, the north-south component becomes more important as the ion gyrofrequency ω_i is greater than unity at these heights[58].

There have been attempts to verify the wind shear theory in the middle latitudes by observing the neutral winds and the electron density profiles at the same time. Layzer[62] compared the wind shear theory with the experimental results obtained by Smith[68] and Manring et al[69] and found a close correspondence between the fine structure of ionization profile and the fine structure of the wind profile, layers of enhanced ionization tending to coincide with narrow layers of zero shear where both the speed and direction of the wind are stationary.

Rosenberg et al[39] are carrying out experiments to connect the wind shears with the sporadic E. They found that generally the high shear region is between 101 to 120 km. They suggested that the shear altitude may vary between night and day[143]. They found that, a natural mechanism exists at night to maintain a concentration of ionization of sporadic E at a selected level over long periods, while at nearby levels an abundance of ionisation is dissipated by apparently normal processes of diffusion and electron loss within a few minutes. They also found that, the sporadic E layers detected from ionograms corresponded to zero velocity in the east-west shear, but not dependent on the direction of this shear. Bowen et al[70] at Hammaguir and Groves[71] from Woomera also found the same result that the sporadic E can occur on both positive and negative

wind gradients. Mac Leod[72], on the other hand, reports that he obtained an excellent agreement between the altitudes of sporadic E layers predicted from observations of horizontal velocities and very accurate ionosonde measurements of sporadic E layer reflections.

Cohen et al[73] observed two types of sporadic E near the magnetic equator. For the first type, which was called by them "equatorial sporadic E", the echoes observed on the ionograms were assumed to be due to a thin stratum of magnetic-field-aligned irregularities embedded in the equatorial E layer. The traces in the ionogram due to second type, called the "equatorial slant sporadic E", were assumed to be due to a mechanism involving propagation in the vertical east-west plane and scattering from these irregularities.

Farley[74] has shown that sporadic E near the magnetic equator arises from an acoustic wave generated by a two-stream instability associated with electrojet.

Thus it is seen that the wind shear theory which appears plausible at middle latitudes has not been fully verified by experiments and its importance near geomagnetic equator is still uncertain.

1.4. METHODS EMPLOYED FOR OBSERVING NEUTRAL UPPER ATMOSPHERE WINDS.

The available data for the neutral upper atmosphere winds are very meager. Till recently no direct tool was

available to study these winds in the upper atmosphere. Only indirect methods, like observing the movements of noctilucent clouds and meteor trails, provided the scant data available.

1.4.1. Observation of noctilucent clouds.

The noctilucent clouds are generally seen in the latitude range 45° to 77°, the region of optimum occurrence being 50° to 65° . These clouds are formed between 79 and 90 km, the average height being about 82 km[75]. They are seen from late May to the middle of August and only during twilight period between 2° and 10° from the horizon. The temperature at the height, where these clouds are formed, is about 130° K[76]. The origin of these clouds is not yet clearly known, but it is believed that they consist of either meteor[77] or volcanic dust[75] particles coated with a volatile material like water[78] . The height and the movement of these clouds can be studied by photographing them from two widely placed cameras. Paton[79] has reviewed recently the different characteristics of these clouds. However, recent observations of the motions of these clouds have not added much to the knowledge of winds at these heights.

1.4.2. Meteor trails.

The meteors, entering the earths atmosphere, penetrate until collisions with atmospheric atoms and molecules are sufficient to disintegrate them into small particles. The passage of a meteor in the denser region of the upper atmosphere

where disintegration takes place, produces two effects. Firstly, the high energy of meteor imparts sufficient energy to air molecules through collisions, to ionise them and produce a dense ionized trail of the order of 10^{10} electrons/cm^3 [80]. Secondly, the hot meteoric particles produce a visible trail in the atmosphere. Various methods have been adopted to study these meteor trails, and determine the wind field in the height range 80 to 110 km, where these meteors appear. Elford[81], and Greenhow and Neufeld[82] have used radio echo methods to observe the meteor trails. The radio echo method is very useful in that the meteors can be observed during day time as well as during night, and thus a large amount of data can be acquired within a short interval of time. Whipple[83], Millman[84], as well as several Russian workers[85] have used photographic methods. This photographic method is useful only during night hours, and only those meteors which produce visible trails can be studied by this method. Lovell[86], Manning[87] and Kuruhata[88] used radar to track down the meteors. Craig[9] reviewed the observations of meteors made by radio echo methods at Jodrell Bank and Adelaid and gave the salient features of the wind field in the 80-110 km region.

1.4.3. Rocket released sodium vapour clouds.

The two methods given above depend on the natural phenomena over which no physical control is possible. In 1950, Bates[89] put forward the idea of injecting chemicals into the upper atmosphere with the help of rockets, and studying the

artificial phenomena thus created, for deriving the information. He thought this would be more advantageous then the observation of natural phenomena. He suggested to inject about 100 g of sodium vapour with the help of rocket at about 70 km during twilight or night. He predicted that the resulting emission due to the resonant scattering of sunlight during the twilight, or due to chemical action during night, would be much higher and the luminosity thus obtained would allow a quantitative study of the following phenomena:

(i) The absolute intensity might give information concerning the equilibrium ratio of free to combined sodium.

(ii) The relative luminosity of clouds ejected at different times of the year might reveal whether the observed seasonal variation of the normal D-lines is caused by a change in the total sodium content or by a change in some property of the atmosphere.

(iii) The decay and the movement of the cloud might reveal information about chemical energy available, diffusion, turbulence and winds.

(iv) Due to the resonance scattering of sunlight during twilight period, the natural sodium of the atmosphere present at about 90 km altitude reveals the characteristics of this region of atmosphere such as temperature and density. If the artificial sodium vapour cloud could be formed at higher altitudes where the natural sodium is absent, this region of the atmosphere also could be studied.

artificial phenomena thus created, for deriving the information. He thought this would be more advantageous than the observation of natural phenomena. He suggested to inject about 100 g of sodium vapour with the help of rocket at about 70 km during twilight or night. He predicted that the resulting emission due to the resonant scattering of sunlight during the twilight, or due to chemical action during night, would be much higher and the luminosity thus obtained would allow a quantitative study of the following phenomena:

(i) The absolute intensity might give information concerning the equilibrium ratio of free to combined sodium.

(ii) The relative luminosity of clouds ejected at different times of the year might reveal whether the observed seasonal variation of the normal D-lines is caused by a change in the total sodium content or by a change in some property of the atmosphere.

(iii) The decay and the movement of the cloud might reveal information about chemical energy available, diffusion, turbulence and winds.

(iv) Due to the resonance scattering of sunlight during twilight period, the natural sodium of the atmosphere present at about 90 km altitude reveals the characteristics of this region of atmosphere such as temperature and density. If the artificial sodium vapour cloud could be formed at higher altitudes where the natural sodium is absent, this region of the atmosphere also could be studied.

(v) Comparison of the cloud formed during night, at different levels, might indicate the dependence on altitude of the rate of excitation.

Following the suggestion of Bates, Edwards et al[90] carried out the first successful experiment of injecting the sodium vapour into the upper atmosphere on 21 January 1955 at Holloman Air Development Centre near Almagordo, New Mexico, using an Aerobee rocket. The sodium was ejected between 50 and 70 km at dusk, but no sodium emission was observed, either during the twilight or on the following night. The second experiment was carried out on 12 October 1955, when the sodium was ejected from 70 to 110 km. The sodium emission was observed at 85 km which could be photographed from the ground. The winds between 85 and 110 km could thus be measured. Dedinger et al[91], in a subsequent experiment of this type, studied the various chemical reactions, which give rise to the observed intensity of the cloud at various heights, from 90 to 140 km, during twilight as well as during night. The spectrographic observations showed no trace of sodium molecular spectrum. An attempt to observe the second doublet of the principal series of sodium (λ=3302 $\mathring{A}$) also failed, which showed only radiation from the first doublet (λ=5890 $\mathring{A}$). Since these first experiments, many scientific groups at different places on the earth are engaged in determining the winds in upper atmosphere by this technique.

The sodium vapour experiments proved very useful

to determine the neutral atmosphere winds up to about 200 km. (The payload construction and data acquisition techniques for this experiments are discussed in detail in chapter II). The drawback in this experiment is that the data are available for a few minutes only, during the twilight periods. The night time ejection of sodium at 80-110 km altitude produces a light emission of only 15 times the normal night sky glow and it is of short persistence and so it cannot be photographed.

1.4.4. Grenades.

After the advent of sounding rockets, the grenade experiments are also being used to determine the winds, temperature, pressure and density of the atmosphere. This technique is mostly useful up to about 90 km. The technique, followed by Smith et al[92] at Wallops Island, is as follows. One and two pound grenades, carried in a sounding rocket, are ejected and exploded at 4 to 6 km intervals. Either a high precision radar or a doppler tracking system or both are used to determine the rocket position and hence the exact position of the explosion. The time of the explosion is detected by small infrared photocells on the rocket and this information is telemetered to the ground. A ground-based array of hot wire microphones, with frequency response peaked at 4 cycles/sec, is used to detect and record the sound waves from each exploding grenade. Thus the measured experimental parameters are the times of the grenade explosions, the positions of the grenade explosions, and the times of arrival of the sound waves at the ground based microphones.

Elevation and azimuth angles are computed for each arriving sound wave front by applying a least squares fit to the arrival times at the array of microphones. Each wave is then analytically traced up through the atmosphere by use of Snell's law. The apparent position of the wave is then compared with the known position of the source of the wave, that is, the grenade explosion. The amount by which the sound wave has been displaced horizontally from one explosion to the next is a measure of the average wind velocity vector in the layer between any two adjacent explosions. The rocket grenade experiments used by Stroud et al[93] at Fort Churchill, Canada, and Groves[94] at Woomera, Australia, have revealed interesting features of wind field up to about 90 km.

1.4.6 Chemiluminescent trails.

While conducting grenade experiments it was found that the grenade shells containing aluminium produce a glow when detonated at about 130 km[96] . It was thought that this glow was due to the interaction of incomplete end products of explosion with the atomic oxygen present in this region. Subsequently various chemicals were tried and Trimethyl aluminium (TMA) was found to be most suitable for the night time study of the wind field[96] . The glow from the trail of TMA persists for a few minutes and it can also be photographed from the ground. The upper limit for this glow is about 160 km, above which the glow cannot persist because of small number of oxygen atoms available at this height.

1.5. NEUTRAL WIND MEASUREMENT AT HIGH LATITUDES.

The available data about the neutral winds is very scanty in the high latitude region. In this region, at only one place, at Fort Churchill, Canada (59° N), the vapour cloud experiments have been carried out. Only five launchings are reported[97] since 1963. The majority of data for this latitude region come from noctilucent clouds. At Mawson, Antarctica (68° S), the winds have been measured from radio observation of drifting meteors[98] between 80 and 100 km altitude. Table 3 gives the summary of results of neutral wind measurements with various methods in high latitude region. It is seen that the meridional component is more prominent in this region. The Fort Churchill data shows that the winds are strong at higher altitudes.

1.6. NEUTRAL WIND MEASUREMENT AT MIDDLE LATITUDES.

The majority of data about the neutral winds in the upper atmosphere come from middle latitudes only. These data are available through the study of meteor trails, grenade experiments and the rocket released chemical vapours. The bulk of meteor data come from two stations, Jodrell Bank in England (52° N), and Adelaide in Australia (35° S). Some observations are also available from Harvard Observatory, United States of America, and Ottawa, Canada. The grenade experiments are conducted mainly from two places, Wallops Island, (37° 50' N), United States of America, and from Woomera (31° S), Australia. The number of

Table 3.

Summary of upper atmospheric wind measurements at high latitudes by different methods

	Observer	Place	Technique	Height	Velocity	Direction	Time and Date
1.	Jone	Germany	Scattered clouds	90 km	100-300 m/sec	towards SE	before mid-night
				177	177 m/sec	towards SW	after mid-night
2.	Stoner	Norway	"	60-90 km	44-55 m/sec	towards SSW	twilight
3.	Sitt. G.	Zorte and Stockholm	"	-	low speeds	towards west or SW	-
4.	Hamilton	Jerwick Observatory Scotland	"	91 km	40 m/sec	towards SE	twilight January
5.	Alford and Murray	Hawaii	Radio observation of meteors	80-100 km	20-40 m/sec	N-S component from evening to late hole N-S component changes direction at about 100 km	69
6.	Bedinger	Fort Churchill	Sodium vapour release	80-170 km	Maximum of 120 m/sec around 110 km and between 100 and 150 km	towards north twilight both morning and evening	67
					Jets winds of 200 m/sec at 130 km		
7.	Strand et.al.	Fort Churchill	Grenade experiment	60-100 km	50-100 m/sec	towards east 60 m/sec towards west	May and Aug. July and Aug.

Downloaded from http://pubs.geoscienceworld.org/gsa/books/chapter-pdf/1127/1/1.pdf

places from where the rocket released vapour cloud experiments are being conducted, are increasing in recent years. Table 4 shows the locations in the middle latitudes where such experiments are being conducted at present. Apart from these locations, NASA has launched some rockets from the ships located near Wallops Island.

The data from meteor trails and the grenade experiments are mainly confined to the height region 80 to 100 km, sometimes extending up to 110 km. Some of the results obtained by these methods are given in Table 5. These results are also supplemented by the vapour cloud experiments at some locations. The main characteristics of this height region are the presence of large number of wind shears, turbulence and eddy diffusion. The meteor and vapour trails are distorted due to these effects. Shears up to 30 m/sec per km are frequently found throughout the altitude region 80 to 120 km. Shears greater than 50 m/sec per km are infrequent and usually occur in the 100 to 110 km region[104]. The meridional and zonal components, present similar distributions of these shears. Below about 102 km, due to turbulent diffusion, small globules appear in the meteor and vapour trails which increase in diameter, rapidly at first and more slowly later. It is seen that the turbulence develops more in winter than in summer. The altitude of transition between turbulent and molecular diffusion also appears to be lowered during summer[36].

The data available above 110 km are very meager and

Table 4.

Location of places in middle latitudes from where vapour cloud experiments are conducted.

Location	Country	Latitude	Longitude
1. Ile du Levant	France	43.0°N	6.0°E
2. Sardinia	Italy	39.6°N	9.5°E
3. Wallops Island	US of America	37.8°N	75.5°W
4. AFB New Mexico	US of America	32.5°N	106.5°W
5. Uchinovera	Japan	31.3°N	131.0°E
6. Hamaguir	Algeria	31.0°N	30.0°E
7. Eglin AFB	Florida (US)	30.4°N	86.7°W
8. Reggan	Algeria	26.7°N	0°
9. Sonmiani	Pakistan	26.0°N	67.0°E
10. Kauai	Hawaii	21.9°N	159.6°W
11. Chamical	Argentina	30.5°S	66.0°W
12. Woomera	Australia	31.0°S	137.0°E

Table 5.

Summary of upper atmospheric wind measurements obtained from meteor trails and grenade experiments in the middle latitudes.

.....

	Observer	Place	Method	Height	Velocity	Direction	Time and season	Reference
1.	Elford and Robertson	Adelaide Australia 35°S	meteor (pulse and continuous wave method)	95 km	70 m/sec	towards SE	summer	81
2.	Groves	Woomera Australia 31°S	Grenade experiment	100-110 km	-	towards east	October	71
3.	Elford	Adelaide 35°S	meteor	-	-	towards east towards west	Dec. to Aug Sept to Nov	145
4.	Greenhow and Neufeld	Jodrell Bank England 51°N	meteor (coherent pulse method)	88-100 km	decreases with height	towards east	summer and early winter	54
					10-15 m/sec	towards south towards north	summer other seasons	103
5.	Manning et. al.	Stanford California U.S.A.	meteor (continuous wave Doppler method)	90-110 km	50 m/sec	towards NE towards north	0300 summer 0600 summer	146
6.	Greenhow	Manchester England 51°N	meteor (pulse method)	-	50 m/sec	towards south towards north	before 0100 winter after 0100 winter	147

come exclusively from the rocket released vapour trails. Manring et al[105] and Kochanski[106] have studied the individual wind V/S height profiles obtained at Wallops Island (the only location where large number of profiles are available) and classified the wind profiles in the following two groups according to their apparent characteristics.

(a) Group one: Typical wind profiles belonging to this group are shown in Fig.6. The main characteristics of the group are:

(i) Rapid variation in the direction of the wind with height, usually less than 90^{o},

(ii) A periodic change in velocity with height, and

(iii) A single high shear, high speed region between 100 and 110 km with a quiescent region from about 140 to 100 km.

(b) Group two: Fig. 7 shows some wind profiles which belong to this group. The principal characteristics of this group are:

(i) The presence of an additional maximum in the 100 to 110 km region, and

(ii) The continuous spiralling change of direction with height. The profile denoted by 'spiral' in Fig.7 belongs to this group.

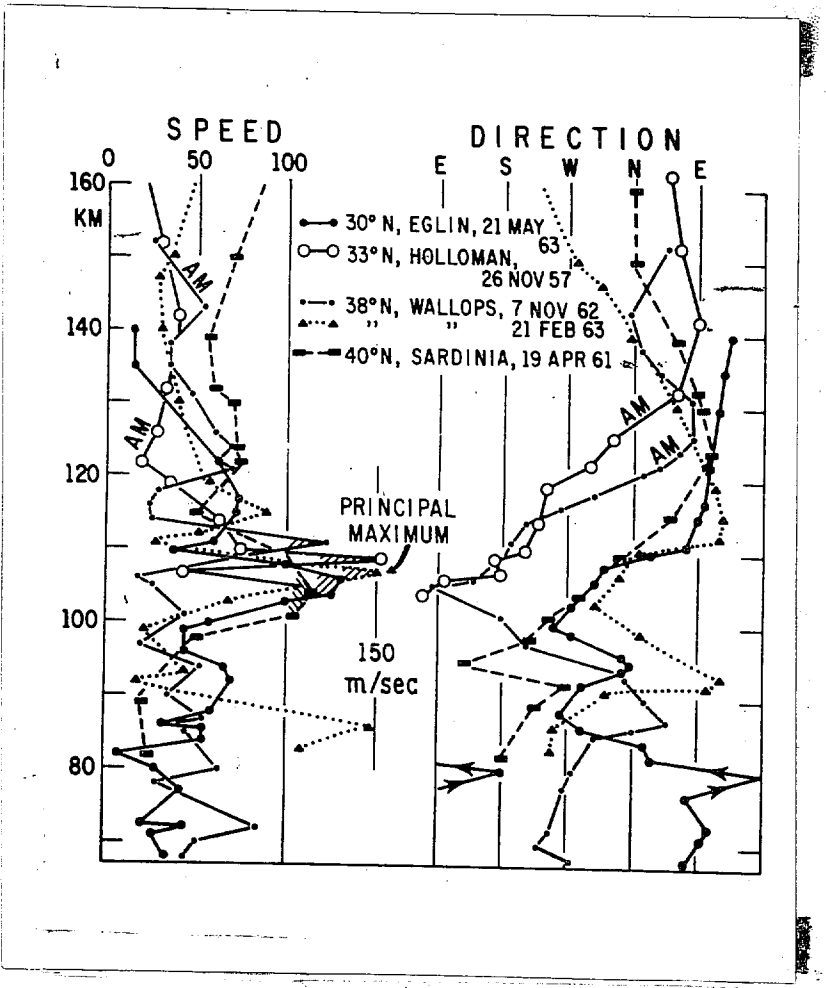

Fig. 6

Typical upper atmospheric wind profiles belonging to Group 1 (Kochanski[107])

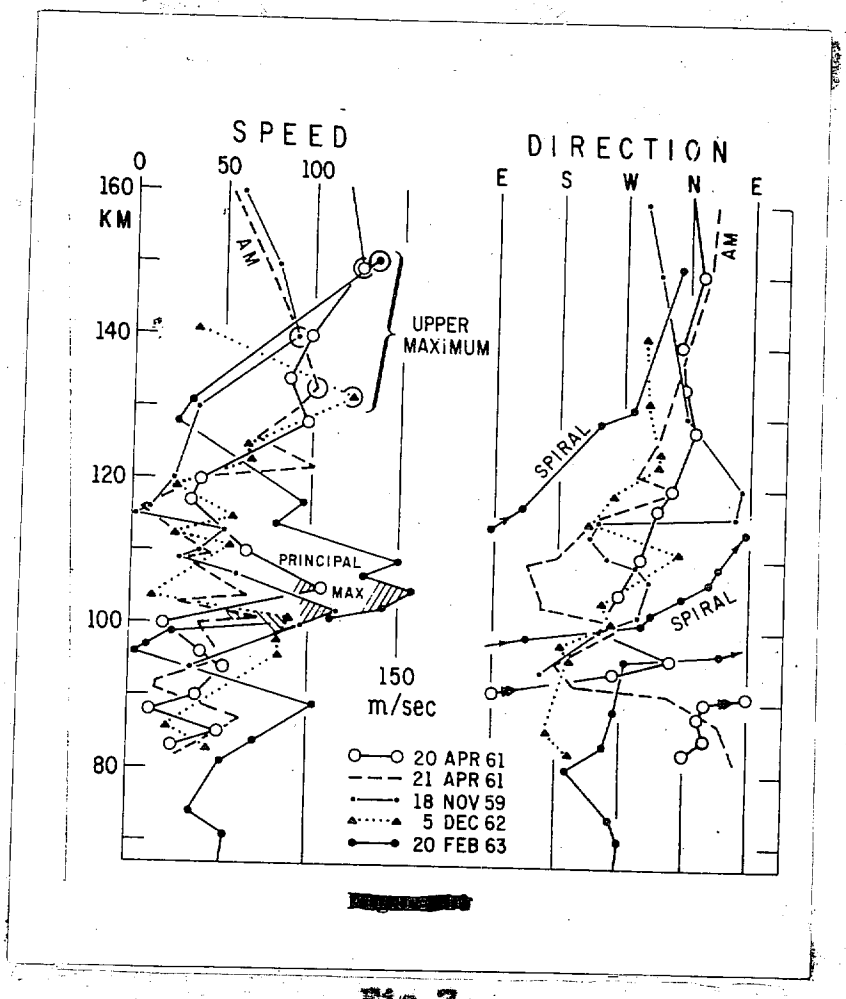

Fig.7

Typical upper atmospheric wind profiles belonging to Group 2 (Kochanski[107])

The two figures show a close similarity of wind profiles for both morning and evening twilight periods in northern hemisphere. All the wind profiles show a principal maximum of speed at an average height of 106 ± 4 km, with average speed of 118 ± 23 m/sec at maximum, bracketed by speed minima below and above this level. The maximum speed is sometimes as high as 150 m/sec. Kochanski suggests that this principal maximum is probably located at or slightly below the level of diffusive separation and its situation between 100 and 110 km suggests a standing wave phenomenon. In summer the direction of principal maximum is nearly always from north-west and in winter the directions are equally divided between north, south and north-west. In southern hemisphere, however, the principal maximum is not evident in the few launchings made at Chemical, Argentina and Woomera, Australia. A maximum wind is found at higher altitudes between 116 and 130 km.

Another important feature of these wind profiles, obtained from middle latitudes in northern hemisphere, is a clockwise turning of the wind vector from 100 to 130 km in majority of wind profiles. In another type of profiles, a continuous spiralling in clockwise direction is observed. In southern hemisphere the wind vector shows opposite rotation in that the winds are anticlockwise up to about 130 ± 10 km and clockwise above this height[102] or anticlockwise throughout the height up to about 160 km[97].

As noted earlier, the region between 80 and 110 km is a high shear region. Above 110 km the shears are very small and between 135 and 160 km the velocity oscillations with increasing height are remarkably small giving rise to a quiescent zone. As can be seen from Table 5, zonal components predominate up to 100 km height, but in 100 to 190 km region, meridional components are equally important. In the northern hemisphere, the meridional winds above about 115 km are mainly southward with an average speed of about 65 m/sec. The experiments at Woomera, and Chamical, show that the meridional winds in southern hemisphere are mainly towards north with the speeds ranging from 0 to 60 m/sec. The zonal winds show that above 110 km the winds from east prevail with speeds of about 80 m/sec at 30° N from May through November, and winds from west with speeds of about 45 m/sec prevail from December through April. No gradual transitions are apparent at these heights. In southern hemisphere the zonal winds give low speeds at about 145 km and maximum speeds of about 100 m/sec or more at 120-130 km level. The maximum winds are directed towards west until late night.[95] As has been noted earlier in section 1.3.3, the effects of solar activity and geomagnetic storms appear to affect the neutral atmosphere wind field. The sodium vapour sounding at Wallops Island, on 24 May 1960, is a typical example, which was carried out during a geomagnetic storm, and which showed a velocity maximum of about 150 m/sec at 117 km altitude.[106]

The meteor data from Jodrell Bank, England[103], show that between 80 and 100 km the winds are towards west in spring and towards east in summer and early winter, increasing in speed with height, ranging from 50 to 100 m/sec. In autumn and late winter the eastward winds decrease with height in this region, becoming westward above 100 km. In Australia also[81,102] the eastward winds in winter decrease with height in 80 to 100 km region, and become westward winds around 100 km. In spring the winds are towards west as in northern hemisphere. The change-over from west winds to east winds and vice versa occurs a month or so earlier at higher levels (90-100 km) than it does at lower levels (70-90 km)[102].

The data acquired so far, at any one location with the vapour cloud experiments, are not sufficient to give a good seasonal picture of the wind field. However, the tentative results from Wallops Island data[107] show that, in summer, the winds between 115 and 180 km are almost exclusively from the north-east, and in winter, between 115 and 130 km they are from north-east, while between 130 and 180 km they are from north, north-west and sometimes north-east. Fig.6, adopted from Kochanski[107], gives the seasonal variation of winds between 70 and 160 km.

The average wind speeds for summer and winter, at Wallops Island, show that the speed at the principal maximum is more in summer than in winter with an average value of about 85 m/sec. Above about 110 km the speed generally increases

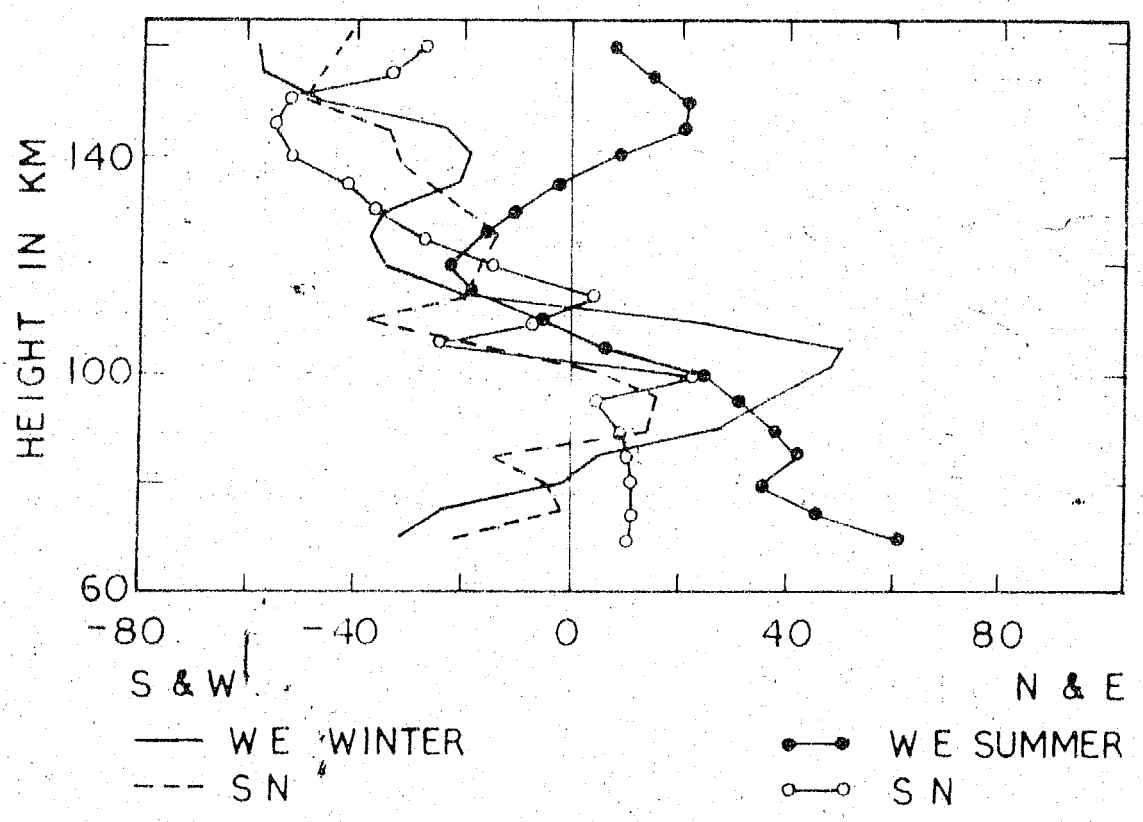

FIG. 8

SEASONAL VARIATION OF THE RESULTANT MERIDIONAL AND ZONAL COMPONENTS OF UPPER ATMOSPHERE WINDS AT 38°N (KOCHANSKI[107]).

with height. This increase appears to be approximately linear and averages 1.8 m/sec per 10 km. Near 160 km a velocity increase in summer and a velocity decrease in winter is observed.

The wind field in the neutral upper atmosphere represents three types of motion, a general drift, the tidal components and internal atmospheric gravity waves, superimposed on one another. Due to the availability of large data from radio observation of meteor trails, it is possible to isolate these components at lower altitudes up to about 110 km. Above this height level, however, due to the meager data available, and also due to the time of observation of vapour trails at present restricted to twilight periods, it is not possible to separate these components unambiguously.

The general drift is similar in character to the prevailing wind at lower heights. At meteor heights the prevailing wind shows irregular day-to-day variations and changes direction, as much as 90^{0}, over a period of 12 hours[9]. It has not been possible to separate the prevailing wind completely from other components with the help of the wind data available from the vapour trails. If the wind velocities during morning and evening twilights at a particular height and location are averaged, the diurnal component, if any, and other irregularities will be smoothed out, and the prevailing component will be obtained, which may also include the semi-diurnal component if it is present. As large data can be

obtained from meteor trails by radio methods, both during day and night, methods of harmonic analysis could be applied to separate the semi-diurnal and diurnal components. By this method it is observed, that the amplitude of semi-diurnal component increases with height, both in summer and winter[103]. At 100 km altitude the semi-diurnal component is towards north at 0600 and 1800 hours at Jodrell Bank. The diurnal component, on the other hand, has little variation with height or season. This component appears to be towards north at about 1200 hours over England, and at about 1800 hours over Australia.

The conventional harmonic analysis cannot be applied to isolate the tidal effects, to vapour cloud data obtained at twilight periods. Individual wind velocity profiles do not reveal any obvious dissimilarities between sodium soundings during evening and morning twilight hours. However, averages of Wallops Island data for the dusk and dawn hours show sizeable differences in the 95 to 125 km region. Large PM to AM wind direction differences, greater than 80°, appear in the 102-122 km region. Speed differences are also large in the 102-122 km region and in the 145-160 km region. The morning speeds appear to be smaller than the evening speeds. However, these observations do not show clearly the presence of a diurnal or a semi-diurnal component. Hines[106] attempted to isolate the diurnal component, from the observed wind profiles, taking advantage of the fact that the dusk and dawn observed points are situated symmetrically on the curve of the diurnal

component. In the method Hines gave, the wind vectors at any one height were separated into dusk and dawn categories and the mean wind vector for each category determined. It was assumed that differences between the two means at a given level could be ascribed to the diurnal tide, which would be roughly in anti-phase at the times of dusk and dawn launchings. The vector common to the dusk and dawn means would represent the prevailing wind and the semi-diurnal tide, which would have completed roughly one full cycle in the dusk-dawn interval. From this analysis it was shown that a real systematic variation of 24-hour component exists over the height range 100-115 km, probably extending over the broader range 96-120 km. This component rotates clockwise, as is given by the tidal theory for northern hemisphere[34]. The theoretical value of the vertical wave-length for the dominant diurnal mode is about 24 km as compared to the wave-length of 20 ± 3 km as given by the analysis of Hines. The amplitude increases with height from 90 or 95 km up to the 105 km level due to the decrease of density of the atmosphere. Above this level, the amplitude decreases due to the dissipation of tidal energy by viscosity and thermal conduction.

Hines further notes, that if the prevailing wind is assumed to be zero, the observed value of the vertical wave-length for the residual or semi-diurnal component is perfectly compatible with the theoretical vertical wavelength of the (2,4) mode of the semi-diurnal tide. Hines, however, cautions

that these results cannot be taken as conclusive and more data should be awaited for.

In a different method to determine the tidal components, Manring et al[105] found that the quasi-periodic components into which the wind pattern between 85 and 135 km could be resolved, might be represented, as a first approximation, by closed loops. When the wind vectors for a given height derived from different launchings were plotted on the same polar diagram, they formed well defined chains of 3 to 8 points. In all the cases, the chains could be connected to form a closed curve consisting of three loops. This indicated that the winds have a quasi-periodic character, rather than non-periodic component, which should give random distribution on the polar diagram. The rate at which the wind vector at a given height traced out its pattern departed substantially from the rate appropriate to strictly periodic motion. The findings of Manring et al are as follows:

(i) At each height, the observed wind vectors define a pattern which is accurately reproduced by a theoretical figure composed of prevailing, diurnal, semi-diurnal and 8-hour components, and the magnitude and directions of the prevailing component determines the position of the centre of the pattern.

(ii) The parameters that define the pattern vary smoothly with height. The magnitude of all components increase to a maximum between 100 and 110 km and the phase angles change rapidly in this region.

(iii) The 8-hour component is dominant at all heights. Sometimes its magnitude is twice that of the semi-diurnal component. The diurnal component is small below about 95 km but increases above this height. The prevailing component varies from near zero to a maximum of 40 m/sec at 105 km. The direction is generally towards east below 120 km and towards west above.

It was suggested by them that though the magnitudes of cyclic components vary smoothly with height, there is a phase anomaly, that is, the phase is a non-linear function of time. It was also suggested that the lack of correlation between the phase anomaly at different heights gives rise to the variability of the wind profiles. The phase anomaly was attributed to magnetohydrodynamic effects, which enhance the effective viscous coupling between adjacent layers, and to variability in the reflection properties of the atmosphere above 135 km. Hines[109], however, criticised this approach of analysis, and rejected these conclusions, on the basis that the appearance of chains of data points has no significance in a statistical sample of the size they employed. Hines has also pointed out that their conclusion that the 8-hour tide was strongest was contrary to the observational evidence available from meteor trails.

The sodium vapour launchings restricted to morning and evening twilight periods are thus inadequate to resolve the periodic motions. The measurement of winds through night

has become possible by the availability of the technique of releasing chemiluminescent trails[110] in the region 90 to 150 km. The periodic components in the atmosphere can be studied by having more than one launching in one night. For a reliable time resolution of the periodic components, a series of about four or more firings is needed. Such a series of launchings are very rare and only three series, two at Eglin Air Force Base, Florida, United States of America[111] and one at Woomera, Australia[102] are so far known.

By analysing the meager data obtained at Woomera, and assuming that only diurnal and semi-diurnal components are of importance, Groves[102] indicates that the amplitudes are approximately equal for both the components.

Thus much more data of this nature are required to determine the periodic tidal components in the upper atmospheric winds.

The internal atmospheric gravity waves, whose properties have been discussed in section 1.2.3 of this chapter, are evident in meteor and vapour trails more prominantly in the height range 80-120 km. All these trails show velocity oscillations at vertical intervals that grow with height, and are of the order of 6 km in the 70 to 120 km region, and of 16 km at 140 km. Kochanski[106] resolved the observed wind profiles into two kinds of motions, the wave motion whose amplitude is W, and a residual term with amplitude R which can be interpreted as the sum of the general drift and tidal motions. The mean speed

attributed to wave motion W shows a peak near 108 km followed by a decrease at higher altitudes. The annual profiles from four locations in northern hemisphere[1] indicate that the amplitude increases from 40 m/sec at 80 km to a maximum of 60 m/sec near 108 km and then slowly decreases with height. The Wallops Island data shows that above about 110 km, the amplitude for summer is larger than the amplitude for winter. The direction of the vector $\vec{W}$ appears to have some preferred directions showing that it is polarized. The energy of internal atmospheric gravity waves, which is proportional to $W^2 \rho$ where ρ is the density, shows an exponential decrease, which was attributed to the viscous dissipation of these waves at higher altitudes. The speed of the residual term R was found to grow rapidly from 70 to 105 km, remain nearly constant from 105 to 130 km, and then slowly increase again with height. At 140 km, it accounted for 78% of the observed wind speed.

1.7. MODELS OF THE GENERAL CIRCULATION IN THE NEUTRAL UPPER ATMOSPHERE.

Many models, theoretical as well as based on the experimental results of the neutral upper atmosphere wind field above 80 km, have been proposed. The majority of the experimental models are based on meteor data, and hence, give the wind field up to about 120 km[112,33,113,114,115] only. Pant[116] and Deb[117] have proposed theoretical models which give winds up to about 300 km at all latitudes.

1.7.1. Models based on the experimental results.

Kellogg and Schilling[112] in their model suggested that at about 80 km the winds are towards west while between 100 and 120 km they are towards east at all latitudes.

Murgatroyd[33] surveyed the available data up to 100 km from different methods till 1957, and gave a plausible model of zonal winds, between 10° and 70° latitude, up to 120 km. According to this model the wind between 30° and 50° in the region 80 to 120 km is towards east in summer and towards west in winter. The wind velocity maximum in summer takes place around 90 to 100 km, which shifts to a higher altitude of about 110 to 120 km in winter. The speed at the maximum, in both the cases, remains constant and is about 70 m/sec.

Batten[113] later gave a zonal wind corss-section for the solstices assuming a hemispherical symmetry. Fig.9 shows the zonal winds according to Batten, which include the data from meteor trail observations, high level balloon observations and anomalous sound propagation measurements. At higher altitudes the results of some vapour cloud experiments are also included. According to this model, like Murgatroyd's model, the winds in summer in middle latitudes, between 80 and 100 km, are towards east. In winter, however, the winds are again towards east between 80 and 100 km, probably changing towards west above. In both these models the wind field near the equator, at higher altitudes, is not given due to the lack of adequate data.

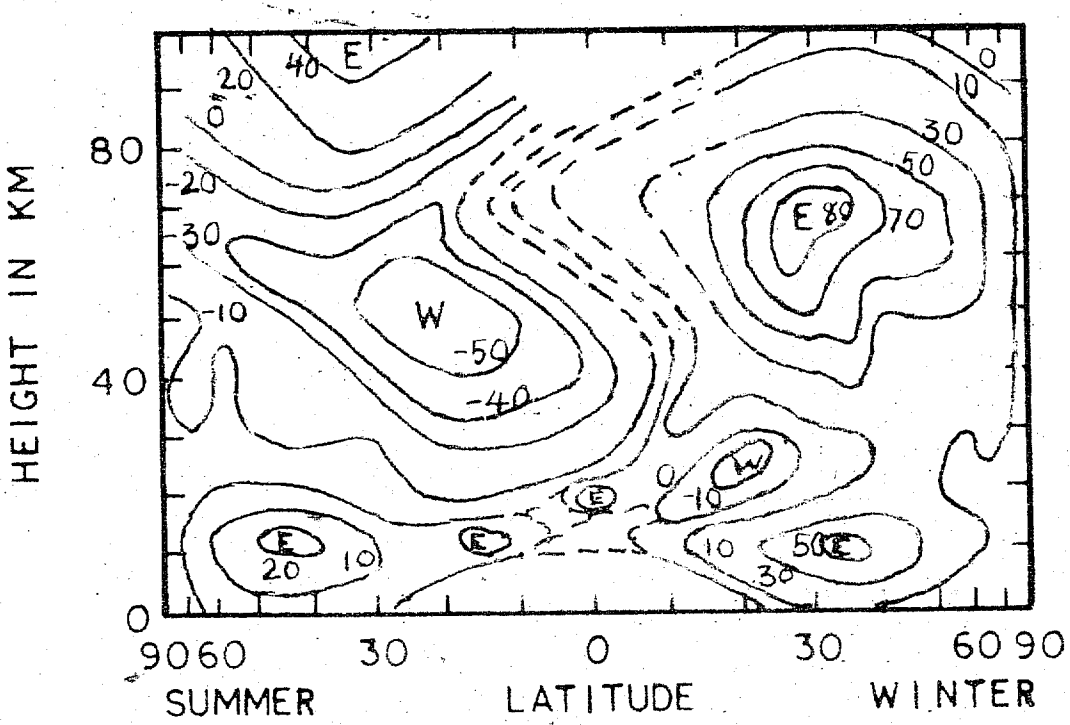

Fig. 9

MODLE OF ZONAL CIRCULATION OF THE UPPER ATMOSPHERE BASED ON EXPERIMENTAL RESULTS (BATTEN[113]). WIND SPEEDS ARE INDICATED IN M/SEC. WIND MOTION TOWARDS EAST IS TAKEN AS POSITIVE .

Kochanski[114] states that there is an exchange of winds between the two hemispheres above 80 km, the net flow being directed from summer to the winter hemisphere. The model for summer shows that at 100 km there is an extensive low pressure system associated with the cold pole, and extending to about 6° latitude. This system slowly gives way at 80 km, where the winds towards west appear near the pole and from 0° to about 18° latitudes. The maximum winds are probably 60 m/sec at 100 km near 30° latitude and 30 m/sec at 80 km. For the equinoxes it is assumed that the semi-annual variation of temperature observed above 200 km[144] is also present at 100 km. The polar region is assumed to be warmest and occupied by an anticyclone. At 100 km, weak winds from west extend from 45° to 0° latitude and at 80 km from 60° to 0° latitude, with maximum winds, only 15-20 m/sec, near 33° latitude. For winter, two alternatives were proposed. In the first model, the polar region was warmest and was occupied by an anticyclone. At about 68° latitude there was a cold belt and cyclonic circulation. Around 38° a zone of westward winds of about 20 m/sec was present at 100 km. At 80 km the eastward winds spread to all latitudes with a maximum of about 60 m/sec at 33° latitude. In the second alternative, the pole was assumed relatively cold but still warmer than the equator and the circulation was almost similar as in the previous model.

More recently Murgatroyd[118] has given an exhaustive survey of the recent models and proposed a model of zonal winds

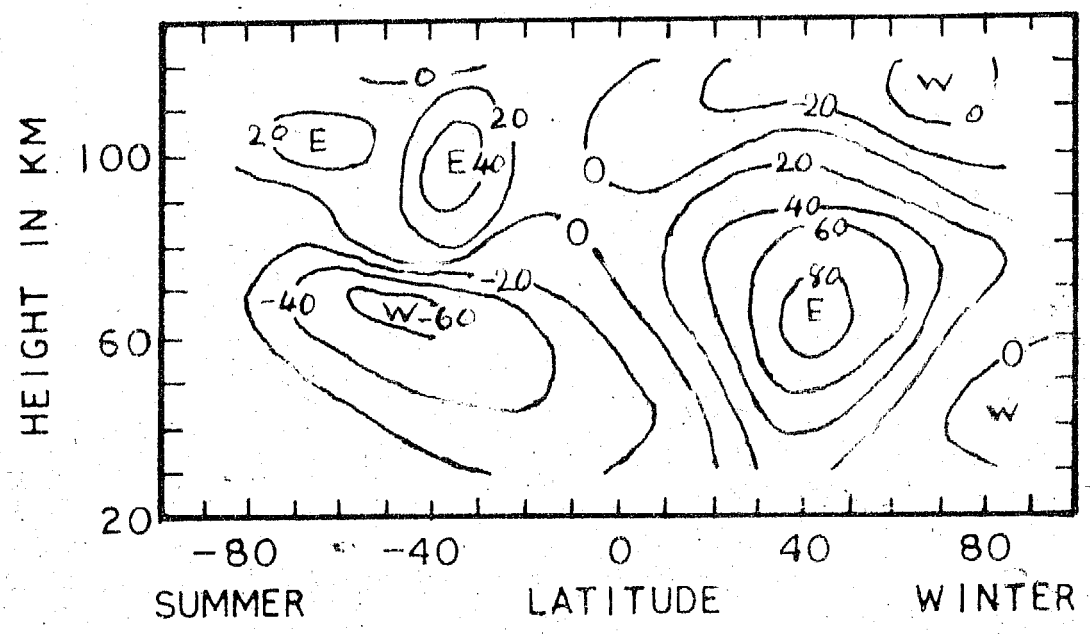

FIG. 10

MODEL OF ZONAL CIRCULATION OF THE ATMOSPHERE AT SOLSTICES (MURGATROYD[118])

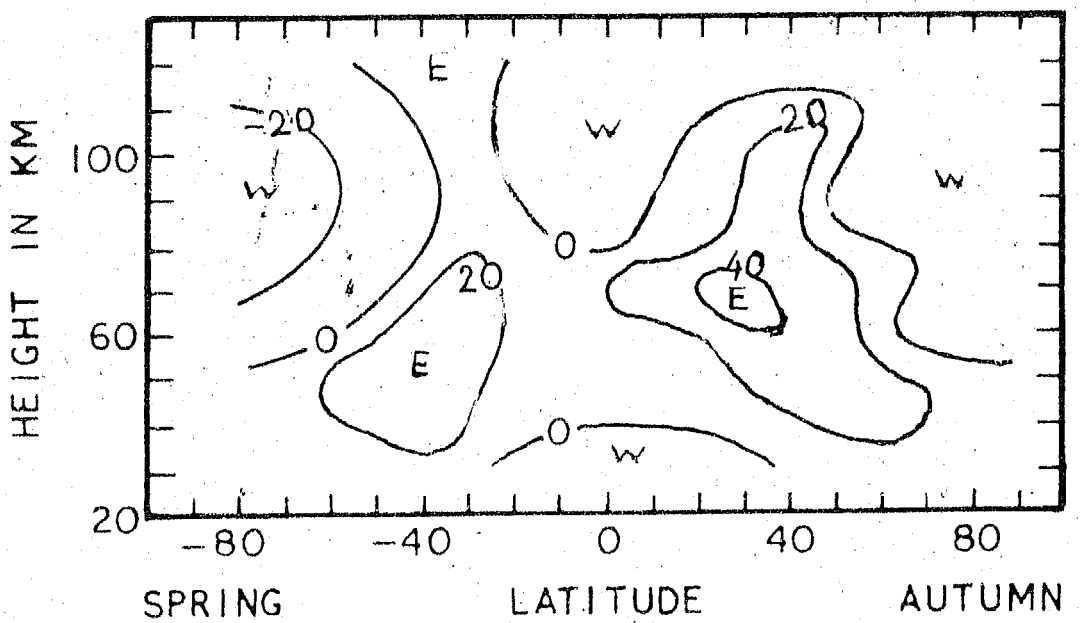

FIG. 11

MODEL OF ZONAL CIRCULATION OF THE ATMOSPHERE AT EQUINOXES. WIND SPEEDS ARE INDICATED IN M/SEC. WIND MOTION TOWARDS EAST IS TAKEN AS POSITIVE (MURGATROYD[118])

from 30 to 130 km. According to this model Fig. 10 shows the zonal winds during solstices and Fig. 11 during equinoxes. According to these figures the winds are towards east in summer above 80 km, probably changing towards west above 120 km. In winter and autumn, the winds are towards west. In spring the winds are towards east in mid-latitudes while at high and low latitudes, they are towards west.

Ragsdale and Wasko[119] attempted to give an experimental model of zonal and meridional winds from about 30 to 200 km considering the very small amount of data from vapour cloud experiments at higher altitudes and from the chaff experiments at lower altitudes. Fig. 12 gives the annual means of zonal and meridional winds at 30° to 40° latitude according to Ragsdale and Wasko. As in other models, this model also shows that up to about 80-90 km, the zonal components are towards east in winter and towards west in summer. Between 90 and 110 km range large changes in wind speed and direction with height occur, and there are also large wind shears, but the overall direction of wind is towards east in all seasons except spring. Up to 130 km the zonal component increases with height being towards west in summer and east in winter with a changeover at the equinoxes. Winds are generally strong, often exceeding 100 m/sec. From 120-140 km the wind speed, as shown, decreases with height, increasing again in 140-180 km region. The meridional winds are large compared to those at lower altitudes (less than 60 km) and higher altitudes (above 200 km).

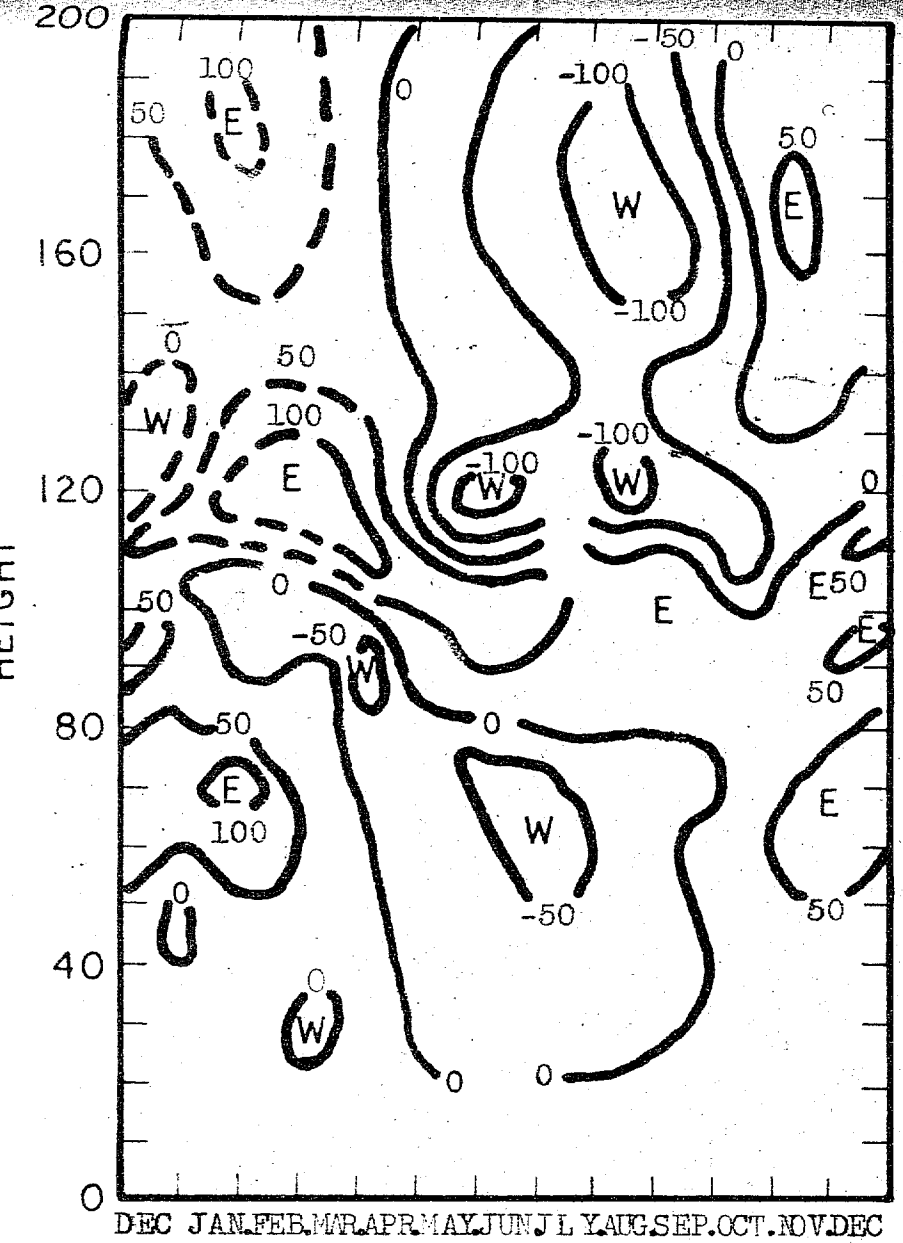

FIG 12 (A)

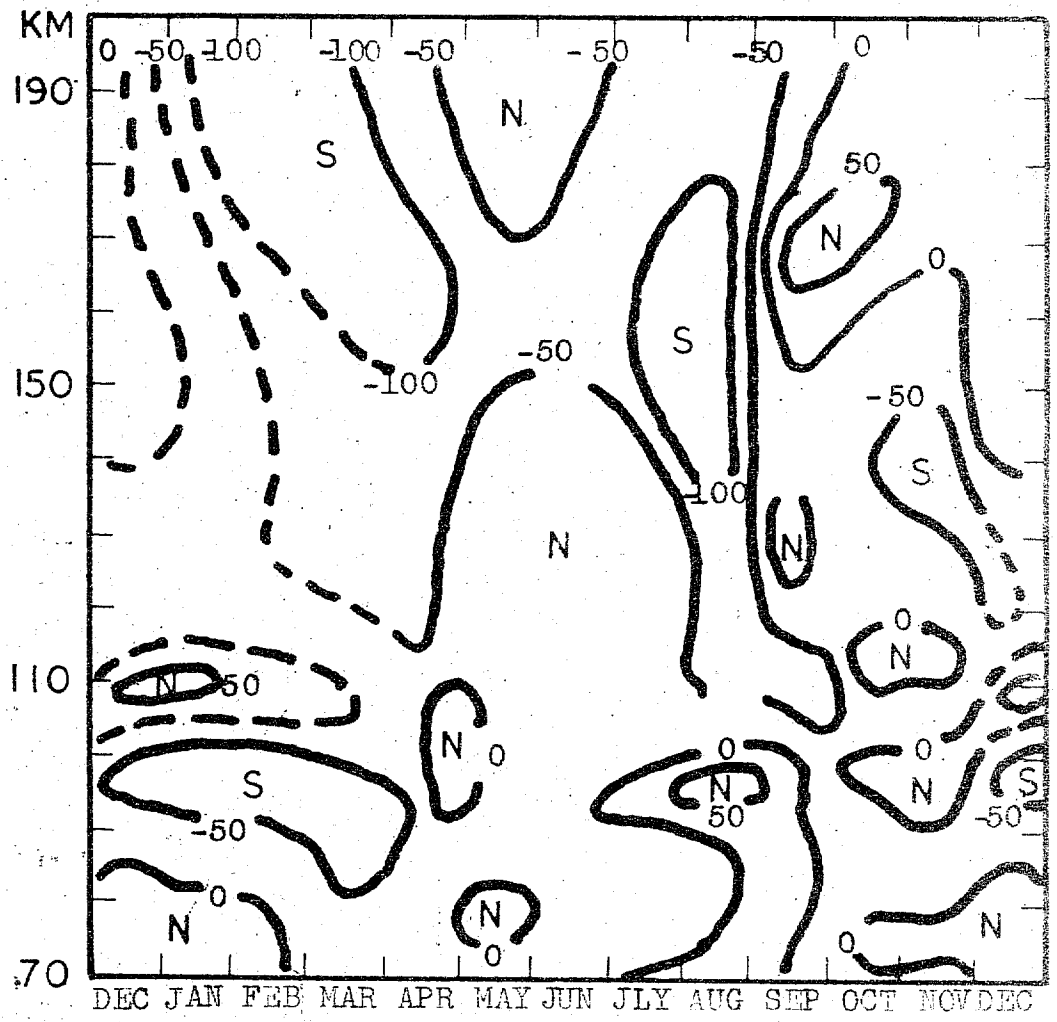

FIG. 12 (B)

FIG. 12

AVERAGE ZONAL (12A) AND MERIDIONAL (12B) UPPER ATMOSPHERIC WINDS AT 30°TO 40°N. SPEED IN M/SEC (RAGSDALE AND WASKO[119])

1.7.2. Models based on theoretical considerations.

Deb[117] theoretically calculated the wind field between 100 and 400 km from the height and latitudinal distribution of temperature. From the known temperature at 90°-80°N, 45°N and 30°N, Deb postulated three atmospheric models for 80 to 400 km altitude region. In the first model, obtained from the temperature difference at 80° N and 45°N, a south to north movement of air was predicted all the year round in this region. His derivations did not give any evidence of any seasonal change in direction. According to this model wind velocity was lower in summer than in winter, being about 25 m/sec in summer and 45 m/sec in winter. He showed that strong vertical gradient of wind velocity also developed above 100 km level. In winter, the velocity at 100 km gave a value of about 45 m/sec and at 120 km about 130 m/sec. Above this level the viscous forces reduced the gradient with height and around 260 km return currents of large velocity were established. Viscosity and Coriolis forces produced in northern hemisphere, a wind blowing towards north-east with a velocity of 20-80 m/sec around 110 km (E region).

In the second model, which depended on the temperature distribution between 90°-80° and 30°N latitudes, a feeble seasonal change was obtained in the 100-120 km region. The winds were from south to north in winter and from north to south in summer. Above 150 km the direction of wind was always from north to south. At 100 km the speed was higher in summer being 40 m/sec

compared to about 17 m/sec in winter. The vertical gradient of wind velocity was small in winter in the 100-160 km region and appreciable above. In summer, the gradient appeared to be moderate in 100-160 km region and very large above. Due to Coriolis force and viscosity, the wind was towards north-east in winter and very light, and towards south-west with a speed of more then 45 m/sec in summer.

In the third model, when the temperature distribution between 45° and 30°N was considered, the direction of wind was from north to south throughout the year with almost same velocity in both summer and winter. A very high vertical gradient of wind speed was present which gave rise to very high speeds of the order of 500 m/sec or more at about 150 km. However, the viscous forces reduced this tendency considerably. The Coriolis force and viscosity gave rise to winds towards south-west with speeds of about 90 m/sec at about 110 km (E region), and with speeds of about 110 m/sec around 180 km (F1 region). Comparing these models with the wind data available from other methods, Deb concluded that the first model gave a fairly representative picture of the atmospheric motions except that the model did not indicate any seasonal changes which were observed by other methods. The other drawback for these models is that the temperatures assumed at different latitudes were only of approximate value.

Pant[116] calculated the meridional winds above 80 km from the zonal winds observed by radio meteors[120] and ionospheric

movements, after giving full consideration to the effects of the kinematic viscosity given by Yerg[121]. His calculations showed that the meridional winds would be from the north in the region where zonal winds were from east, and from south in the region where zonal winds were from west. The meridional motions thus obtained reached their maximum, around 200 km, where the Kinematic viscosity reached its maximum. Pant's calculations also showed that the return meridional flow would take place between 200 and 300 km. Thus it is seen that above 100 km, the meridional component is as important as zonal component, as is shown by Kochanski[106] from the sodium vapour trail studied.

1.8. NECESSITY FOR THE PRESENT STUDY

From the foregoing discussions, it is seen that very little is known about the neutral atmosphere wind motions above 80 km altitude, and practically no data on neutral winds were available at these heights from the low latitudes till 1963. The ionospheric drifts have been measured near the equator and other low latitudes at some places. But the identity of these drift measurements with the motion in the neutral upper atmosphere is doubtful as the ionospheric motions are affected by the earth's magnetic field, while the neutral atmosphere motions are not directly affected. There are only indirect calculations of the neutral atmosphere wind fields at lower latitudes above 80 km as discussed in section 1.7.2.

The study of the winds in the upper atmosphere is of very great geophysical importance. The occurrence and movements of the sporadic E, which plays an important role in the ionospheric studies, are thought to be connected with the neutral atmosphere turbulence, winds and the wind shears present at these heights. The coupling between the neutral and the ionised components of the atmosphere through the collisions of the neutral and ionised air molecules and atoms, and hence, the transfer of effect of the earth's magnetic field on the movements of the ionised components to the movements of the neutral components, and such other phenomena, are all unknown factors which could be studied by knowing neutral atmosphere wind field.

The winds in this altitude region are studied, in the middle and high latitudes, by release of chemicals from rockets. The location on the earth of these places from where such experiments are conducted are given in Table No. 4 on page 53. These experiments coupled with other experiments such as electron probes and the magnetometers help in understanding the interaction of neutral wind with ionised particles.

While these experiments greatly enhance our knowledge of the upper atmospheric motion pertaining to the neutral components, they are confined to the temperate and high latitudes only. To understand the world wide general circulation of the neutral upper atmosphere, and also flow of air between two hemispheres, observations at lower latitudes and at the equator

are absolutely necessary. The lack of any observations of upper atmosphere winds in the tropics and near the equator, where the geostrophic wind equation does not hold good, had been a great set back even in developing the theoretical work in this regard.

As has been discussed earlier, the upper atmosphere winds may have pronounced effects on geomagnetic phenomena. Near the geomagnetic equator, where intense electric current, called the equatorial electrojet, flows in a narrow band extending to a few degrees on either side of the equator, in the E layer around 110 km, the observation of winds may lead to very interesting results. The occurrence of sporadic E, as explained by Whitehead, may be proved in temperate latitudes. But near the geomagnetic equator the occurrence of sporadic E cannot be explained by his theory, as the magnetic dip angle here is zero. Only the simultaneous experimental observations of the distribution of electron densities and the wind shears at the geomagnetic equator will throw some light on this phenomenon.

With above mentioned objectives in view, the Indian National Committee for Space Research (INCOSPAR) established a rocket launching station at Thumba in 1963, which is almost on the geomagnetic equator, being only 30 km south of it. Its geographic latitude is only 8.6°N. Thus from this station the effects of both geomagnetic and geographic equators on the wind field in the upper atmosphere can be studied.

1.9. STATEMENT OF THE PROBLEM.

In collaboration with the National Aeronautics and Space Administration (NASA) of the United States of America and Center Nationale D'Etude Spatiales (CNES) of France, Physical Research Laboratory at Ahmedabad, India, has started a programme, sponsored by the Indian National Committee for Space Research (INCOSPAR) to study the upper atmosphere neutral winds near the geomagnetic equator. The major objectives of this programme are as follows:

(i) To determine winds in the 80 to 200 km height region of the neutral upper atmosphere at the magnetic equator and near the geographic equator.

(ii) To study the diurnal, semi-diurnal and other periodic changes in these wind motions.

(iii) To participate in the global, zonal and regional synoptic studies of the upper atmosphere, to get insight of the general circulation at these heights.

(iv) To study the relation between the neutral gas wind and the ionospheric drift measurements.

(v) To study the correlation between wind shears, sporadic E and equatorial electrojet currents.

(vi) To study turbulence and diffusion in the upper atmosphere.

(vii) To measure the atmospheric temperature by the study of the sodium resonance emission line widths.

The present study has been taken up as a first step in fulfilling the above mentioned objectives. Neutral winds above 100 km, have been measured during morning and evening twilight in November 1963, January 1964 and November 1964. The dates and times are given below.

1.	21	November	1963	Evening twilight
2.	8	January	1964	Evening twilight
3.	12	January	1964	Morning twilight
4.	6	November	1964	Morning twilight
5.	9	November	1964	Evening twilight
6.	10	November	1964	Morning twilight

The November 1964 experiments formed part of the global synoptic wind measurements.

An ionospheric drift recorder has been established at Thumba by the Ionospheric Group of the Physical Research Laboratory, in prior to study the relation between the neutral gas wind and the ionospheric drift measurements.

CHAPTER - II

EXPERIMENTAL TECHNIQUE

In the morning before sunrise or in the evening after sunset, when the sun is 6^{0} or more below the horizon, the sky background light is negligible, because the major portion of the atmosphere is under the earth's shadow. At this time, if a cloud is generated by the release of sodium vapour above 80 km in the atmosphere, the region which is still sunlit, the cloud appears as a bright object due to the resonance scattering of the sunlight and could be used as an excellent marker for the study of atmospheric motions above these heights.

The present chapter deals with the technique of the release of sodium vapour, data acquisition by photography from two or more camera stations, of the vapour trail thus generated, and the determination of the atmospheric motions by triangulation technique from the photographic data. Sections 2.1 and 2.2 deal with the rockets and payloads used, and section 2.3 deals with the photography of the vapour trail. In section 2.4 selection of the camera sites, from where the trail is photographed, is discussed and the location of the camera sites used in the present experiment are given. Section 2.5 gives a method of data analysis developed by the author. This method is based on the earlier methods of Broglio[122] and Smith[123]. IBM 1620 electronic computer was used for the computations. Section 2.6 deals with the errors involved in the method and the estimation of these errors in determining the height and the wind velocity.

2.1. ROCKETS

American made Nike-Apache rockets were used for these experiments which were supplied by the National Aeronautics and Space Administration (NASA), United States of America, under a collaboration agreement with the Indian National Committee for Space Research (INCOSPAR). Nike Apache is a two stage rocket. The booster burns out at an altitude of about 1.6 km when the rocket attains a velocity of about 975 m/sec. The Apache second stage ignites at an altitude of about 12.2 km when the rocket is coasting at a speed of about 550 m/sec and burns out at an altitude of 19.2 km when the rocket attains a velocity of about 1950 m/sec. The maximum acceleration attained is about 37 G. At 100 km altitude, when the sodium vapour is released, the rocket would be coasting at a speed of about 1.6 km/sec. The maximum altitude attainable is about 200 km. Above data are calculated for a 60 lb payload and 60° launch angle. If the payload weight or launch angle is changed, the performance of the rocket also changes. Fig 13 gives some performance curves for the Nike Apache rockets for 60° launch angle and three different payload weights. In Fig. 14 a rocket on the launch pad is shown.

2.2. ROCKET PAYLOAD FOR THE RELEASE OF SODIUM VAPOUR TRAIL

The payloads used for the present experiments were supplied by the Centre National d' Etudes Spatiales (CNES) of France, under a collaboration agreement with the INCOSPAR. A typical sodium vapour rocket payload consists of two parts;

Fig. 13

Performance curves for Nike Apache type rockets for three different payload weights

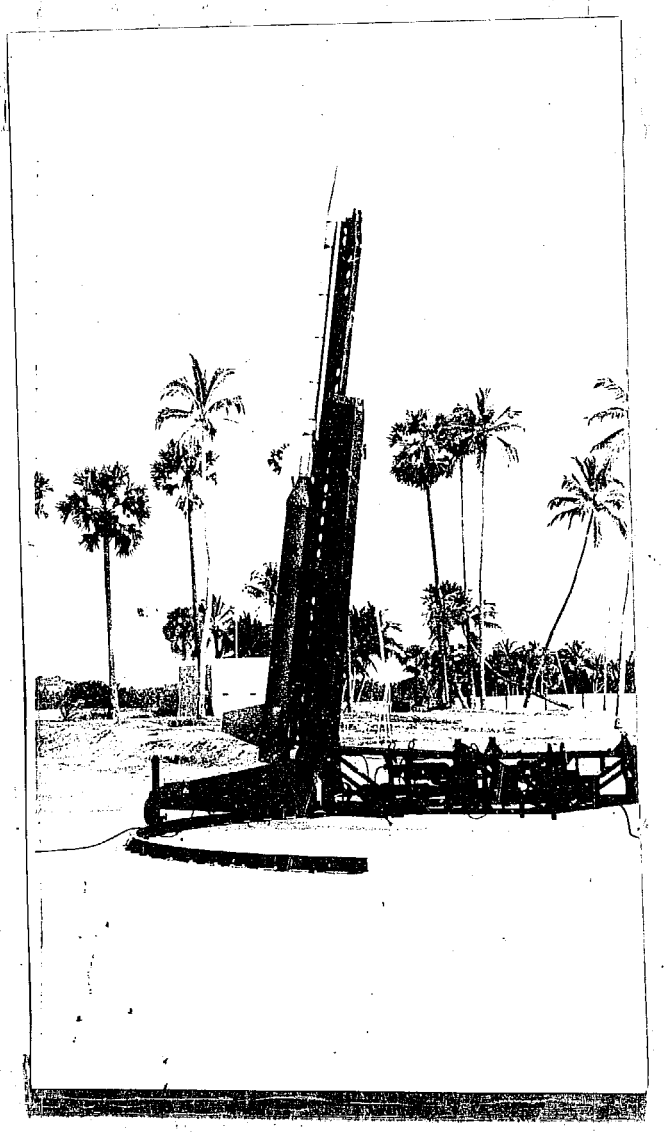

Fig. 14

Nike Apache rocket on the launch pad at TERLS

a vaporiser and a timer to ignite the vaporiser at a pre-determined time. The vaporiser is described in section 2.2.1. Electronic timers were used for the present experiments and the timer used is described in section 2.2.2.

2.2.1. Sodium vaporiser.

The sodium vaporiser is a pyrotechnic device. Its function is to eject a constant stream of sodium vapour from the rocket in the desired altitude range. The heat from burning iron-oxide-aluminium thermite is used to vaporise metallic sodium. The exothermic thermite reaction is

$$Fe_2O_3 + 2\,Al \longrightarrow Al_2O_3 + 2\,Fe \qquad (1)$$

Following method of preparing the sodium vaporiser is given by Geophysics Corporation of America in its Technical Report[134].

To prepare satisfactory thermite, the commercial iron oxide, Fe_2O_3, is dried in shallow pans in a drying oven, keeping the temperature of the oven below 100°C. A higher temperature is not desirable for drying, as it decomposes the oxide and reduces its efficiency in the thermite. A 100 mesh Aluminium powder is mixed with iron oxide. The thermite reaction (1) requires a mixture of 76% Fe_2O_3 and 24% Al by weight. Much care is required during preparation and loading of the vaporiser as it is a pyrotechnic device. Also care is to be taken to ensure predictable and reproducible results.

The sodium is extruded into small pellets and mixed with the thermite. Sodium pellets of about 1/8" to 1/4" in diameter and about 1/4" long are found quite satisfactory for the vaporiser preparation. The mixture is tightly packed into a cylindrical stainless steel container which is sealed except for vent holes through which the sodium vapour escapes.

When sodium is added to the mixture, Al_2O_3 is still the most stable oxide that is formed; however, it is seen that Na_2O is also produced, the overall reaction being

$$Fe_2O_3 + 2Al \longrightarrow Al_2O_3 + 2Fe$$

$$Fe_2O_3 + 6Na \longrightarrow 3Na_2O + 2Fe$$

$$3Na_2O + 2Al \longrightarrow Al_2O_3 + 6Na$$

The thermite reaction goes well when sufficient energy is available for the sodium to attain about 1000°C which is about 38 K cal/mole of sodium vapour. This means approximately 3.2 g of thermite is required to vaporise one gram of sodium at 1000°C. If sufficient aluminium is present, the formation of sodium oxide can be minimised. To attain this, 73% Fe_2O_3 is mixed with 27% Al by weight. Thus the requirements for vaporising one kilogram of sodium are

Sodium pellets	1.0 kg
Red Oxide, Fe_2O_3	2.19 kg
Aluminium granules	0.81 kg
Total weight	4.00 kg

The final thermite-sodium mixture for filling the payload is prepared as follows:

The iron oxide and aluminium are first mixed thoroughly to a homogeneous mixture in a bucket. The dry sodium pellets are then added to the mixture and mixed thoroughly. This mixture is loaded in the canister, in small quantities, and each quantity thus added is pressed to the desired compactness. The sodium and thermite are packed in canisters at a pressure of 1000 p.s.i. Approximately 0.5 kg of thermite, containing no sodium, is lightly packed on the top of the main charge to aid ignition.

The rate of burning of a vaporiser may be varied by varying thermite to sodium ratio in the mixture. The burning rate is also dependent on the granular size of the aluminium powder, the packing pressure and the vaporiser configuration. In the present experiment 6 kg of thermite and 2 kg of sodium were used to prepare the vaporiser. A typical vaporiser is shown in Fig.15.

2.2.2. Electronic timer.

The circuit diagram of the electronic timers used for the present experiments is given in Fig.16. The power to the circuit is supplied by an 18 V nickle-cadmium battery. An electric pulse is supplied to the gate of the silicon controlled rectifier CR_1 (2N 1596) when the inertia switch becomes

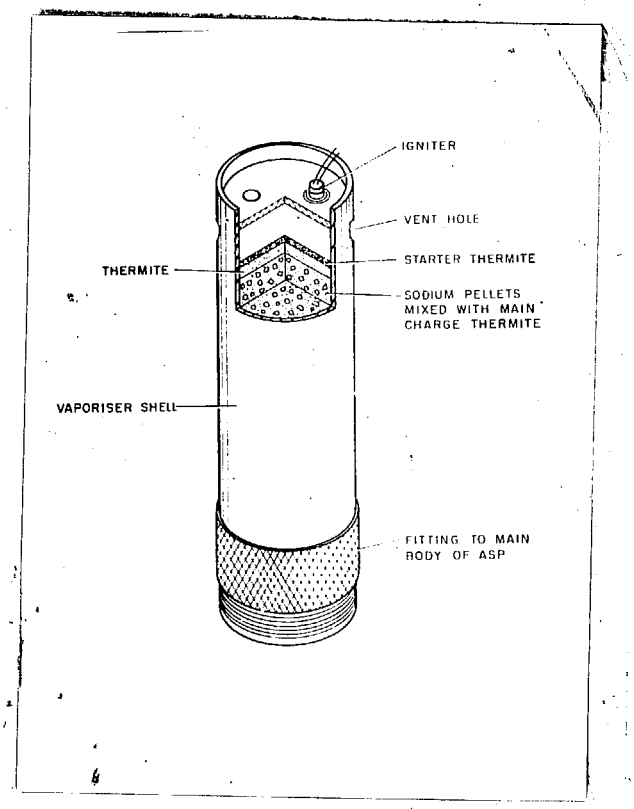

Fig. 15

A typical sodium vaporiser

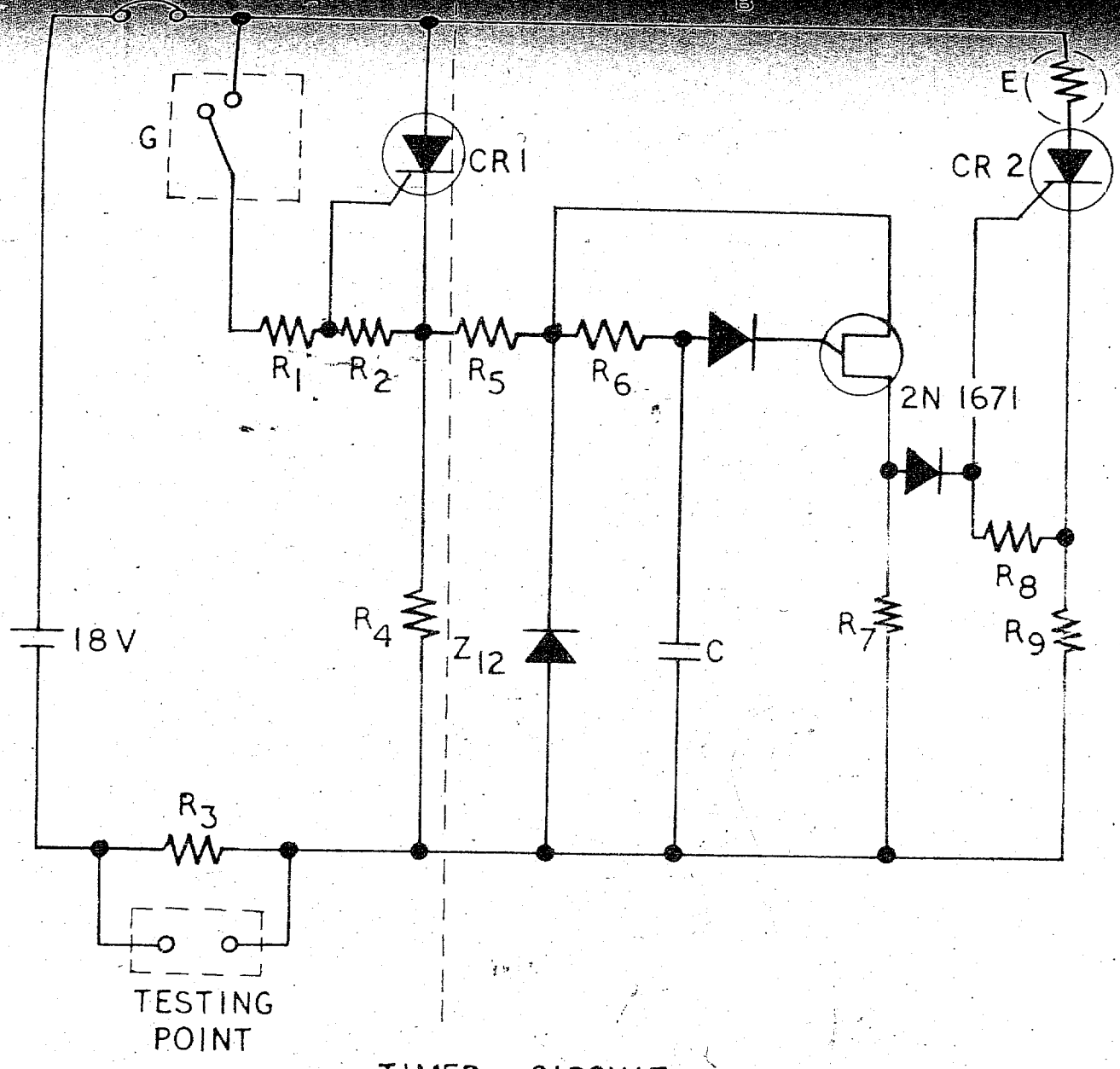

TIMER CIRCUIT

FIG. 16

CIRCUIT DIAGRAM FOR AN ELECTRONIC TIMER

momentarily on due to the acceleration at the time of rocket take-off. This makes CR_1 conducting and a constant voltage across the zener diode Z_{12} is developed. The RC time circuit which is charged at this constant voltage consists of a precision resistance R_8 and condenser C. This RC circuit ensures the required time for the build up of the required voltage at the unijunction transistor 2N 1671. This serves as a potential divider and when fired gives about 6V to the gate of the second silicon controlled rectifier, CR_2(2N 1596), in whose anode circuit the igniter squib is kept. When CR_2 conducts, it initiates the squib which starts the burning of the thermite in the vaporiser. The resistance R_9 is adjusted so as to get the required current of about 300 mA to fire the squib E which has a resistance of about 2 ohms.

For the sake of redundency, two such timer circuits were used with each vaporiser, each timer controlling a separate squib. The two independent timer circuits are triggered simultaneously by an inertia switch when the rocket is fired. The two circuits are coupled by a resistance, so that, if any one controlled rectifier is not functioning satisfactorily, the current from this circuit passes to the second circuit through this resistance. To ensure that the batteries are fully charged and the circuit receives proper voltage, the nickle-cadmium battery is charged on the day of rocket launch.

Following precautionary measures are taken to ensure

that the squibs are not fired accidentally while the rocket is on the launch pad. The squibs are short circuited and the power is connected only one hour before the launch time. About half an hour before the launch time, when the nose cone is fitted to the rocket, this short circuit is removed. From this time onwards, only inertia switch keeps the circuit open. At the time of take-off of the rocket the inertia relay is closed and the timer circuit starts functioning, which fires the squib E at the preset time accomplished by the RC circuit.

The electronic component and the batteries are mounted on a rigid circular plate which is mounted, in turn, on an adapter ring forming the connection with the sodium canister.

The timers in the present series of experiments were set for 60 seconds. This ensured the release of vapour at an altitude of about 100 km in the form of a trail.

2.3. PHOTOGRAPHY OF THE VAPOUR TRAILS

To get good pictures of the vapour trail, suitable for triangulation, the important factors to be considered are the time of the experiment, the selection of proper cameras, the film and filter to be used and the processing of the film. These factors are discussed here briefly.

2.3.1. The time of experiment.

As mentioned earlier in the introduction to this chapter, the sodium vapour cloud experiment is carried out either during

dusk or dawn. The time of the rocket launch is selected such that during major portion of the observation time, the atmosphere below the vapour trail is in the earth's shadow so that the sky background is very little. In Fig.17, let A be the projection of the starting point of the trail on the ground and let the sun's rays BC graze the surface of the earth at C. Let the solar depression angle at this time be δ. Then the earth's shadow at A is given by AB equal to X. If the radius of the earth is denoted by R, the relation between the height of the earth's shadow and the solar depression angle is given by

$$\cos \delta = \frac{R}{R+X}$$

or $$X = R (\sec \delta - 1)$$

Measurements on the sky background during twilight periods have shown that the major portion of the atmosphere responsible for background, because of the scattering of light, is below 35 km altitude. Therefore, if the earth's shadow is to be 35 km, the solar depression angle comes to about 6°.

The curve in Fig.18 gives the relation between the solar depression angle and the height of the earth's shadow. If the sodium vapour is ejected from the rocket at the height of 80 km during evening twilight, the trail can be observed till the earth's shadow reaches this height. This will happen when the solar depression angle is 9° (from Fig.18). Thus during the time the solar depression angle changes from 6° to 9°, the trail can be observed at a height of 80 km. At the

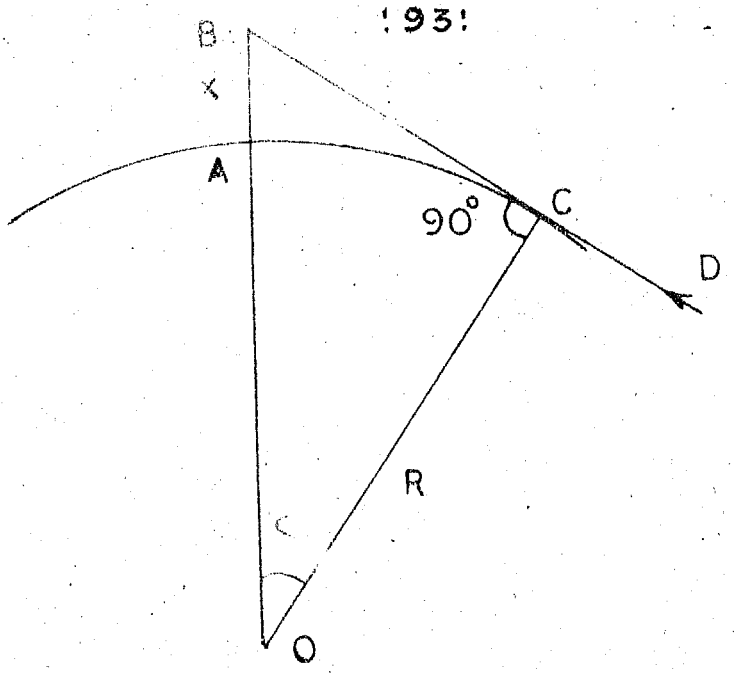
B
X
A
90°
C
D
R
O

FIG. 17

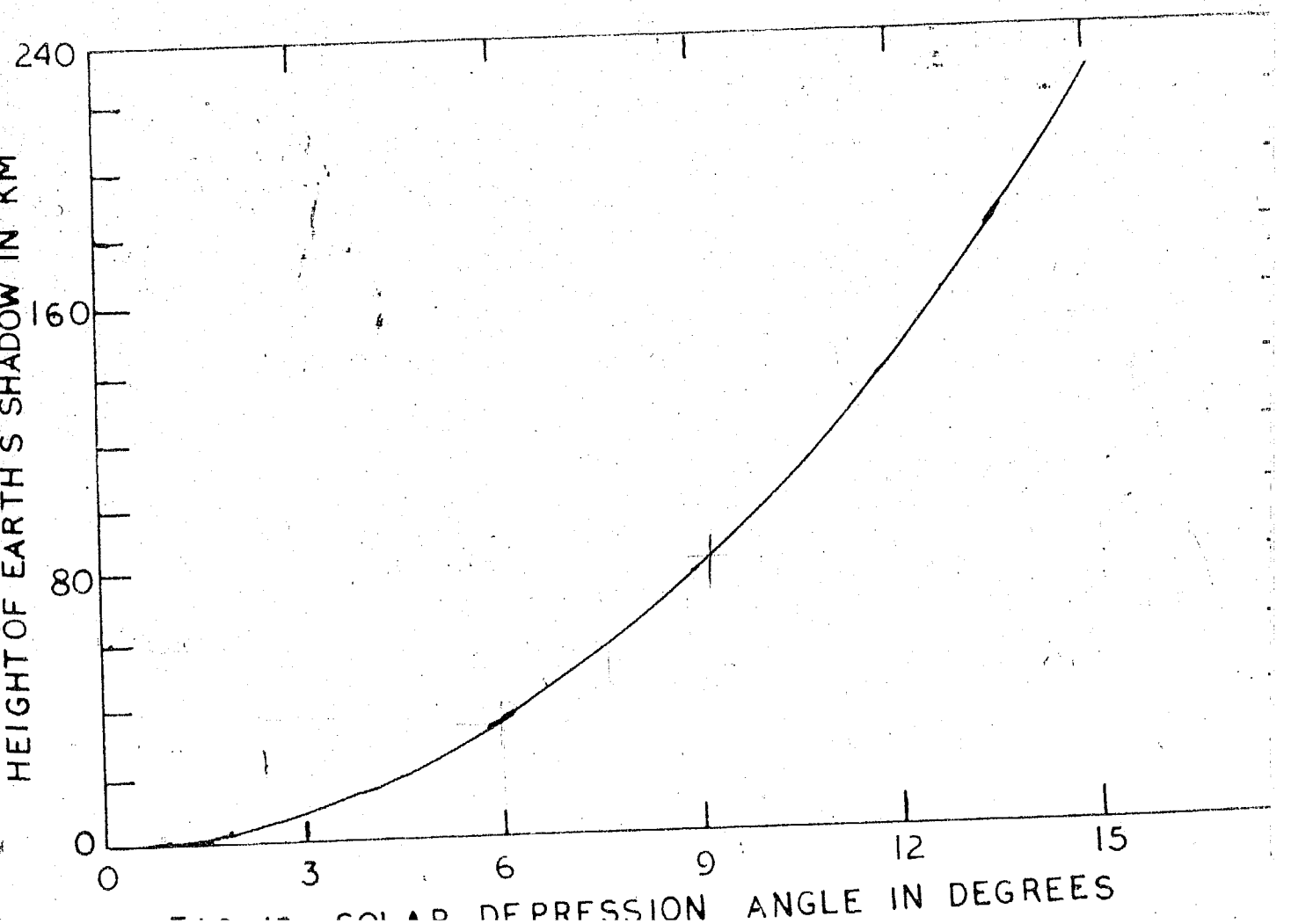
240
160
80
0
HEIGHT OF EARTH'S SHADOW IN KM
0
3
6
9
12
15
SOLAR DEPRESSION ANGLE IN DEGREES

latitude of Thumba this time is about 12 minutes. If the vapour is ejected at 100 km, we can observe it for 15 minutes if the launching of the rocket takes place at 6° solar depression angle. In the case of morning twilight the rocket is launched when the solar depression angle is 10° when the earth's shadow is up to a height of 100 km.

In the Nautical Almanac, the times of sunset and sunrise along with the end and beginning of the astronomical twilight period, when the solar depression angle is 18°, are given at an interval of 4 days and at an interval of 10° latitude. By the method of interpolation, the time of sunset and the end of astronomical twilight period or the time of sunrise and the beginning of astronomical twilight period are obtained for the latitude concerned for each day of the launch period. By another curve of interpolation, the time when the solar depression angle is 6° in the evening and 10° in the morning is obtained for these days.

It is also to be noted that all the days of the month are not suitable for this type of experiment. Particularly when there is lot of haze, the moon light contributes largely to the sky background and the experiment is not possible in the presence of the moon. For a single experiment of this type, any morning twilight after the new moon day or an evening twilight before the new moon day, is suitable. If, however, the experiment is to be carried out at successive twilight

periods to compare the atmospheric motions, three days centred around new moon day are best suited. On the new moon day the experiment can be satisfactorily performed either during morning or evening twilight.

Another factor which decides the period of experiment is the weather. For this experiment the sky should be clear of clouds at the camera sites from where the photographs are taken. Thus, the rainy season, when the sky is invariably cloudy, is most unsuitable for this experiment.

2.3.2. Camera for the photography of vapour trails.

Selection of an appropriate camera for the vapour trail photography is very important. While selecting the camera one has to keep in mind the following points:

(a) It should be possible to operate the camera by remote control switch so that the camera is not disturbed from its position while taking the picture.

(b) The camera should be able to take many pictures in sequence at the desired time intervals.

(c) The camera should be able to get clear, distinct photographs of the sodium vapour trail for sky background conditions of twilight. For this purpose the camera should have the arrangement for changing either the aperture or the time of exposure.

(d) The camera should use a fast lens with large field of view. This will enable the camera to get good pictures of even a faint vapour cloud and increase the accuracy of data reduction.

(e) The camera should be rugged, reliable, portable, and easy to install. This will ensure the easy handling of the camera.

The Kodak K-24 aerial reconnaissance camera satisfies many of the above requirements. This camera has been used by many workers at other places for this experiment. Eight K-24 cameras have been supplied by NASA to INCOSPAR under a collaboration agreement for the vapour trail experiments. These cameras were used for the present experiments. The K-24 camera takes a maximum of 110 pictures on a film roll 5½" x 66'. The format of the pictures is 5" x 5". The camera is operated by a built-in motor which runs on 24V direct current.

The exposures can be taken and the film wound by a single electric switch connected to the camera by a long chord so that the operation does not disturb the camera orientation. The camera can be used for making instant exposures at varying shutter speeds or making time exposures of required time. The shutter used is of focal plane type. Three easily changeable curtains with three different openings, giving exposures of 1/300, 1/450 and 1/150 seconds and one

night curtain with full aperture opening for time exposures, are provided with the camera. For the present work where the exposure timings were always more than one second, only the night curtain was used. The camera has a 7 inch focal length, f/2.5 Aero Ector lens which gives a $40^{\circ} \times 40^{\circ}$ field of view which is sufficient to photograph large luminous clouds without complicated tracking or directing equipment. As the camera requires 24V, 15 amp while winding the film, heavy duty car batteries are used for supplying the power.

On the glass plate which keeps the film in position, fiducial marks are made which are illuminated by a small fiducial lamp run by 1.5V batteries. These marks are necessary as reference points while the coordinate measurements are made on the film. In order to operate this lamp at the same time when the film is exposed, an electronic circuit utilising one shot multivibrator, was used. This made the fiducial lamp on for the required duration during each exposure. The electronic circuit used is given in Fig.19. Fig.20 shows a typical vapour trail photograph taken by this camera. The four cross marks are the fiducial markings.

The camera is fixed on a sturdy stand. This consists of a wooden tripod stand about 4 feet high, on top of which is fixed a base plate divided into 360°. Over this rotates another plate fixed to a U-shape frame made of aluminium casting. This has a protractor reading on a side

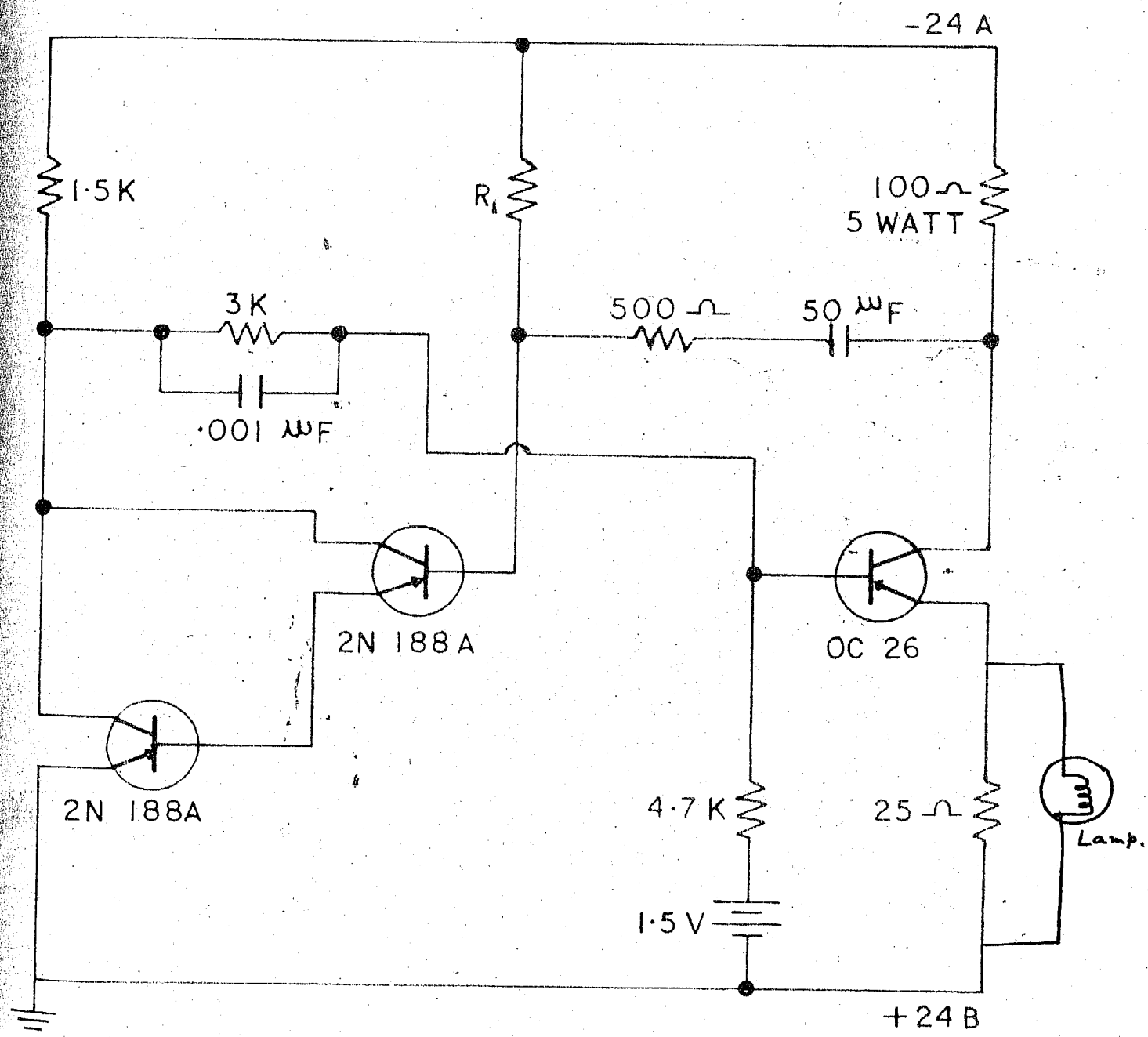

FIG. 19

CIRCUIT USED FOR OPERATING FIDUCIAL LAMP

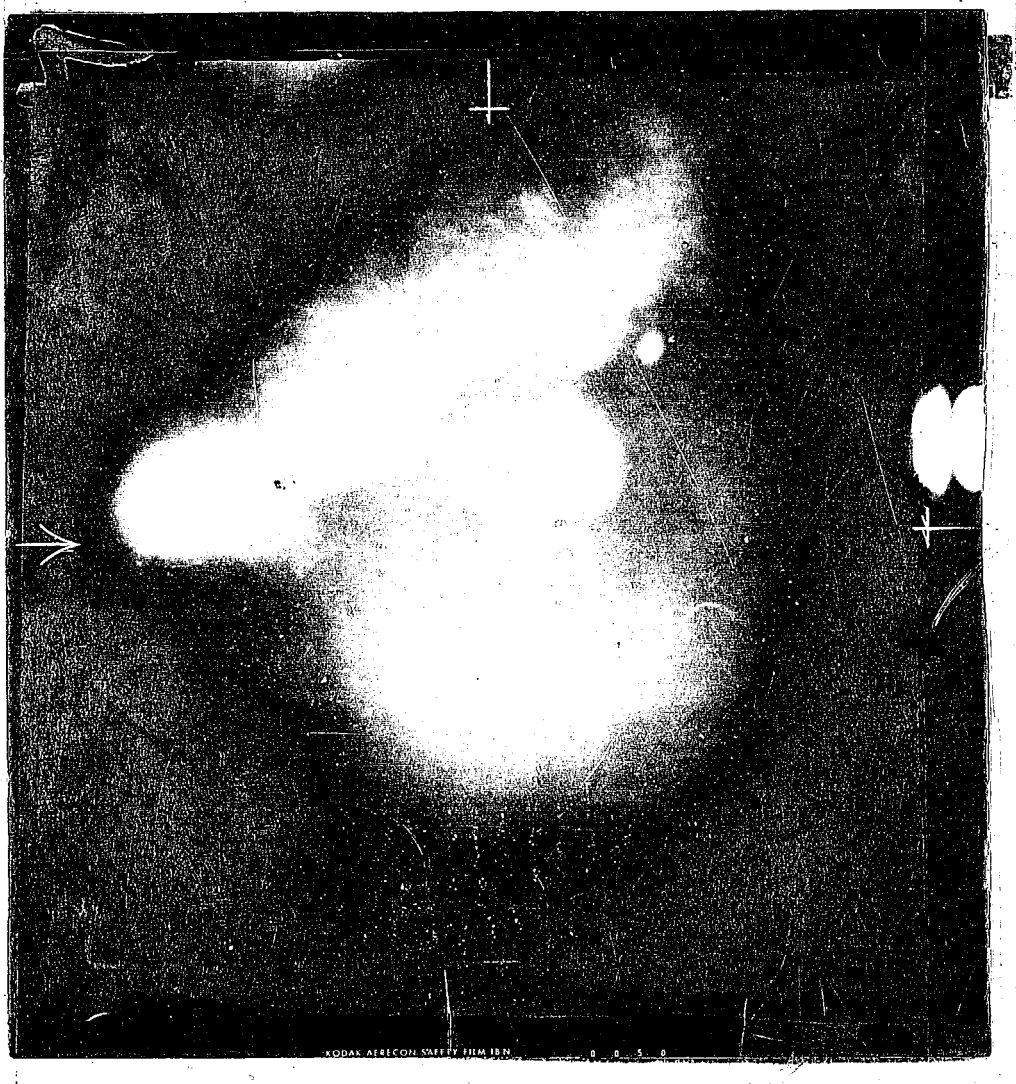

Fig. 20

Photograph of a sodium vapour cloud taken by a K-24 Camera

from 0 to 90°. An index attached to a ring moves on it. The camera is fixed in the ring which can be rotated from 0 to 90° in elevation. The position of the camera is fixed at the desired elevation and azimuth angles using two handles. A view finder, attached to the ring, which can be aligned to get the same field of view as obtained on the film, enables to keep a track of the trail while it is photographed. A schematic diagram of the camera stand is shown in Fig. 21.

2.3.3. Selection of films and filter for the sodium vapour trail photography.

A sodium vapour cloud, due to about 100 gms of sodium released by rocket at 80 km altitude at twilight period, emits about 4 x 10^{24} photons/sec due to resonance scattering of sunlight[80]. Its astronomical magnitude is -9. In comparison to this, venus at her most brilliant is -4.3 and full moon is -12.6. The intensity of vapour trail diminishes rapidly. Cooper[125] observed that the intensity of sodium line in a vapour cloud diminishes by about 3 orders in 10 minutes. To photograph a vapour cloud of such a changing intensity, proper film and exposure times must be selected.

For good contrast and optimum photographic registration of the cloud profile, a film which possesses the required contrast, sufficient sensitivity at the desired wavelength and insensitivity to longer wavelengths of the sky background is necessary. Filters are used to increase the contrast

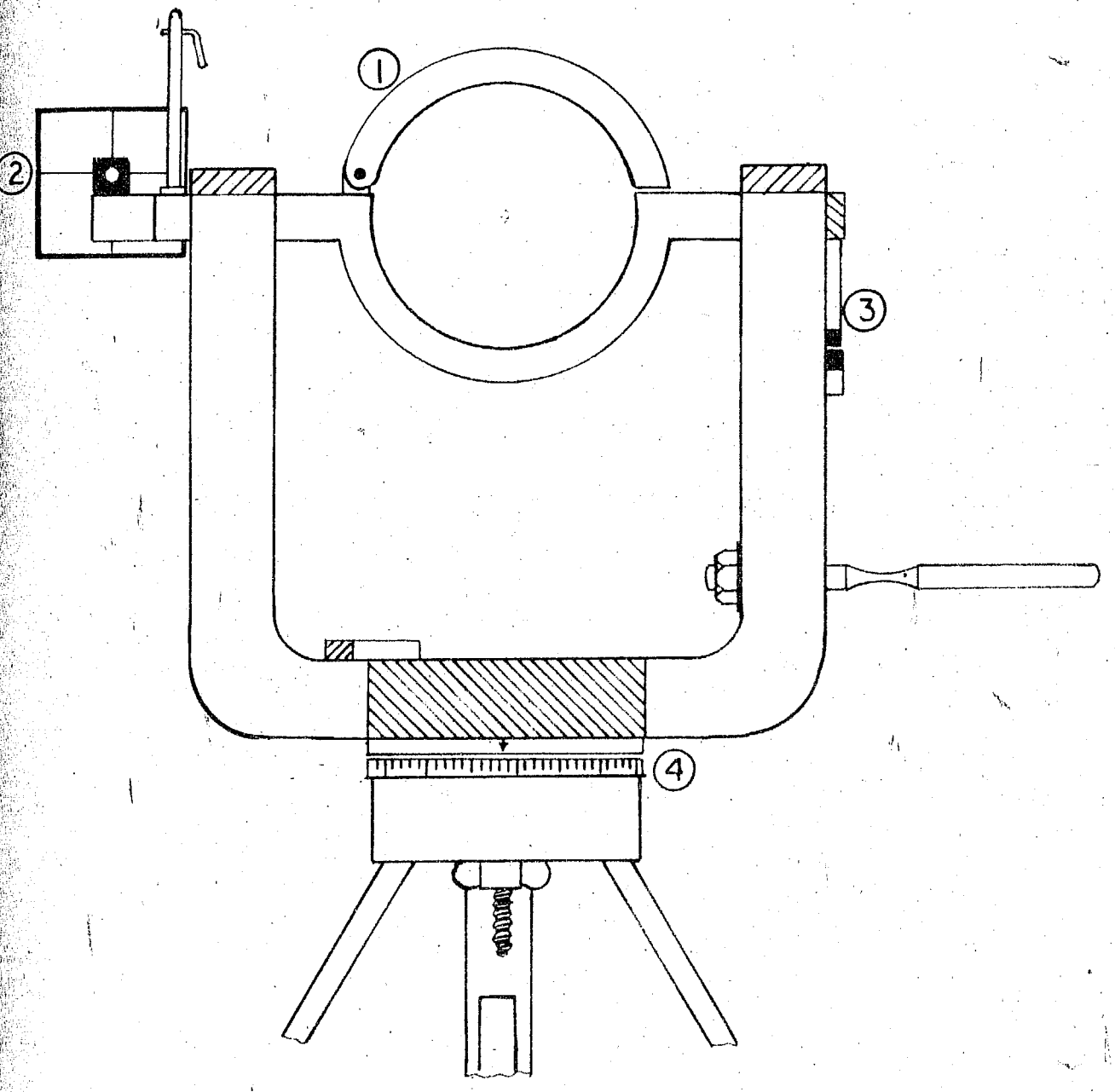

FIG. 21

1 CAMERA RING

2 VIEW FINDER

3 PROTRACTOR

4 BASE PLATE

A SCHEMATIC DIAGRAM OF THE CAMERA

between the vapour cloud and sky background. Filters are chosen which cut off the sky background to the short wavelength side of the desired resonance emission of the cloud.

The physicists at the Geophysical Corporation of America, after the study of various film-filter combinations, have recommended Kodak Panchromatic film with Wratten series 23A filter for photographing the sodium vapour cloud[126]. Panchromatic materials are sensitive to all visible colours including red. Tri-X panchromatic film was chosen for the present study. Tri-X films have thin, strongly hardened emulsion which provides high image sharpness and makes it suitable for high temperature rapid processing. The colour sensitivity curve for Tri-X emulsion is given in Fig.22. The Wratten series 23A filter which is light red in colour absorbs ultraviolet, violet, blue and green rays. Its dominant wavelength is 6055 Å and it transmits 69.6% of 5900 Å wavelength. The absorption curve for Wratten series 23A filter is given in Fig.23. The colour sensitivity of the combination of Panchromatic film with Wratten series 23A filter is given in Fig.24 which shows the spectral region of the sodium cloud, that is, 5890 - 5896 Å, is well within this range.

In order to provide a margin of safety against under-exposure and also to register even faint details of the cloud, the exposure is to be adjusted on the straight

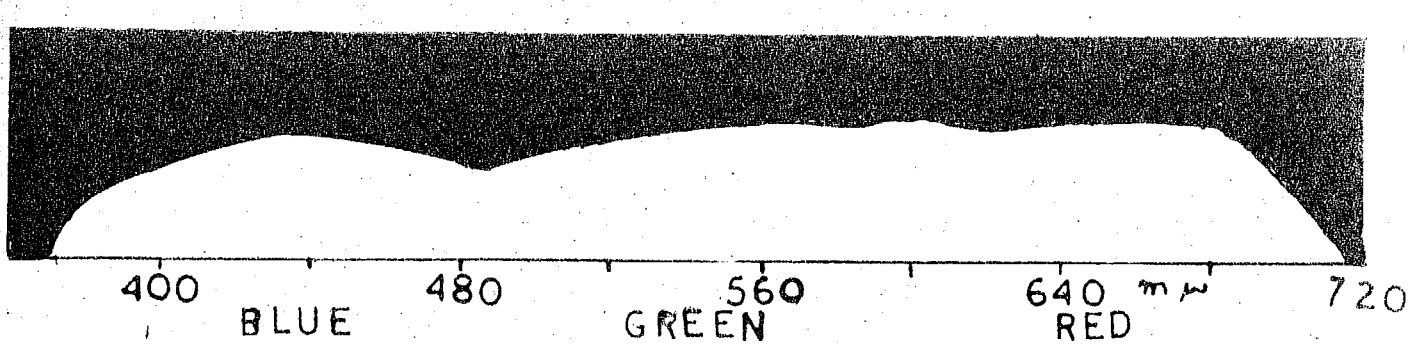

FIG. 22 SENSITOMETRIC DATA FOR TRI-X

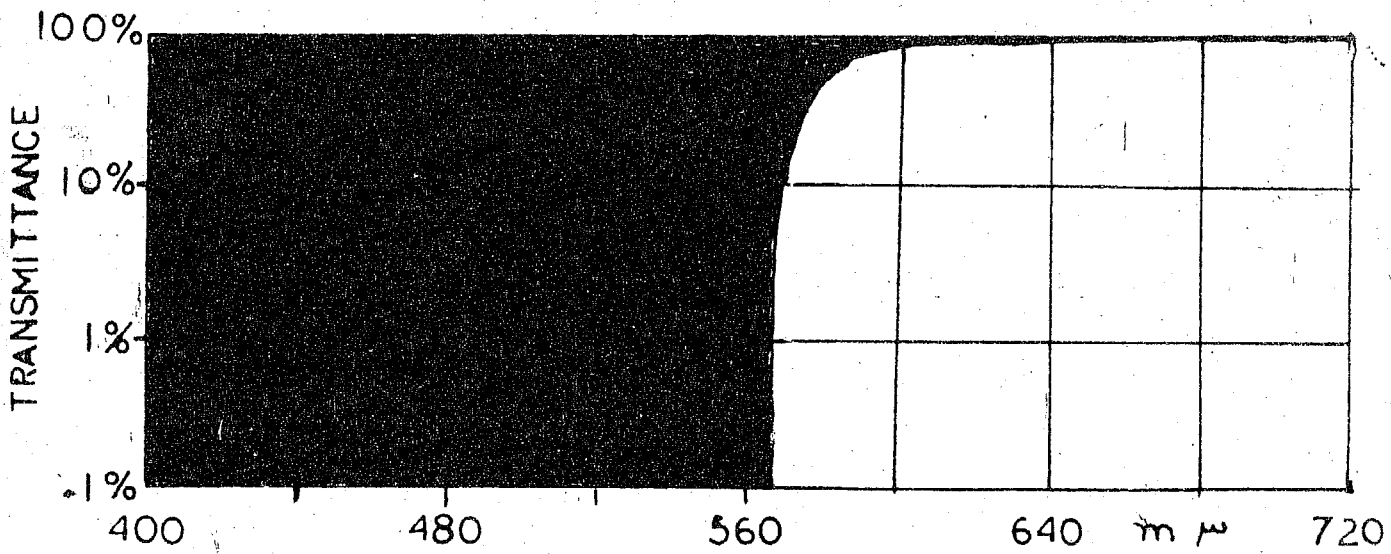

FIG. 23. TRANSMITTANCE DATA FOR THE FILTER
(WRATTEN 23 A)

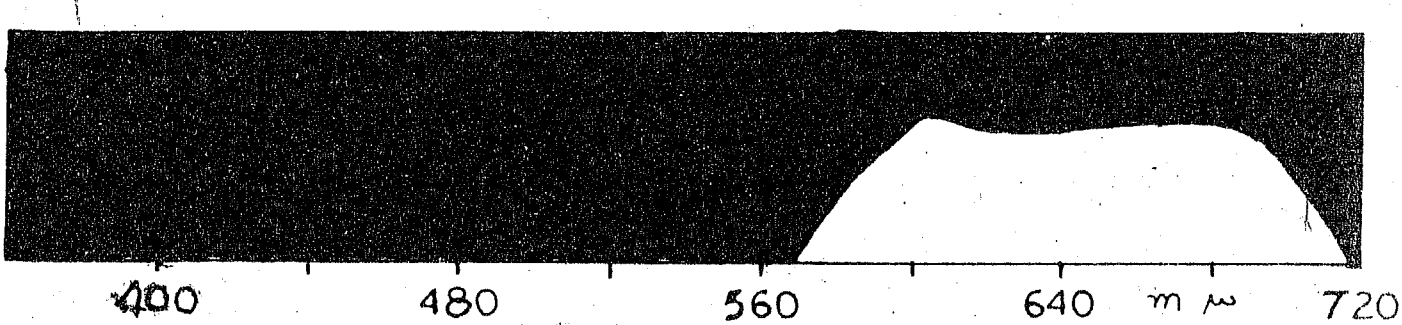

FIG. 24. SENSITOMETRIC DATA FOR FILM AND FILTER COMBINATION

portion of the film characteristic curve. This ensures the sky background level at photographic density 0.2 to 0.4 above chemical fog[126] . The chemical fogging can be kept low by preserving the unused film at low temperature before they are used for photographic purposes. After exposure the films are to be processed as early as possible. Otherwise there may occur a gain in speed for low densities at a rate roughly proportional to the logarithm of the storage time after exposure.

The developer recommended by Kodak for Tri-X Panchromatic film is D-19. This was used for processing the pictures obtained in the first launching. This developer gives high contrast, but will not give high effective film speed. So, for later launchings the developer D-163 was used.

The developing was carried out in a specially made developing tank which enabled continuous agitation of the film and ensured uniform development of the film.

2.3.4 Camera adjustments and preparations for the vapour trail photography at twilight.

To take the photographs of the sodium vapour cloud during the twilight period, each camera was adjusted in the following way. The tripod stand (Fig 21) was adjusted so that there was no obstacle in the line of sight towards the expected zone of interest. The zone of interest was decided

from the knowledge of the rocket trajectory and the expected height range of the vapour trail. The zero mark on the camera stand was pointed towards north and the tripod stand levelled properly using a spirit level. After the U-stand was adjusted on the tripod stand, the camera was fixed on it in the ring provided for it. The camera was adjusted to be horizontal when the protractor reading on the U-Stand showed zero. Removing the magazine of the camera, the view finder on the camera stand was adjusted so that the same field of view was obtained through the view finder as obtained on the glass plate of the camera. The camera was loaded with a full length of the roll film in perfect darkness and the magazine fitted to the camera about half an hour before the time of rocket launch. The freshly charged battery was connected to the camera motor through a junction box. This junction box enabled the use of the same battery to operate two cameras. The aperture of lens was opened fully giving f/2.5 and the Wratten series 23A filter was fitted in its proper place. Two fresh 1.5V cells were adjusted in the cell box provided for them. These cells lighted a lamp, which put the fiducial marks on each picture frame. Five minutes before the launch time the camera was oriented towards the predetermined zone and the elevation and the azimuth noted down. When the cloud was released about one minute after the rocket launch, minor adjustments of the camera for elevation and azimuth were made looking through

the view finder, so that the entire vapour cloud was acquired in the centre of the field of view. An experienced camera operator can adjust the camera direction in such a way that it has not to be changed often or too much during the observation time. The camera operation was started 3 minutes after the launch and the pictures were taken according to the predetermined exposure sequence.

To know the exact direction in which the camera is oriented, the star pictures, obtained during the photography, of the trail were used. In addition to this, for getting the same information about the direction of pointing of the camera, from the readings on the zenith and azimuth angle protractors on the camera stand, following procedure was used. The camera was oriented to a known configuration of stars before the launch in the case of morning launchings, and after the launch in the case of evening launchings, and the elevation, and the azimuth as shown on the camera stand, were noted down. At a correctly noted time an exposure of one minute was given. From this the orientation of the camera axis was calculated and compared with the noted values which gave the necessary correction to be applied to the readings on both the scales.

2.3.5. Exposure sequence.

The basic requirement in the present work is to get time coincident pictures of the vapour trail from two or

more camera sites at regular intervals. This is accomplished by using synchronised, accurate stop-watches at each camera site. The stop watches used in the present experiment kept time correct to ± 1 second in 2 hours. The stop-watches, at all the camera sites, were adjusted to the accurate range timing half an hour before the launch, by a time signal supplied to the camera sites. In order to have a uniform programme of exposures, a predetermined exposure schedule was used at all camera sites.

The following points were kept in mind while fixing the exposure schedule.

(1) The image of vapour trail in the film should have good contrast from sky background. Though the sodium vaporiser is standardised to give uniform results, it is found that the intensity of the cloud changes from launch to launch. Hence the photographic conditions will not be similar for all the experiments. It would be difficult to judge the correct exposure and change the diaphragm of the camera to suit different intensities of the sodium vapour trails during the experiments. Moreover, the intensity of sodium trail will change rapidly during the observation time due to the diffusion. To get good contrast of the image of vapour trail from sky background, the exposure time could be changed properly, so that it takes care of the changing intensity of the cloud. The exposure determination is discussed in detail by Dubin[127].

(ii) Experiments on the sky background light intensity have shown that the exposure of more than 3 seconds on Tri-X film at f/2.5 would over-expose the film and good results are not possible till the solar depression angle is 7°. Similarly, an exposure of more than 10 seconds till the solar depression angle is 7.5° and of more than 30 seconds till the solar depression angle is 8.5° would not give good results. However, if the haze is present, the sky background gets enhanced and conditions become much worse.

(iii) To determine the accurate direction in which the camera axis is oriented while photographing the vapour trail, at least two stars must be visible on the photograph for that direction of sight. The bright stars get recorded by an exposure of 10 seconds, but to get a good star picture an exposure of at least 30 seconds is necessary. In order to get many stars to facilitate the identification of them, an exposure of about a minute is essential.

(iv) During evening twilight launching, the intensity of the cloud diminishes as the background sky intensity also diminishes. Reverse is the case during morning twilight launching - the intensity of cloud diminishes as the background intensity increases.

Considering all these factors the following exposure schedules were fixed for morning and evening launchings.

In the case of morning launching, the time of rocket launch was selected when the solar depression angle was 10^{0}. The photography of the vapour trail was started 3 minutes after the launch of the rocket, at a solar depression angle slightly more than 9^{0}. For solar depression angles 9^{0} or more the sky background is minimum, while immediately after the release, the intensity of the vapour cloud is maximum. Only short duration exposures are sufficient to get good vapour cloud pictures under such conditions. The sky background slowly increases with time at dawn while the intensity of vapour cloud decreases due to diffusion. Thus longer exposures are necessary to record the vapour cloud at later time. After the solar depression angle reaches 6^{0}, the sky background becomes very large and longer exposures do not give good results. For this period, again, a few short exposures become necessary.

The observation time was divided into groups of exposures, each group having 3 minutes time duration. In turn, each group was divided into 3 sub-groups of 1 minute each. In the first group each sub-group had three exposures of 1 second, 3 seconds and 10 seconds duration. In the second, third and fourth groups exposures of 3 records, 9 seconds and 27 seconds were given in each sub-group. In the last two groups the exposures were again 1 second, 3 seconds and 10 seconds for each sub-group.

In the case of evening launching, the rocket launch time was selected so that the solar depression angle was 6° and the photography of the vapour trail was started 3 minutes after the launch, when the solar depression angle was about 7°. At this time the sky background is large, and longer exposures do not give good results. Besides, the intensity of vapour trail is also large and shorter exposures give good results. As the solar depression angle increases, the sky background diminishes enabling the longer exposures to be taken which become necessary as the vapour trail becomes faint. In this case also the observation time was divided into groups and sub-groups as before. For the first three groups of 3 minutes each, exposures of 1 second, 3 seconds and 10 seconds were given in each sub-group. For the later groups longer exposures of 3 seconds, 9 seconds and 27 seconds duration were given in each sub-group. Taking three different exposures in each sub-group ensured atleast one good exposure for each minute. This method also helped in identifying frames and keep track of missed exposures, at the time of data reduction.

If the axis of the camera was to be changed, to keep track with the moving vapour cloud, the usual exposures of one sub-group were suspended and one exposure of 55 seconds was given to obtain a star picture before the camera axis was changed. The exposure sequences for morning and evening twilight launchings are given in appendix I.

A one minute exposure of a known star configuration was taken and the camera axis readings were recorded at the noted time, after the photography of trail, in the case of dusk firing; and before the photography of the trail in the case of dawn firing.

2.4. THE CAMERA SITES

2.4.1. Selection of a camera site.

The sodium vapour trail released at and above 80 km by the rocket is photographed from at least two different sites. The important factors to be kept in mind for the selection of a camera site are as follows:-

(1) The distance of the camera site from the expected vapour trail should be such that large pictures of the trail are obtained. The perspective from the camera site should be such that the complete trail is photographed.

A curve showing the angle subtended by the trail at different distances from it can be obtained. This gives the perspective of the trail at different distances.

Let CE in Fig.25 denote the surface of the earth with E as the camera site, A a point in the vapour cloud, and C the projection of A on the surface of the earth. ED denotes the horizontal plane at E with D as the horizon. Let EC be denoted by X and AC by h and the distance between

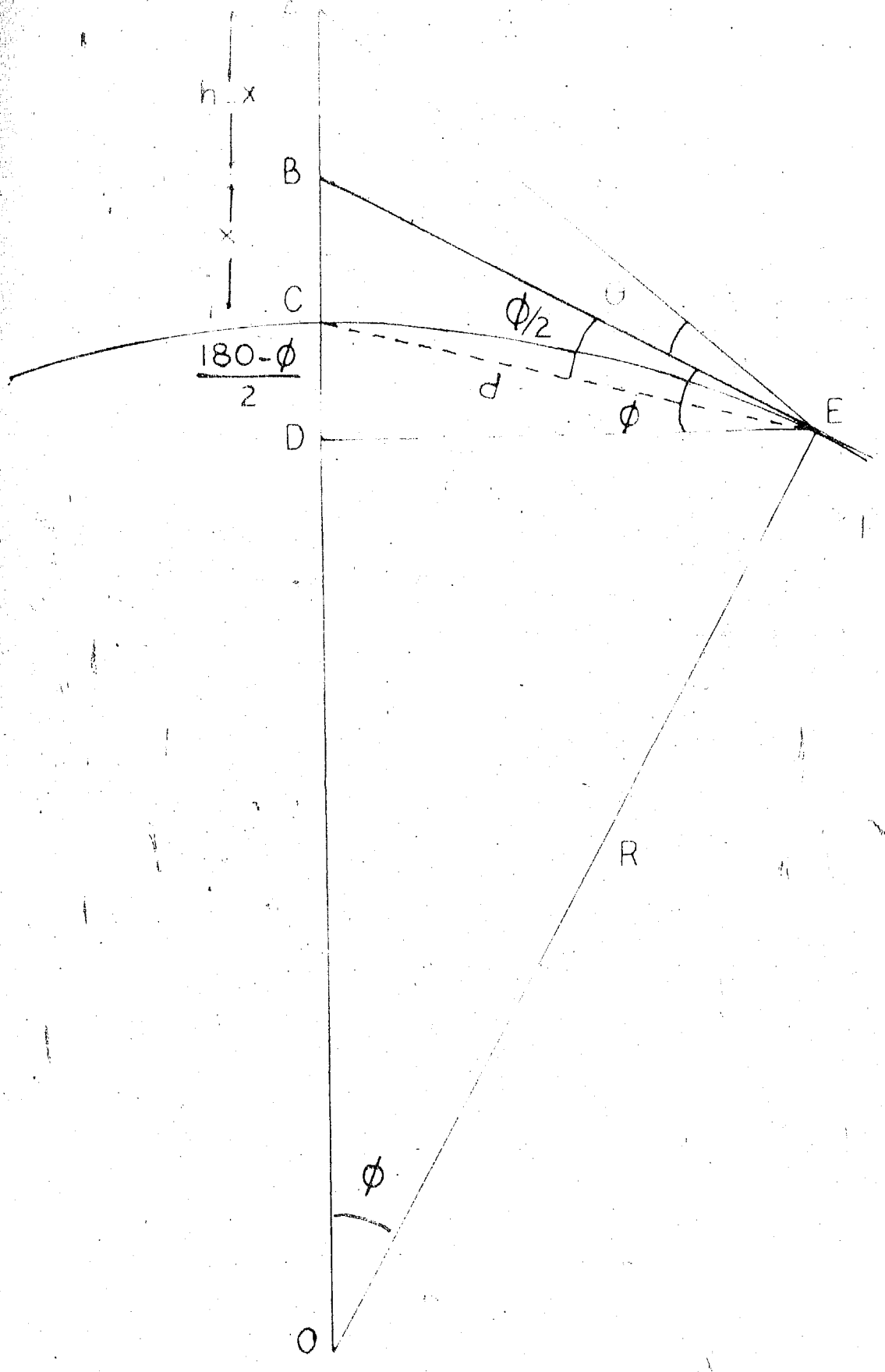

FIG. 25

C and E by d. Angle AEB, that is, the elevation angle subtended by the vapour cloud point A at E, is denoted by θ. As d is small compared to R, the radius of the earth, the angle ϕ also will be small,

then $R\phi = d$

and $X = d\frac{\phi}{2} = \frac{d^2}{2R}$

Then $\frac{h-X}{\sin\theta} = \frac{AE}{\cos\phi}$

But $AE = \sqrt{R^2 + (R+h)^2 - 2R(R+h).\cos\phi}$

and $\cos\phi = \frac{R}{R+X}$

Then $\sin\theta = \frac{R(h-X)}{(R+X)\sqrt{R^2 + (R+h)^2 - 2R^2\left(\frac{R+h}{R+X}\right)}}$

For different values of d and h the angle θ is calculated. If the vapour cloud is released from, say, 70 km to 180 km then h_{min} = 70 km and h_{max} = 180 km. The elevation angles θ subtended at different distances by points at the above heights are calculated and plotted in Fig. 26. Curve 'a' in the figure is for the highest point h_{max} situated at 180 km and curve 'b' is for the lowest point h_{min} situated at 70 km. The angle subtended by the whole trail at the observation

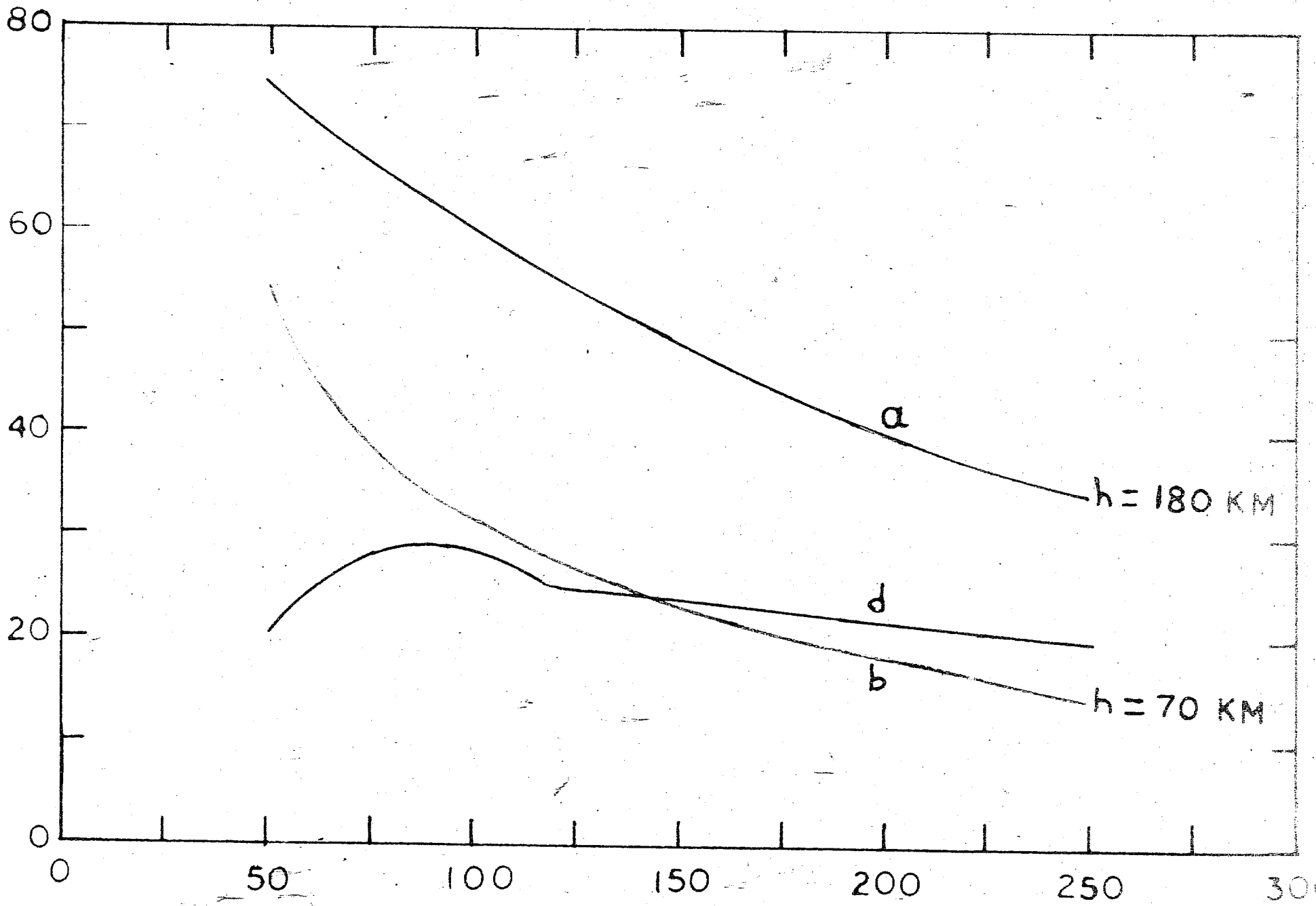

FIG. 26

CURVES SHOWING RED ANGLES SUBTENDED BY VARIOUS REAL RAYS AT DIFFERENT DISTANCES

point is given by the difference between the values of θ given by h_{max} and h_{min}. This difference curve also is plotted in Fig. 26 as curve 'd'. The slopes of the curves 'a' and 'b' show that up to a distance of about 100 km of the observing station, the elevation angle of lower point changes rapidly while that of the higher point changes slowly. This means that up to this distance equal segments of the trail subtend different angles thereby giving a bad perspective of the trail. Beyond this distance however, equal segments of the trail subtend almost equal angles. This gives a good perspective and thus the minimum camera site distance is about 100 km.

(ii) The camera site should not be too far from the launch site, so that the elevation angle for the lower point of the vapour trail is less than 16^{o}. At smaller elevation angles than 15^{o}, haze and absorption in the atmosphere decrease visibility by a large extent. The maximum suitable distance for a camera site from launch site is found to be about 260 km.

(iii) For triangulation purpose the accurate distance between two camera stations is required. To calculate this distance, latitude and longitude of the place must be known correct to a second of an arc. Also, the height of the camera position from the sea level must be accurately known.

(iv) The zone of interest, that is, the portion of

the sky where the vapour cloud is seen, should have a good view from the camera site without any physical obstructions.

(v) The camera site should have the electric power and telephone connections. The telephone connection is necessary because, the weather conditions at the camera sites are to be informed at regular intervals on the day of firing to the project scientist at the launch site. The project scientist, on the basis of such information decides whether to proceed with the experiment or not on that day, after considering the weather informations from all camera sites. The telephone connection is also necessary because the correct time signal has to be given from the launch site to all camera sites about half an hour before the launch. The correct time signal would enable the stop watches to be adjusted for correct time at each camera site. Correct time is necessary to get time coincident pictures of the vapour trail from different camera sites and also to take star pictures at accurately known times.

(vi) The camera site should have a provision for a good dark room. It is absolutely essential that the cameras are loaded in perfect darkness. After the experiment is over, the films are also to be unloaded in absoluto darkness and preserved in light-tight cans.

(vii) The camera site should be easily approachable and must be able to provide good accommodation to the camera crew.

2.4.2. Position of camera sites in relation to launch site.

For determining the heights of vapour points by triangulation, at least two camera sites are necessary from where the vapour trail is photographed. Usually more than three camera sites are selected to make sure that at least two are free of clouds. This will also ensure the photography of the complete trail even if, due to winds, the vapour trail moves over one of the camera sites. If a camera site is situated behind the trajectory, different portions of the trajectory might get mixed up in the picture and good perspective might not be obtained. So, while selecting the camera sites, a narrow zone of $\pm 10^{\circ}$ from the plane of trajectory, is avoided. Fig. 27 shows the launch site with the trajectory and the zone in which the camera sites can be selected with advantage. The shaded portion is the area in which the camera sites should be avoided. Marine camera stations on ship cannot be used as the roll of the ship would disturb the cameras while taking the pictures.

Considering these factors and also those given in section 2.4.1, the following places were selected for camera sites.

(i) Travellers' Bungalow, Kottayam,
(ii) Solar Physical Observatory, Kodaikanal,
(iii) Travellers' Bungalow, Palayamkottai. This was subsequently changed to St.Xavier's College, Palayamkottai,
(iv) Kerala House, Cape Comorin,
(v) St.Thomas College, Trichur.

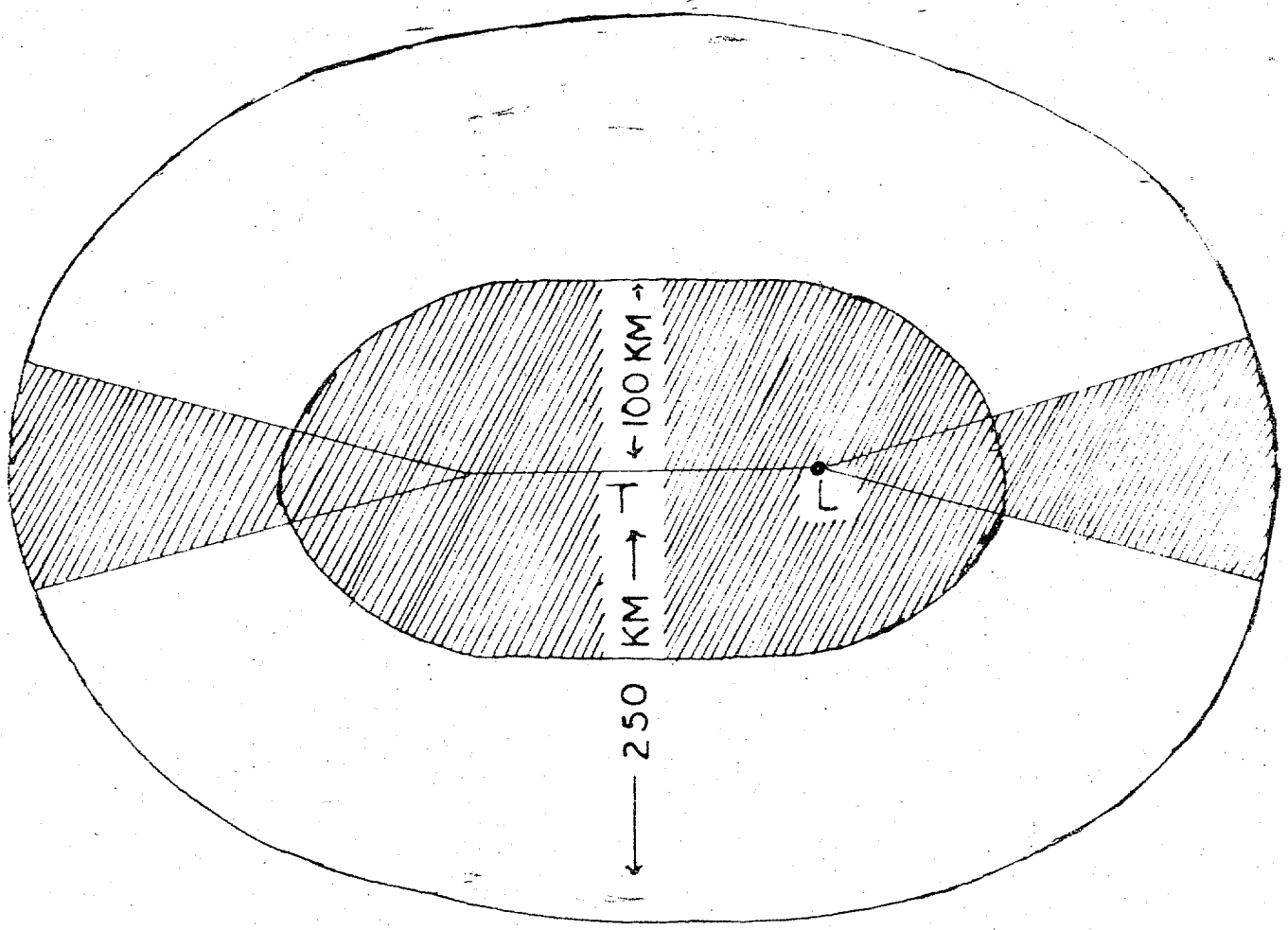

L → LAUNCH SITE T → TRAJECTORY

FIG . 27

SCHEMATIC DIAGRAM SHOWING THE ZONE IN WHICH CAMERA SITES CAN BE SATISFACTORILY LOCATED. CAMERA SITES SHOULD NOT BE LOCATED IN THE SHADED AREA.

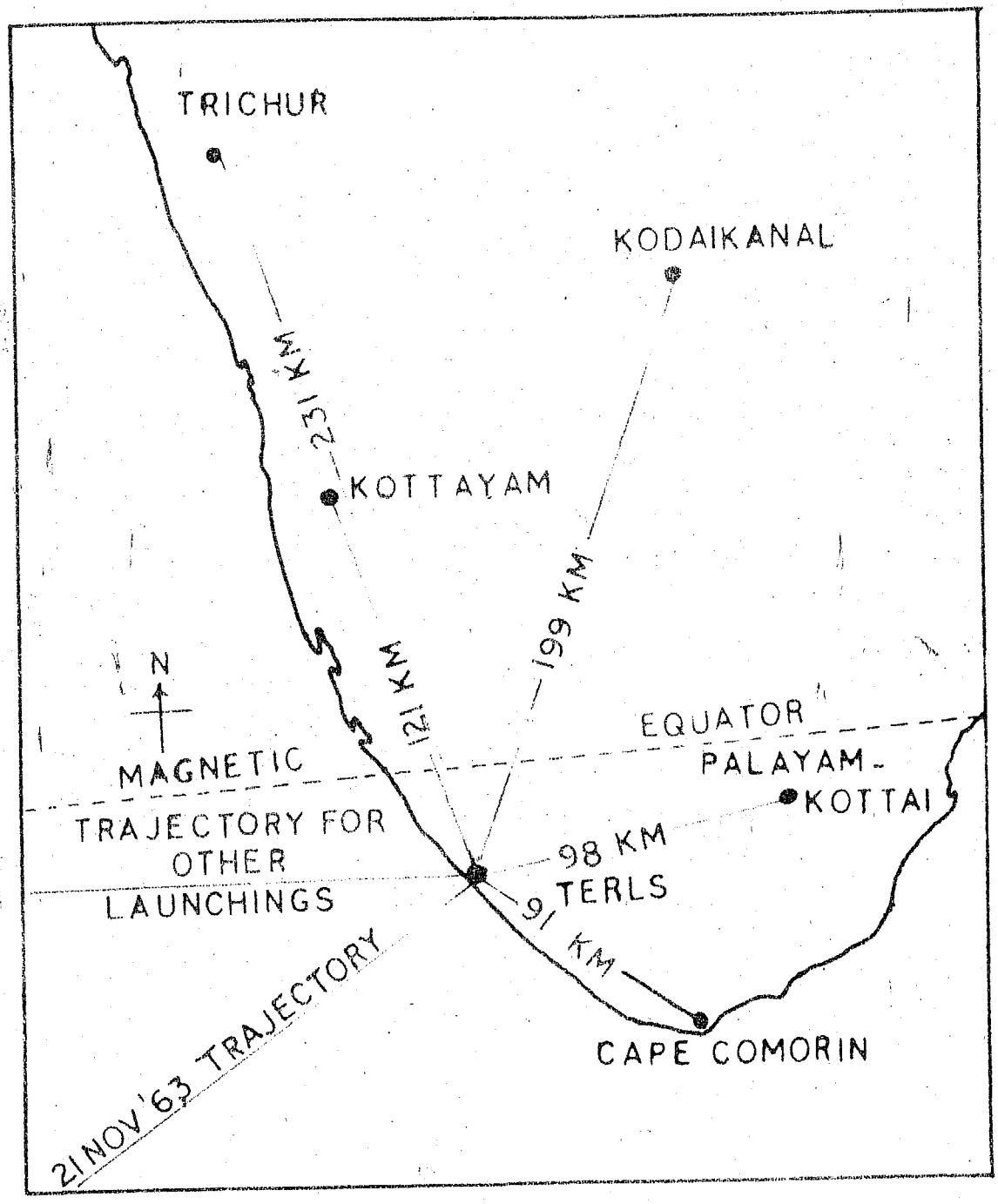

FIG. 28

MAP OF SOUTHERN PART OF INDIA SHOWING CAMERA SITES AND THE LAUNCH SITE

Latitudes and longitudes of the camera sites.

Camera site	Latitude ^{o} N	Longitude ^{o} E	Height above sea level in feet.	Distance from launch site in km.
1. Kottayam (Traveller Bungalow)	9° 34' 51"	76° 31' 26"	83	121.5
2. Kodaikanal (Solar Observatory)	10° 13' 43"	77° 27' 53"	7665	199.2
3. Palayamkottai (St. Xavier's college)	8° 43' 00"	77° 44' 04"	141	98.1
4. Cape Comorin (Kerala House)	8° 04' 44"	77° 32' 56"	108	91.5
5. Trichur (St. Thomas college)	10° 31' 21"	76° 13' 12"	38	231.5

The positions of these camera sites and the launch site at Thumba are shown on the map in Fig.2.8. No camera site was established west of the launch site as there is no land mass or suitable island available within permissible distance. Table 6 gives other relevant data concerning the camera sites.

The latitudes and longitudes of the place were taken from a previous work by Gulatee[126] who did gravity survey at these places. The distances were calculated from these values and the latitude and longitude of Thumba.

2.6. DATA REDUCTION

The primary aim of this experiment is to determine the neutral atmosphere motions by using the sodium vapour trail as a marker. The vapour trail is released at altitudes greater than 100 km, at twilight, with the help of a rocket. At these heights the sodium remains in atomic form[91] and attains ambient conditions very quickly[129]. The sodium atoms pick-up the motions of the surrounding gas and drift along with the air particles. Thus if the velocity of sodium vapour cloud at different altitudes is measured, the velocity of the neutral wind at these heights is obtained. To accomplish this, the sodium cloud is photographed from atleast two widely separated camera sites, using K-24 cameras, as given in section 2.3.4. Using the triangulation technique, the heights of different points of the vapour cloud are determined and utilising the photographs taken at different times, the

velocity and the direction of the neutral atmosphere wind are calculated.

There are basically two methods of data analysis for this experiment. The first, namely the analogue method, was adopted by Manring et al[130]. In this method the simultaneous photographs of the trail were projected on the screens placed at proper distances from projectors kept at points corresponding to the original camera sites on an appropriately scaled-down model of the firing range. Jarret et al[131] used the same method with slight modifications. This method can be advantageously used up to about 120 km altitude because, up to this altitude, some of the points on the trail can be well identified. Baguett[132] used an 'apparatus of restitution' which gave the coordinates of the cloud points at various heights. The second method is a numerical method in which trigonometrical relations are used in calculating the heights of vapour points by triangulation. Broglio[122] used this method supplemented by graphical solution. Smith[123] used the numerical method and used computer to determine the positions of vapour cloud points at different times and hence the atmospheric motions. The method used for the present study is based on Smith's method with some modifications adopted from the method suggested by Broglio. In what follows the method adopted by the author is given in detail. Some of the corrections suggested by Justus et al[133] are also

included in this section. The possible errors in the method and their magnitudes are discussed in section 2.6.

2.5.1. Determination of distances between the camera sites.

To determine the space coordinates of vapour cloud point utilising the triangulation technique, the knowledge of the correct distance between the two observation points is necessary. These distances were calculated from the known values of latitude and longitude of the camera sites. The distance between any pair of two camera sites was calculated as follows. First the geographic latitudes were converted to geocentric latitudes for these two camera sites and thus the correction for the oblateness of the earth was applied. The relation between geographic latitude ϕ' and geocentric latitude ϕ is given by

$$\tan\phi = K_1 \tan\phi'$$

where $$K_1 = \left(\frac{\text{Polar radius of the earth}}{\text{Equatorial radius of the earth}}\right)^2$$

Since the earth is assumed to be symmetric about its polar axis, the geographic and geocentric longitudes are same.

Due to the oblateness of the earth, the radius of the earth at a place is a function of geocentric latitude of that place and is given by

$$R = \frac{R_p}{\sqrt{(1 - K_1 \cos^2\phi)}} \qquad (2)$$

where R_p is the polar radius of the earth and $K_2 = 1 - K_1$.

In the following calculations the radius of the earth R at the camera site includes the height of camera from the mean sea level as it is added to the value of R calculated above.

In Fig. 29 let N denote the north pole of the earth, E and F the two camera sites and G_1 and G_2 the colatitudes of these two camera sites respectively. The angle subtended by the two camera sites at the north pole is given by the difference of the longitudes and is denoted by S. By solving this spherical triangle, the angles at E and F and the arc EF can be calculated. The relations giving these quantities are[135]

$$\cos EF = \cos G_1 \cos G_2 + \sin G_1 \sin G_2 \cos S \quad (3)$$

$$\sin E = \frac{\sin S \quad \sin G_2}{\sin EF}$$

$$\cos E = \frac{\cos G_2 - \cos G_1 \cos EF}{\sin G_1 \quad \sin EF} \quad (4)$$

$$\sin F = \frac{\sin S \quad \sin G_1}{\sin EF}$$

$$\cos F = \frac{\cos G_1 - \cos G_2 \cos EF}{\sin G_2 \quad \sin EF} \quad (5)$$

In Fig.30 E and F denote the same two camera sites given in Fig. 29 and O the centre of the earth. The angles β_1 and β_2 denote, respectively, the angles between the local

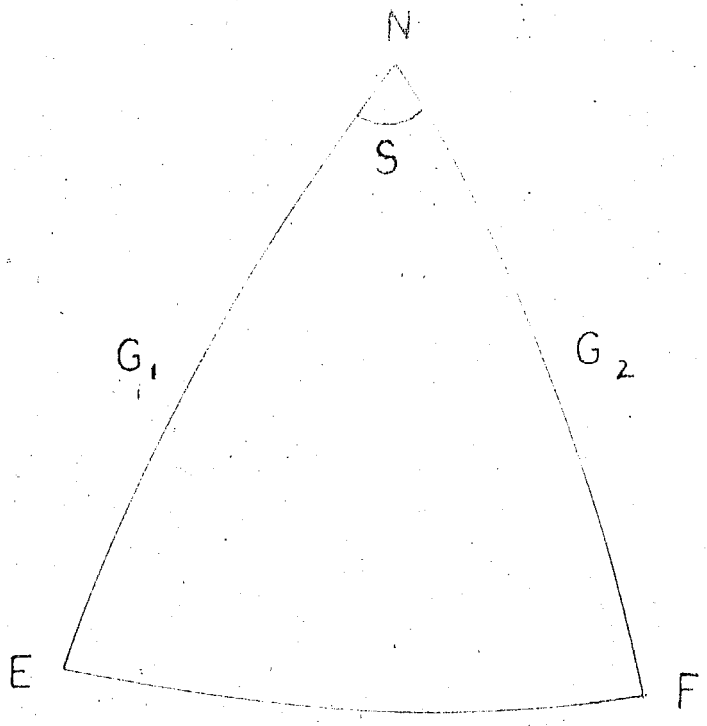

FIG. 29

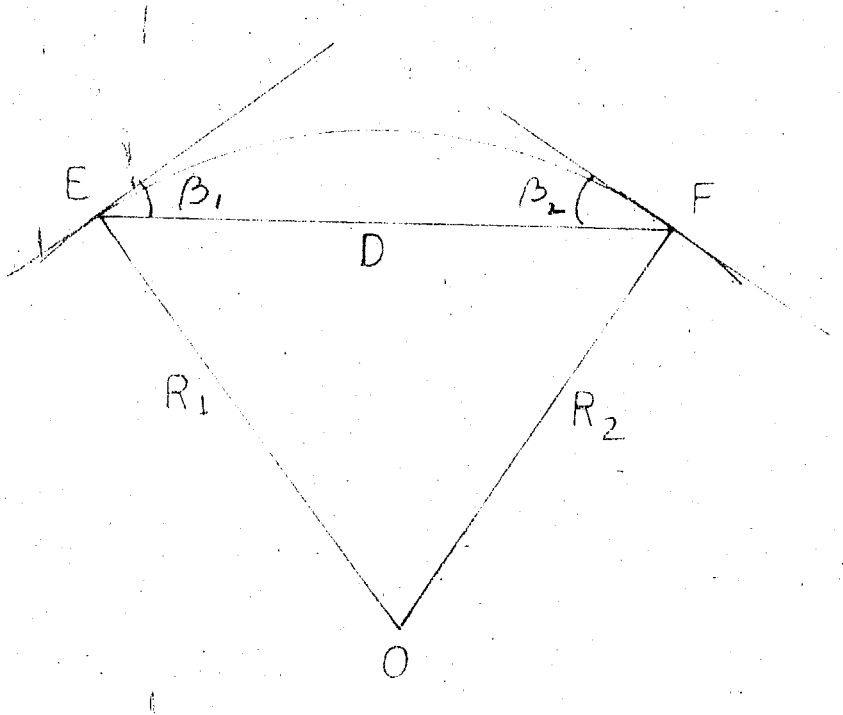

FIG 30

horizontale and the line joining the two camera sites. The horizontal distance between the two sites given by the arc EF was assumed to be equal to the chord D as it is very much small compared to the radius of the earth. Thus the distance D is given by

$$D = \sqrt{R_1^2 + R_2^2 - 2\ R_1\ R_2 \cos EF} \qquad (6)$$

Also β_1 and β_2 are given by

$$\sin\beta_1 = \frac{R_1^2 + D^2 - R_2^2}{2\ R_1\ D}$$

$$\sin\beta_2 = \frac{R_2^2 + D^2 - R_1^2}{2\ R_2\ D} \qquad (7)$$

2.6.2. Determination of the direction of the camera axis.

To determine the orientation of the camera axis more accurately than given by the elevation and azimuth scales on the camera stand, the images of two known stars obtained at known time, during the photography of the vapour trail were utilised. To do this, it was necessary to know the time of photography in sidereal time. To identify the stars, a star atlas[134] was used.

The time of exposure, given in Indian Standard Time, was first converted to Universal Time and the sidereal equivalent of this was obtained from the Nautical Almanac. To

this time was added the sidereial time at zero hours on that day as obtained from Nautical Almanac. This total time was converted back to the local time of camera site. This gave the sidereial time of the star exposure at the camera site.

Using a two-dimensional X-Y coordinate measuring microscope, the plate coordinates of the stars were read accurately. For this purpose the lines joining the opposite fiducial marks on the film were taken as axes and the centre of the film, which is the point of intersection of these lines, as the origin of the coordinate system x'oy'. The right ascensions and declinations of the identified stars were obtained from the Nautical Almanac. A spherical triangle with the zenith of the camera site, the north pole and one of the two stars as vertices was formed. If the right ascension and declination of the star are α_1 and δ_1 respectively, the angle at the north pole, called the hour angle of the star, is given in time units by

$$H = \alpha_1 - \text{sidereial time}$$

This was converted into degrees by multiplying by 15 as the entire celestial sphere rotates once in 24 hours and so each hour angle is equal to 15^0.

In Fig. 31, Z is the zenith and N is the north pole, so ZN gives the colatitude of the camera site and is given by $(90^0 - \phi)$. S_1 is the star and so NS_1 gives the codeclination

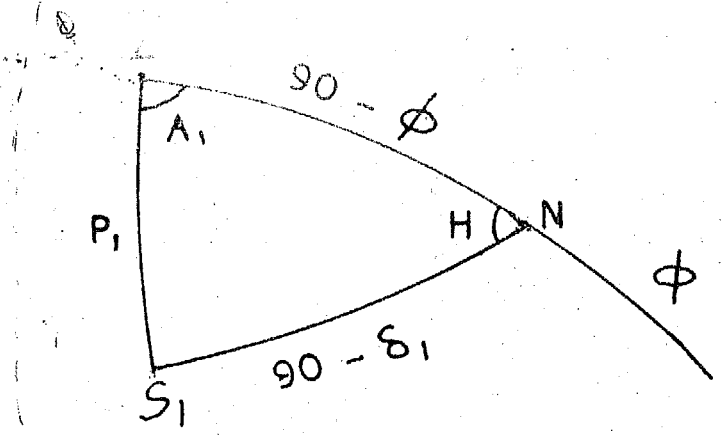

FIG. 31

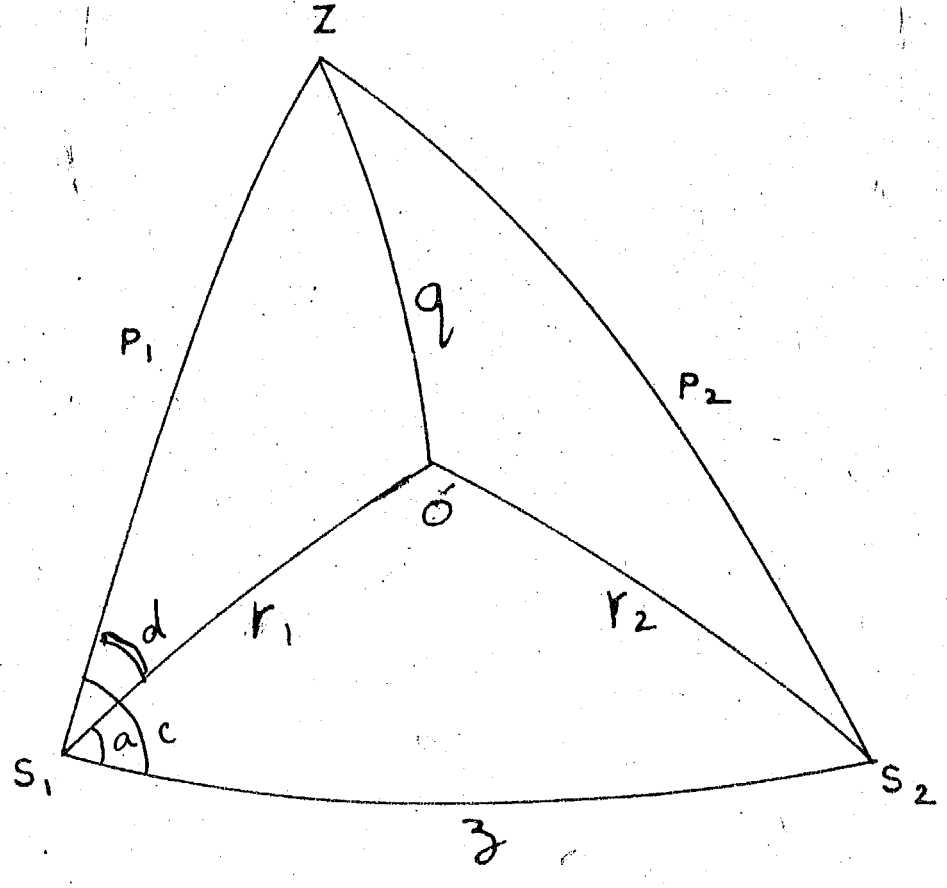

of the star and is given by $90^{\circ}-\delta_1$. If ZS_1, the coelevation of the star, is denoted by p_1, the spherical triangle can be solved to determine p_1 and angle A_1 the azimuth of the star. These are given by

$$\cos p_1 = \sin\phi \sin \delta_1 + \cos \phi \cos \delta_1 \cos H_1 \qquad (8)$$

$$\cos A_1 = \frac{\sin\delta_1 - \sin\phi \cos p_1}{\sin p_1 \cos\phi}$$

and

$$\sin A_1 = \frac{\cos\delta_1 \sin H_1}{\sin p_1} \qquad (9)$$

where $H_1 = H \times 15$ is the hour angle in degrees. The last two equations were necessary to determine the quadrant of A_1 from which the azimuth of the star was calculated. The azimuth was taken from north through east, that is, in clockwise direction from north. Similarly the azimuth of the second star A_2 also was calculated from another spherical triangle. The angle made by the two stars, A, at the zenith on the celestial sphere is given by the difference of the azimuths of the two stars.

Thus $$A = \left| A_1 - A_2 \right|$$

Another set of spherical triangles was now formed with the zenith Z, the two stars S_1 and S_2 and the point O' on the celestial sphere where the axis of the camera meets it. Fig. 32 illustrates the set of spherical triangles so formed.

The coelevations of the stars S_1 and S_2 are p_1 and p_2 respectively. Let the coelevation of the point where the camera axis meets the celestial sphere be q and let the angular distances of the stars from the camera axis be r_1 and r_2 respectively. The angle $S_1 Z S_2$ is the angle A calculated above and p_1 and p_2 were also calculated. So in the spherical triangle $Z S_1 S_2$, the arc $z = S_1 S_2$ is given by

$$\cos z = \cos p_1 \cos p_2 + \sin p_1 \sin p_2 \cos A \qquad (10)$$

On the photographic film the image of O' is the centre of the film or the origin of coordinate system having ox' and oy' as axes and the images of S_1 and S_2 have the coordinates (x'_1, y'_1) and (x'_2, y'_2) respectively (Fig.33). So the distance $O' S_1$ on the film is

$$d_1 = \sqrt{x'^2_1 + y'^2_1}$$

similarly the distance $O' S_2$ on the film is

$$d_2 = \sqrt{x'^2_2 + y'^2_2}$$

and the distance $S_1 S_2$ on the film is

$$d_3 = \sqrt{(x'_2 - x'_1)^2 + (y'_2 - y'_1)^2}$$

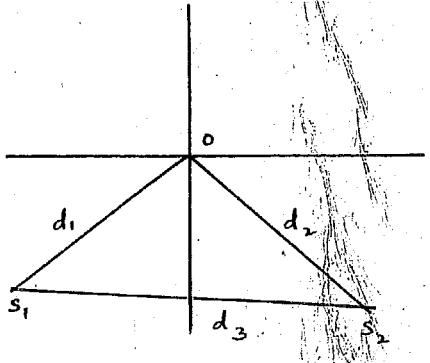

FIG. 33.

The angle $S_1 O' S_2$ is given by

$$\cos (S_1 O' S_2) = \frac{d_1^2 + d_2^2 - d_3^2}{2 d_1 d_2}$$

Now the arcs r_1 and r_2 are given, respectively, by (Fig.32)

$$\tan r_1 = \frac{d_1}{f}$$

and $$\tan r_2 = \frac{d_2}{f}$$

where f is the focal length of the camera lens. To check up the calculations, we can again find out z by the equation

$$\cos z = \cos r_1 \cos r_2 + \sin r_1 \sin r_2 \cos(S_1O'S_2) \quad (11)$$

Angle $O' S_1 S_2$ denoted by a is obtained by the equations;

$$\sin a = \frac{\sin r_2 \sin (S_1O' S_2)}{\sin z}$$

$$\cos a = \frac{\cos r_2 - \cos z \cos r_1}{\sin z \sin r_1} \quad (12)$$

In the triangle $Z S_1 S_2$, the angle $Z S_1 S_2$ denoted by c is obtained from equations

$$\sin c = \frac{\sin p_2 \sin A}{\sin z}$$

$$\cos c = \frac{\cos p_2 - \cos p_1 \cos z}{\sin p_1 \sin z} \quad (13)$$

These two equations were required to fix the complete angles as these angles have values lying between 0 and 2π. From these two values of a and c and the configuration of the stars, the angle $Z S_1O'$, denoted by d, was obtained by algebraic subtraction.

Now in the spherical triangle Z S_1 O' we have

$$\cos q = \cos r_1 \cos p_1 + \sin r_1 \sin p_1 \cos d \qquad (14)$$

This gave the coelevation of the camera axis, and so the elevation was calculated as

$$\varphi_0 = 90^0 - q \qquad (15)$$

Also from the same triangle

$$\sin (S_1 Z O') = \frac{\sin r_1 \sin d}{\sin q}$$

Now according to the position of the first star S_1, the azimuth of the camera axis is given by

$$\theta_0 = A \pm S_1 \hat{Z} O' \qquad (16)$$

Thus the azimuth and elevation of all the camera orientations from all the camera sites were obtained when a good star field was photographed.

2.6.3. Determination of the focal length of the camera lens.

The K-24 camera is equipped with a multi-element 7 inch focal length (178 mm) f/3.5 lens. The focal length, given by the manufacturer, is not given up to an accuracy required in this experiment. The focal length can be calculated very accurately using the same stars which are used to determine the direction of the camera axis. The following method used,

is adopted from Justus et al[131].

Let f be the correct focal length. Then,

$$\tan r_1 = \frac{d_1}{f}$$

and $$\tan r_2 = \frac{d_2}{f}$$

From this we have

$$\sin r_1 = \frac{d_1}{\sqrt{d_1^2 + f^2}}$$

$$\cos r_1 = \frac{f}{\sqrt{d_1^2 + f^2}}$$

$$\sin r_2 = \frac{d_2}{\sqrt{d_2^2 + f^2}}$$

and $$\cos r_2 = \frac{f}{\sqrt{d_2^2 + f^2}} \qquad (17)$$

In the spherical triangle $O' S_1 S_2$ (Fig.32) z is given by

$$\cos z = \cos r_1 \cos r_2 + \sin r_1 \sin r_2 \cos (S_1 O' S_2) \qquad (18)$$

Knowing the values of cos z and cos $(S_1 O' S_2)$ and using the relations obtained above, the following relation was obtained.

$$f^4(\cos^2 z - 1) + f^2\left[(d_1^2 + d_2^2)\cos^2 z - 2 d_1 d_2 \cos (S_1 O' S_2)\right]$$

$$+ d_1^2 d_2^2 \left[\cos^2 z - \cos^2 (S_1 O' S_2)\right] = 0$$

From this, the value of f was calculated as

$$f = \left[\frac{-V \pm (V^2 - 4UW)^{\frac{1}{2}}}{2U} \right]^{\frac{1}{2}} \qquad (19)$$

where $U = \cos^2 s - 1$

$$V = (d_1^2 + d_2^2) \cos^2 s - 2 d_1 d_2 \cos(\theta_1\theta', \theta_2)$$

$$W = \left[\cos^2 s - \cos^2(\theta_1\theta', \theta_2) \right] d_1^2 d_2^2$$

Thus two values of f were obtained. From this the value which had minimum deviation from the nominal value quoted by the manufacturer was taken as the correct value for the focal length of the lens.

2.5.4. Camera tilt.

If the camera is mounted perfectly horizontal during the photography, the line on the celestial sphere joining the zenith with the point where the axis of camera intersects the celestial sphere gives a projection on the photographic film which coincides with y' - axis of the coordinate system of the film. But due to unavoidable reasons, the camera will invariably be tilted. The following procedure, to determine this tilt of the camera, was also adopted from Justus et al[131]. We can form a new system of coordinate axes xoy on the film such that the y - axis coincides with the projection of the celestial line ZO'. Let the angle between these two coordinate systems be θ' which gives the camera tilt (Fig. 34).

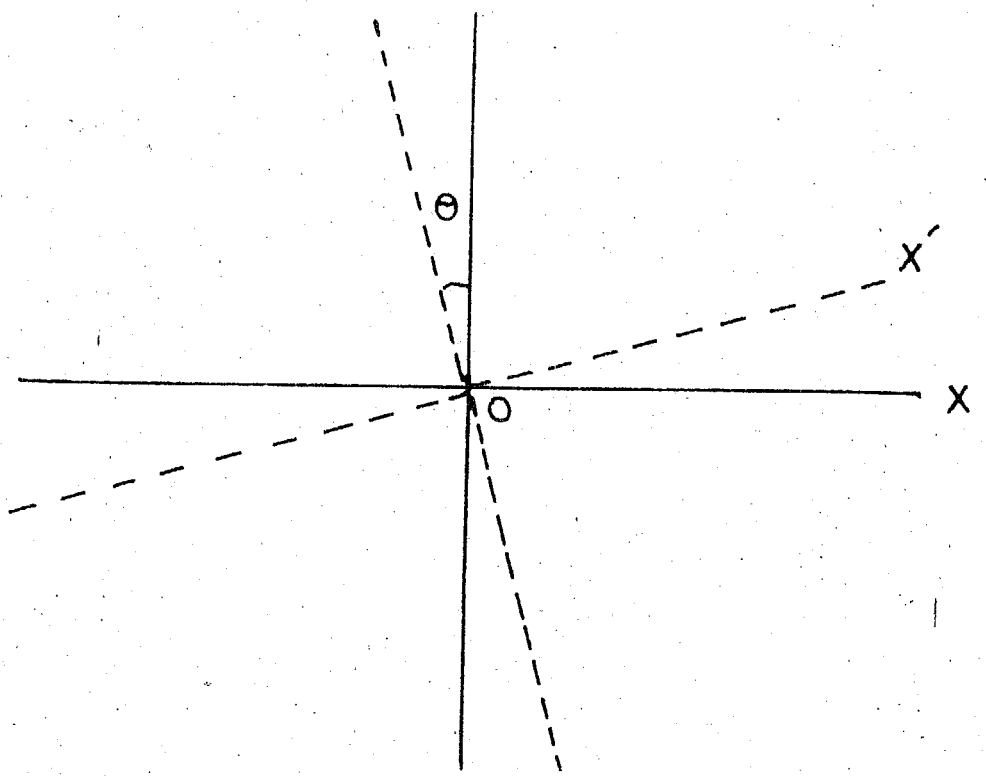

FIG. 34

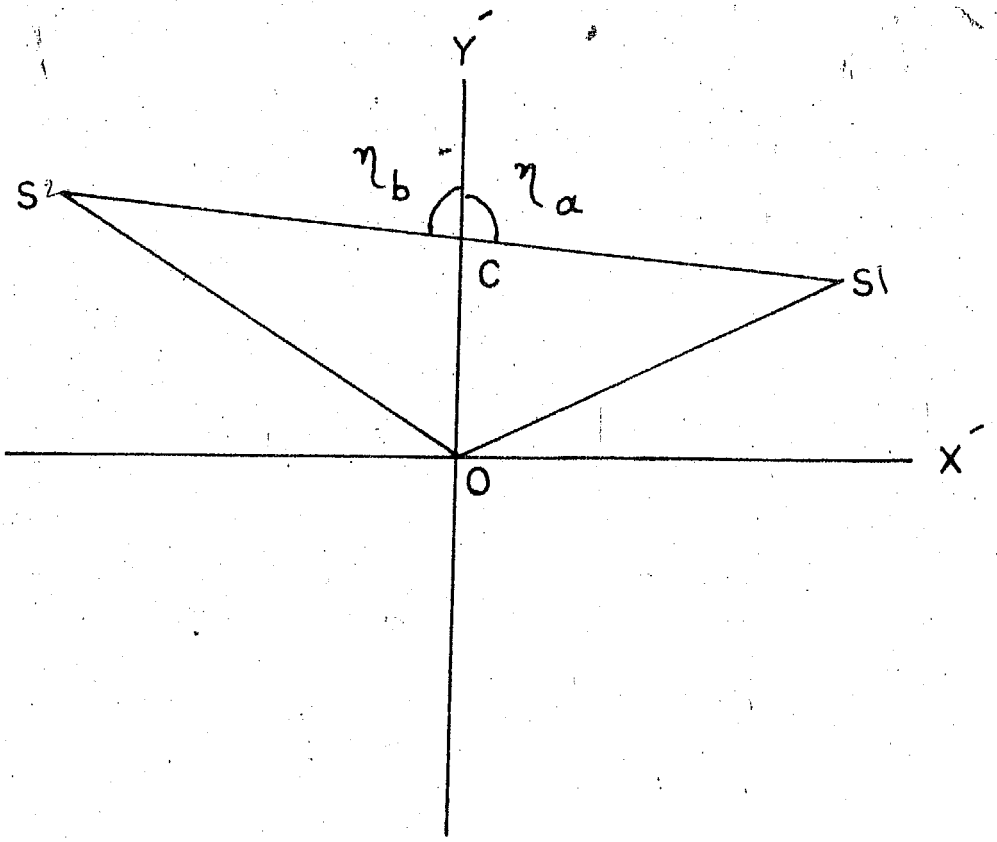

Let the stars S_1 and S_2 have the images s_1 and s_2 on the photographic film (Fig.35). Let the distances of these stars from the centre be d_1 and d_2 respectively and the distance between them d_3 . C is the point of intersection between the line joining star images and the y-axis. The angle between s_1 C and y-axis is η_a while the angle between s_2 C and y-axis is η_b .

The coordinates of s_1 and s_2 are (x'_a , y'_a) and (x'_b , y'_b) as measured in x'-y' coordinate system and (x_a, y_a) and (x_b, y_b) in x-y coordinate system .

Then
$$x_a = x'_a \cos\theta' + y'_a \sin\theta'$$
$$x_b = x'_b \cos\theta' + y'_b \sin\theta'$$
$$y_a = y'_a \cos\theta' - x'_a \sin\theta'$$
$$y_b = y'_b \cos\theta' - x'_b \sin\theta' \qquad (20)$$

and
$$x_a - x_b = (x'_a - x'_b)\cos\theta' + (y'_a - y'_b)\sin\theta'$$
$$y_a - y_b = (y'_a - y'_b)\cos\theta' - (x'_a - x'_b)\sin\theta' \qquad (21)$$

The slope of the line $s_1 s_2$ denoted by y_x is given by

$$y_x = \frac{(y'_a - y'_b)\cos\theta' - (x'_a - x'_b)\sin\theta'}{(x'_a - x'_b)\cos\theta' + (y'_a - y'_b)\sin\theta'} \qquad (22)$$

Solution of this equation gave

$$\tan \theta' = \frac{(y'_a - y'_b) - y_x (x'_a - x'_b)}{y_x (y'_a - y'_b) + (x'_a - x'_b)} \qquad (23)$$

This gave the tilt of the camera provided the slope y_x was known. The slope y_x was determined from the angles η_a and η_b given by

$$y_x = \tan (\eta_a - \frac{\pi}{2}) \quad \text{if } x_a \text{ is negative}$$

$$y_x = \tan (\frac{\pi}{2} - \eta_a) \quad \text{if } x_a \text{ is positive}$$

or

$$y_x = \tan (\eta_b - \frac{\pi}{2}) \quad \text{if } x_b \text{ is negative}$$

$$y_x = \tan (\frac{\pi}{2} - \eta_b) \quad \text{if } x_b \text{ is positive} \qquad (24)$$

To determine the values of η_a and η_b a set of spherical triangles were formed on the celestial sphere by the zenith Z, the stars S_1 and S_2 and O' the intersection of camera axis with celestial sphere as in Fig. 36. The various angles are given in the figure. In this set of spherical triangles the values of θ_1 S_2 , that is z, r_1, r_2, p_1, p_2 and q are known. Also the angles c, a and d and $S_1 \hat{Z} O'$ are known. Let ZO be denoted by q_o . In the spherical triangle Z S_1 C we have

$$\cos \eta'_a = -\cos(S_1 Z C) \cos c + \sin(S_1 Z C) \sin c \cos p_1 \qquad (25)$$

and

$$\sin q_o = \frac{\sin p_1 \sin c}{\sin \eta'_a} \qquad (26)$$

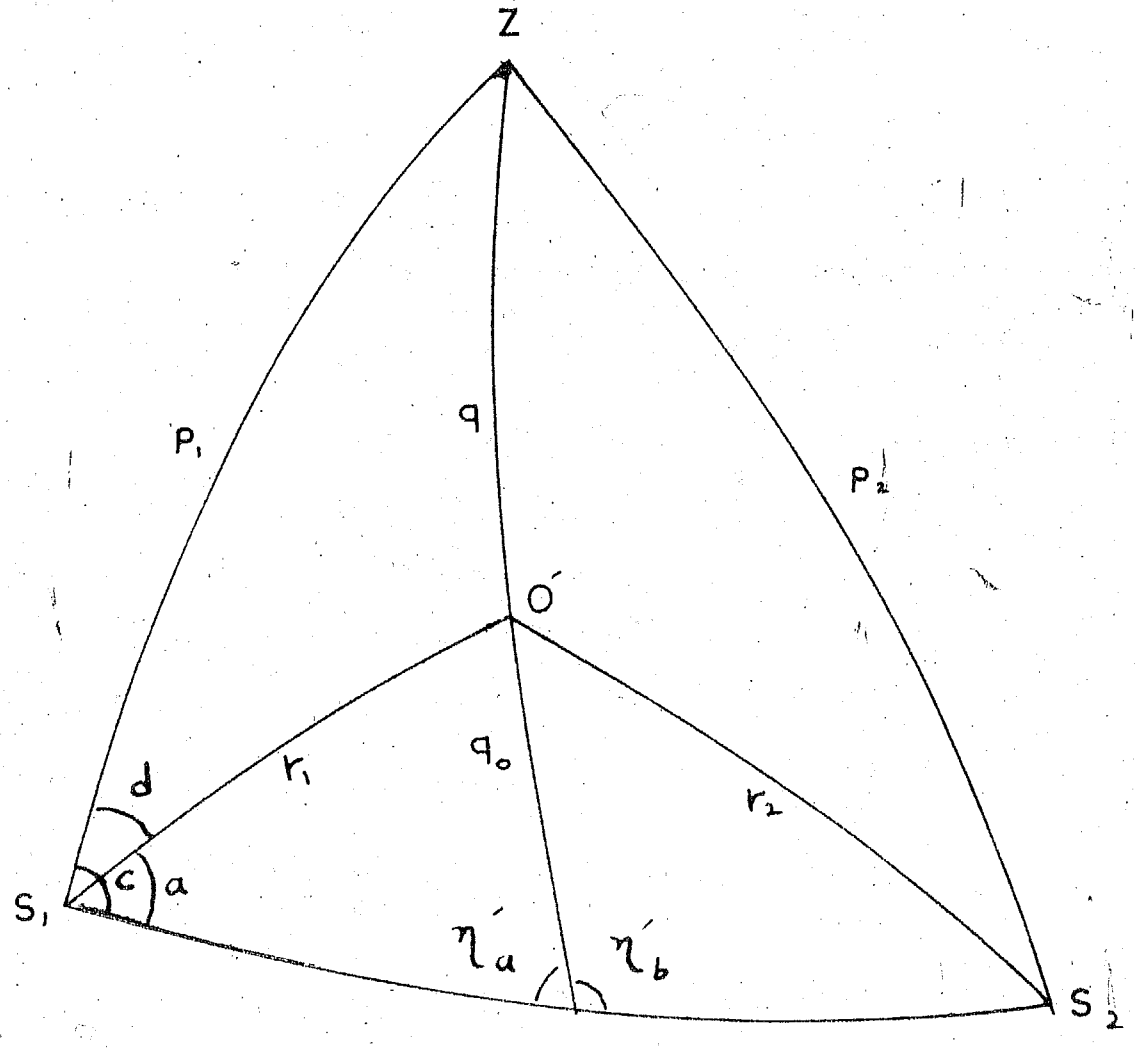

FIG. 36

According to the configuration of stars, O' C was obtained. In Fig. 36

$$O'C = \omega = q_0 - q$$

η'_a is related to the corresponding angle η_a on the photographic film as

$$\tan \eta_a = \tan \eta'_a \cos \omega \qquad (27)$$

Similarly the relation between η_b and η'_b can be determined. Knowing either of these values, the slope y_1 of the line $S_1 S_1$ in Fig. 35 was calculated as per the equations given above. Then the camera tilt θ' was obtained from equation (23).

A correction was applied for tilt to all the points of the vapour cloud read on the photographic film using the equations

$$x = x' \cos \theta' + y' \sin \theta'$$
$$y = y' \cos \theta' - x' \sin \theta' \qquad (28)$$

where (x', y') are the coordinates of the point as read on the film and (x, y) are the coordinates after correction.

2.5.5. Determination of the elevation and the azimuth of the vapour cloud points.

A pair of simultaneous photographs from two stations were selected, which gave good vapour trail images. Assuming the cloud has a cylindrical symmetry at each height, a centre line was drawn on the cloud representing the axis and the coordinates of about 200 points placed conveniently on this line, were read accurately using a two dimensional microscope.

To determine the elevation and the azimuth of these points as seen from one camera site, a spherical polar coordinate system was established with the camera site as the origin O". The elevation φ was taken from the local horizontal and the azimuth θ was taken anticlockwise from the X-axis pointing towards east. Y-axis pointed towards north and Z-axis vertically upwards. The coordinates of the point as read on the film could be related with the elevation φ and azimuth θ of the point of vapour cloud and the elevation φ_0 and azimuth θ_0' of the camera axis. Here θ_0' is the azimuth of the camera axis in anticlockwise direction from X-axis. In Fig. 37, let O" be the centre of the lens, and o' the centre of the film. Then

$$\sin\varphi = \frac{O''M}{O''P} = \frac{O''N + NM}{O''P}$$

now $$O''P = \sqrt{f^2 + x^2 + y^2}$$

where f is the focal length of the camera,

$$O''N = f \sin\varphi_0$$

and $$NM = y \cos\varphi_0$$

then $$\sin\varphi = \frac{f \sin\varphi_0 + y \cos\varphi_0}{\sqrt{f^2 + x^2 + y^2}} \qquad (29)$$

This gave the elevation of vapour point from the camera site.

In Fig. 38 let O"X be the X-axis pointing towards east and O"Y the Y-axis pointing towards north. O" is the lens centre. The azimuth angles of the camera axis and the line of sight to

θ_0' θ

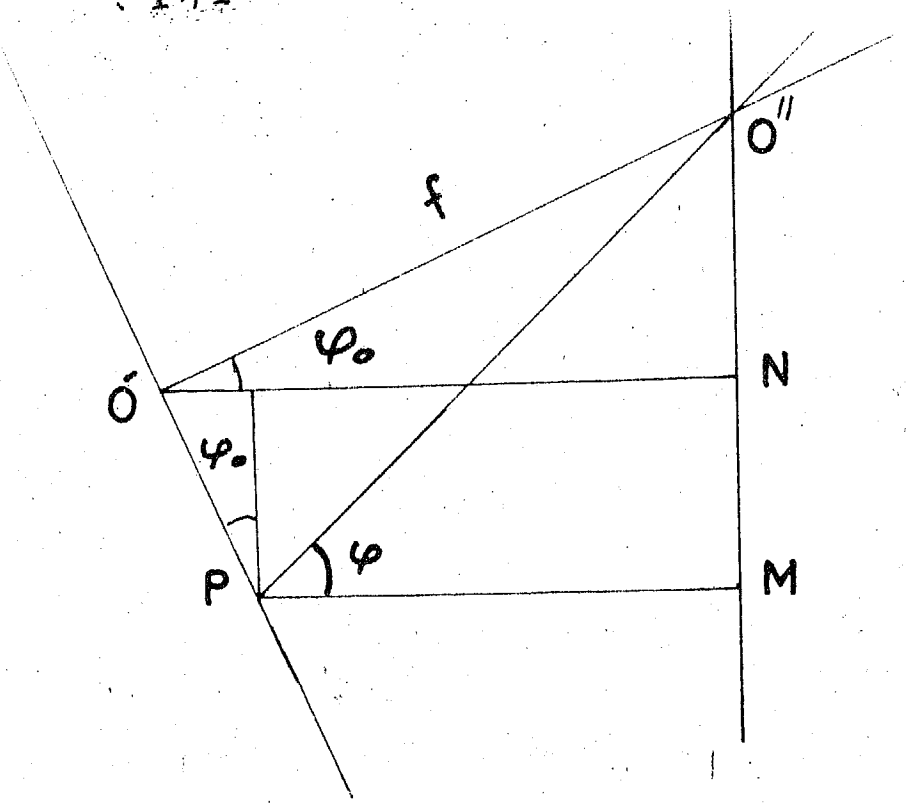

FIG. 37

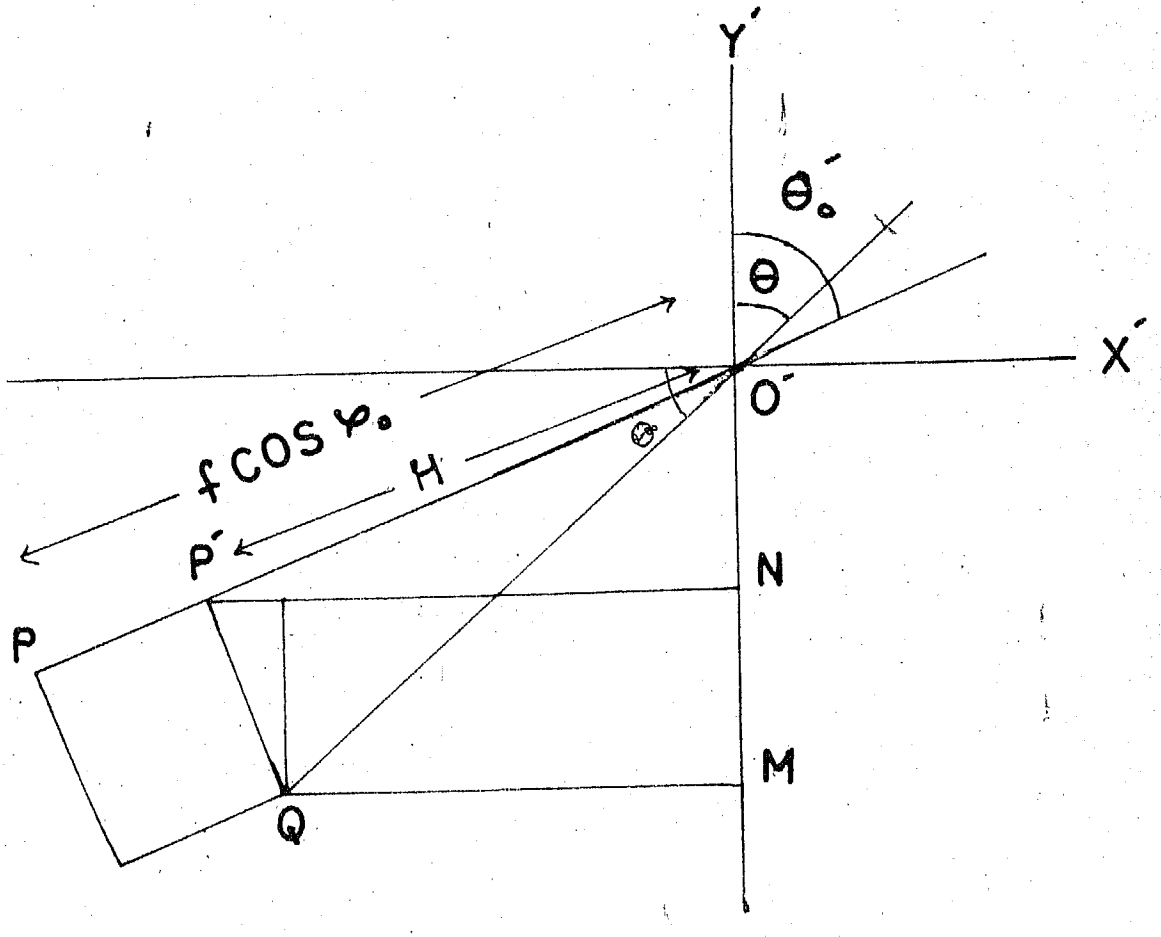

FIG. 38

the vapour point are θ'_o and θ respectively. On the left hand side of $\bar{O}T'$ in Fig. 38, the projections of different quantities on the horizontal plane are drawn. P is the projection of the centre of the film and Q the projection of the vapour point image. Then $\bar{O}P$ is given by $f \cos\varphi_o$ and PP' by $y \sin\varphi_o$. Then $\bar{O}P' = H$ is given by

$$H = f \cos\varphi_o - y \sin\varphi_o$$

From the figure the following relation was derived:

$$\tan\theta'' = \frac{H \sin\theta'_o - x \cos\theta'_o}{H \cos\theta'_o + x \sin\theta'_o} \qquad (30)$$

This gave the azimuth of the vapour point from the X-axis in anticlockwise direction. Using this relation, the true azimuth θ of this vapour point was calculated.

2.5.6. Determination of the space coordinates of points on a vapour cloud.

An arbitrary point on the surface of the earth approximately below the centre of the rocket trajectory was chosen. A plane passing through this point and the two camera sites was established. This point was taken as the origin O'' of the cartesian coordinate system with the X, Y and Z axes pointing towards east, north and vertically upwards respectively. With respect to this origin the coordinates of the camera sites were taken as (X_1, Y_1) and (X_2, Y_2) respectively. From the

points read on the centre line of the vapour cloud image, a group of five points were selected, and their elevations and azimuths with respect to the camera site were determined. These elevations and azimuths were then converted with respect to the common plane as follows.

Let E and F be the camera sites (Fig.39) and P the projection of a vapour point, from the selected group of points, on the common horizontal plane. The elevation of the

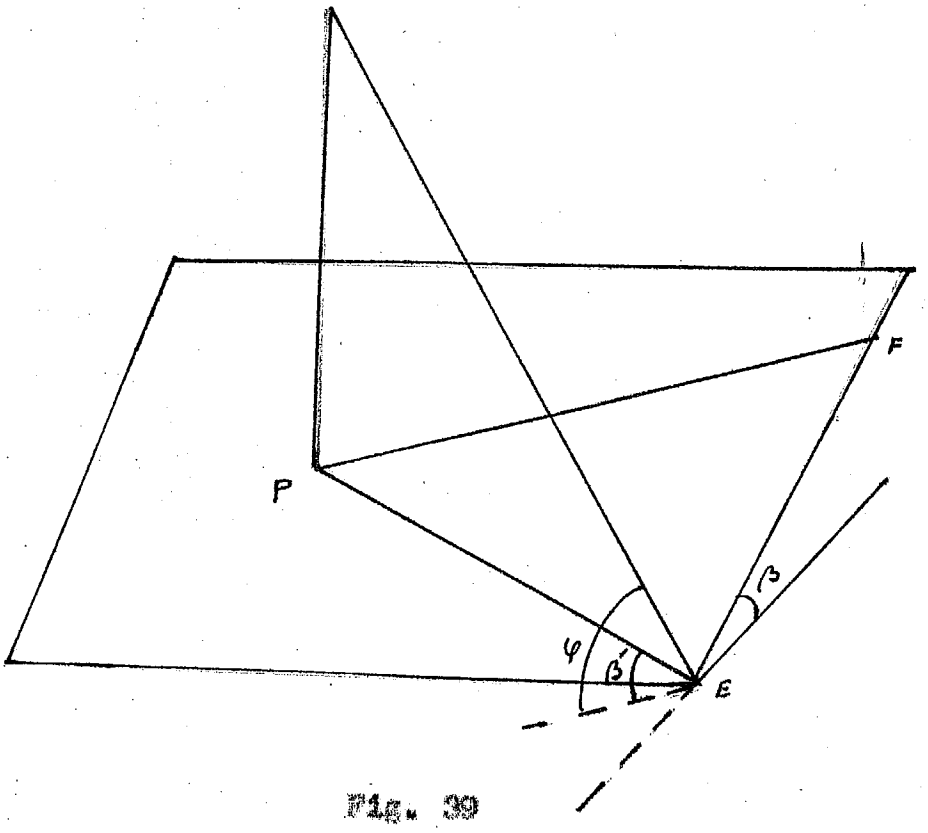

Fig. 39

point from the local horizontal at the camera site, say E, is φ. The angle between the local horizontal and the line joining the two camera sites is β as calculated earlier. This angle

will become in the

$$\beta' = \beta . \cos (FEP) \qquad (31)$$

in the direction of EF. Angle FEP can, in turn, be calculated from the known angle at E in the spherical triangle with north pole and the two stations E and F as vertices (Fig.29). Then the elevation angle of the point with respect to the common plane will become

$$\varphi = \varphi + \beta' \qquad (32)$$

The azimuth of the point in anticlockwise direction from X-axis is given by

$$\theta = \theta'' \cos \beta' \qquad (33)$$

where θ'' is the azimuth of the point from X-axis in anti-clockwise direction.

The direction cosines of the lines joining the selected points to the camera were determined using the equations

$$\begin{aligned} \cos \alpha &= \cos \varphi \cos \theta \\ \cos \beta &= \cos \varphi \sin \theta \\ \cos \gamma &= \sin \varphi \end{aligned} \qquad (34)$$

Approximately same points on the vapour trail image from a simultaneous photograph from the second camera site were selected and the direction cosines of their lines of

sight determined in the same way. One point each from the two groups of five points from the simultaneous photographs were considered and the minimum perpendicular distance between the lines of sight joining these points to the respective camera sites was calculated by using the formula[136] :

$$D = \frac{(X_2 - X_1)(\cos\beta_1\cos\gamma_2 - \cos\gamma_1\cos\beta_2) + (Y_2 - Y_1)(\cos\gamma_1\cos\alpha_2 - \cos\alpha_1\cos\gamma_2)}{\sqrt{\Sigma(\cos\beta_1\cos\gamma_2 - \cos\beta_2\cos\gamma_1)^2}} \qquad (35)$$

where (X_1, Y_1) and (X_2, Y_2) are the coordinates of the two camera sites E and F, Z coordinate being neglected, as the plane passes through the two camera sites. $(\cos\alpha_1, \cos\beta_1, \cos\gamma_1)$ and $(\cos\alpha_2, \cos\beta_2, \cos\gamma_2)$ are the direction cosines of the lines of sight to the selected vapour points from camera sites E and F respectively.

If the two points on the two simultaneous photographs selected are such that they refer to the same point on the vapour trail, the minimum perpendicular distance D will come out equal to zero. In practice, however, due to experimental errors, this will have a small finite value. If this value is very much large it means the two points selected do not represent the same point. Let the points selected from the first photograph be denoted by $E_1, E_2, \ldots E_5$ and those from

the second photograph by F_1, F_2.....F_5. Keeping the line of sight from E to E_1 fixed, the minimum perpendicular distances between this line and the lines of sight joining F to F_1, F_2 ..... F_5, were calculated successively. If E_1 corresponds to any of F_1, F_2..... F_5 , the minimum perpendicular distance between them would become zero or near zero. If however, E_1 lies between two points, say $F_2$and F_3, the minimum perpendicular distances, between E_1 and F_2 and E_1 and F_3 will have finite values but their signs will be changed. If, on the other hand, point E lies on one side of the points F_1,.....F_5, there will not be any change of sign in the minimum perpendicular distances. The process was repeated with other points E_2,.....E_5 from first photograph. If there was no cross over for any of these points it meant that the same group of points were not selected from the two photographs. Hence the points from one photograph or the other were properly shifted so as to get the cross over for at least two points of the group. When a cross over was obtained, a point was determined on the trail which was the centre of the shortest perpendicular distance. The coordinates of this point were determined as follows, which were taken as the space coordinates of a point on the vapour trail in the coordinate system selected.

Let the shortest perpendicular meet the two lines of sight from the two camera sites in C_1 and C_2 respectively.

Then the coordinates of C_1 and C_2 can be written, respectively, as $(X_1 + k_1 \cos\alpha_1, Y_1 + k_1 \cos\beta_1, k_1 \cos\gamma_1)$,

$(X_2 + k_2 \cos\alpha_2, Y_2 + k_2 \cos\beta_2, k_2 \cos\gamma_2)$

where k_1 is proportional to the distance of C_1 from the first camera site with coordinates (X_1, Y_1) and k_2 is proportional to the distance of C_2 from the second site with coordinates (X_2, Y_2).

The direction cosines of C_1 C_2 are now proportional to

$$X_1 - X_2 + k_1 \cos\alpha_1 - k_2 \cos\alpha_2$$

$$Y_1 - Y_2 + k_1 \cos\beta_1 - k_2 \cos\beta_2$$

$$k_1 \cos\gamma_1 - k_2 \cos\gamma_2$$

Since C_1 C_2 is at right angles to both lines of sight we have

$$\cos\alpha_1(X_1 - X_2 + k_1 \cos\alpha_1 - k_2 \cos\alpha_2) +$$
$$+\cos\beta_1(Y_1 - Y_2 + k_1 \cos\beta_1 - k_2 \cos\beta_2) + \cos\gamma_1(k_1 \cos\gamma_1 - k_2 \cos\gamma_2) = 0$$

$$\cos\alpha_2(X_1 - X_2 + k_1 \cos\alpha_1 - k_2 \cos\alpha_2) +$$
$$+\cos\beta_2(Y_1 - Y_2 + k_1 \cos\beta_1 - k_2 \cos\beta_2) + \cos\gamma_2(k_1 \cos\gamma_1 - k_2 \cos\gamma_2) = 0 \quad (36)$$

By solving these equations for k_1 and k_2 the following values are obtained:

$$k_1 = \frac{(X_2-X_1)(\cos\alpha_1 - p\cos\alpha_2)+(Y_2-Y_1)(\cos\beta_1 - p\cos\beta_2)}{1-p^2}$$

$$k_2 = \frac{(X_2-X_1)(p\cos\alpha_1 - \cos\alpha_2)+(Y_2-Y_1)(p\cos\beta_1 - \cos\beta_2)}{1-p^2} \quad (37)$$

where $p = \cos\alpha_1\cos\alpha_2 + \cos\beta_1\cos\beta_2 + \cos\gamma_1\cos\gamma_2$ (38)

The coordinates of the middle point of C_1 C_2 with respect to origin O" are then given by

$$x' = (X_1 + X_2 + k_1\cos\alpha_1 + k_2\cos\alpha_2)/2 \quad (39)$$

$$y' = (Y_1 + Y_2 + k_1\cos\beta_1 + k_2\cos\beta_2)/2 \quad (40)$$

$$z' = (k_1\cos\gamma_1 + k_2\cos\gamma_2)/2 \quad (41)$$

which are the space coordinates of the point on the vapour trail.

The elevation and azimuth of this point with respect to the origin are then given by

$$\tan\varphi' = \frac{z'}{\sqrt{x'^2 + y'^2}} \quad (42)$$

and $$\tan\theta' = \frac{y'}{x'} \quad (43)$$

Equation (43) gives the azimuth in anticlockwise direction from x-axis and can be converted to the true azimuth, that is, from north through east by taking into consideration the proper

quadrant in which the projection of this point falls on the horizontal plane through the camera sites.

This procedure was repeated for all the points of the group which gave the change of sign and then was extended to all the similar groups of points on a pair of vapour trail pictures taken at a time.

The height Z' obtained above is not the true height as it gives the height of the point above the plane containing the origin and the two camera sites. To obtain the true height of the vapour point above the earth's surface, consider Fig. 40 in which O is the centre of the earth, Q' is the point of projection of the vapour point on the earth's surface, O'' is the origin and P is the vapour point whose height is being determined. Let the radius of the earth at O'' be R. PQ' is the true height H and PP' equal to Z' is the height as obtained in equation (41). In the triangle PO O'' we have,

$$PO^2 = \delta^2 + R^2 - 2R\delta \cos(90^\circ + \varphi')$$

where $\delta = \sqrt{x'^2 + y'^2 + z'^2}$

Thus the true height H is given by

$$H = PO - R$$

where R is the radius of the earth being taken on the same latitude as O''.

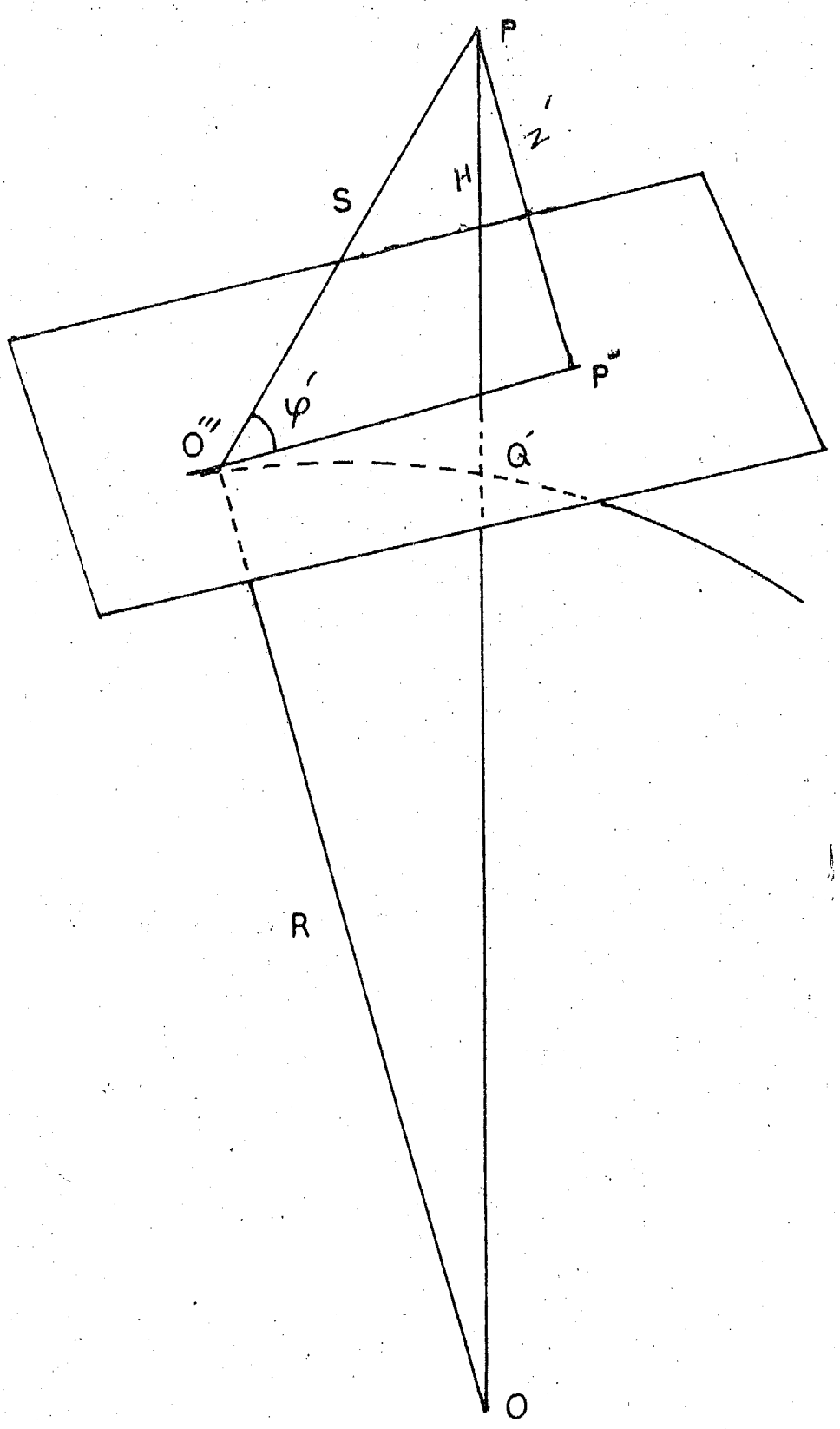

FIG . 40

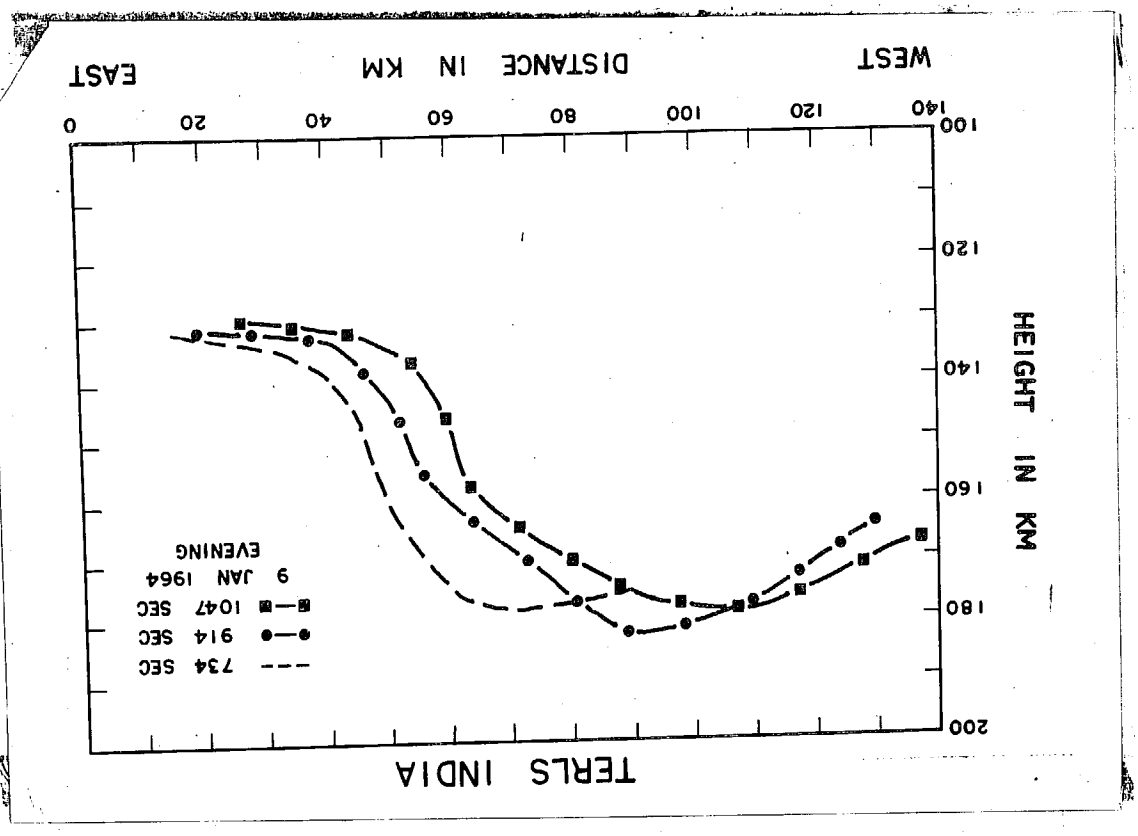

Fig. 41

Projections of the vapour trail released on 9 November 1964 1964 on east-west vertical plane at three different times.

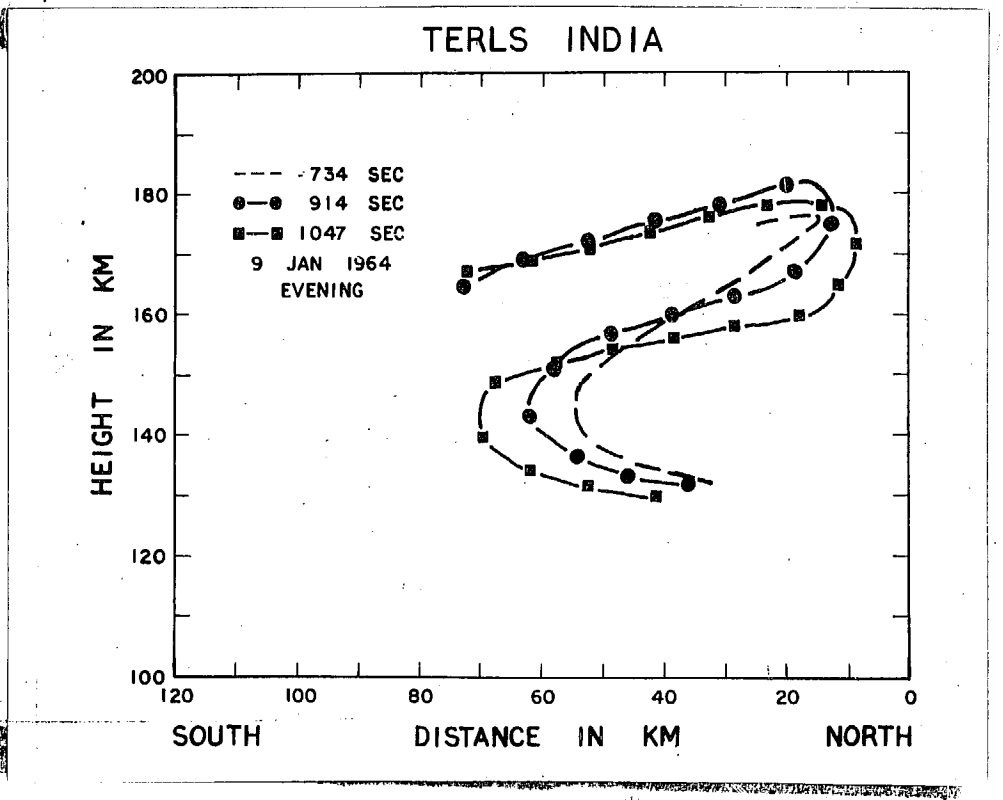

Two vertical planes, one in the east-west direction along the X-axis and the other in the north-south direction along the Y-axis were established at O'', the origin, with Z-axis as the line of intersection. The vapour points as obtained above were then projected on these two vertical planes. When these projections were joined by a smooth curve, they gave projections of the vapour trail on the east-west and north-south planes at a particular instant. This procedure was repeated for all the simultaneous photographs obtained at the time of observation of the vapour trail from the two camera sites. This gave the east-west and north-south projections of the complete vapour trail at different known times. Fig. 41 and Fig. 42 give, respectively, the projections of the vapour trails at different times on the east-west and north-south vertical planes for the launching on 9 November,1964. From these projections, the east-west and north-south displacements of the trail at different altitudes were read out and the velocity components were calculated, from the knowledge of the time interval between the first and the last projection. When these velocity components were compounded vectorially, the wind velocity and direction at different altitudes were obtained.

2.6. ERRORS IN DETERMINING HEIGHTS AND THE WIND VELOCITY

It is very difficult in the vapour cloud experiments to estimate the order of errors, as there are many sources of errors. These errors can be divided into two main groups viz. systematic errors and accidental errors.

2.6.1. Systematic errors.

Systematic errors are those errors whose causes can be easily detected and the corrections applied. In this experiment, there are many sources for such errors. Some of these sources are:

(i) the distortion produced in the vapour trail image by the camera lens,

(ii) the distortion in the objective of the micro-scope used for determining the X-Y coordinates on the trail photographs,

(iii) the refraction through the atmosphere, and

(iv) the refraction of the vapour cloud image through the glass plate which keeps the film in position.

Most of these errors are very small in magnitude compared to the accidental errors.

The distortion due to camera lens is most effective at the periphery of the field of view. The error due to this defect increases with the distance from the centre of the image field. The preliminary results have shown that up to 3 cm from the centre, the error due to lens distortion is only about 0.2%. As in most cases the major portion of the trail image fell within about 4 cm from the centre of the frame, no correction was applied for the distortion of the lens. Assuming that the error introduced is negligible, no attempt

has been made in the present work to determine the lens distortions and the estimation of this error.

The distortion produced by the objective of the microscope, while determining the coordinates, was ineffective, as all measurements were made by bringing the point under observation at the cross wires kept at the centre of the field of view.

The effect of refraction through the atmosphere is to displace the direction of the observed object towards the observer's zenith. This effect is more pronounced near the horizon than at higher elevations. In the present case the elevation of the camera axis was well above the horizon for all camera positions, the minimum being about 25° from Kodaikanal. At this elevation the correction for refraction[137] is only 2' 4". As this correction for other camera sites is much more less compared to the other errors, this correction was also not applied either for star positions or the vapour cloud points.

Before the image is formed on the film, the rays pass through a glass plate, which keeps the film flat and in its position. The image formed on the film would not be a correct reproduction of the trail, but the error would be proportional to the distance of the image point from the centre of the field of view. If the refractive index and the thickness of the glass plate are taken into account to calculate this error,

the maximum error due to this factor at a distance of 9 cm from the centre would be about 0.001 cm[133]. As the limit of accuracy of the microscope used was only 0.01 cm and in general the farthest point of the vapour trail image was much less than 9 cm from the centre of the film, this error was considered negligible.

2.6.2. Accidental errors.

These errors are due to unknown causes and to rectify these errors statistical methods may have to be used. These accidental errors are by far the most important errors in this experiment. These errors may arise

(i) due to the incorrect determination of the latitude and longitude of the camera position,

(ii) due to error in identifying the stars and reading the correct coordinates,

(iii) due to the error in drawing the central line on the vapour trail image and

(iv) due to the limit of accuracy of the coordinate measuring instrument. These errors are cumulative and add up. It is necessary to eliminate or reduce these errors as far as possible or to know correctly the extent of error due to these factors in determining the height of a vapour cloud point or the velocity of the wind at a particular height.

The values of latitudes and longitudes of the camera sites were taken from an earlier determination by Gulatee[128].

The cameras were set up as close to these points as possible and the necessary corrections were made whenever required. The determination of correct latitude and longitude could not be undertaken by the author.

To fix the orientation of the camera, the background starfield is used as discussed in section 2.5.2. If the stars are not properly identified, the determination of the orientation of the camera axis, the tilt of the camera and the focal length of the camera lens may all give wrong results. It is not only necessary to identify the stars correctly, but it is also necessary to read the coordinates of the stars accurately. If star picture exposed for a longer time is used for this purpose, the stars appear as long lines and it is necessary to read the star position either at the beginning or end of the exposure time in order to get the uniform observations. To reduce these errors considerably, many stars were identified in one frame of exposure and different pairs of the stars were used to determine the orientation of the camera axis, tilt of the camera and the focal length of the camera lens. The average of these values were taken to be correct values.

For the purpose of determining the winds at different heights, the vapour cloud is assumed to be cylindrically symmetrical and a central line is drawn on the vapour cloud image representing its axis. This is done by visually judging

the diameter of the cloud image and drawing the central line as accurately as possible. The error in drawing the central line visually is small at lower altitudes where the edges of the trail image are generally sharp. This error becomes large at higher altitudes, above about 120 km, where the trail image becomes diffused. It was assumed that the maximum error in drawing the central line is 1 mm below 120 km and about 3 mm above. The partial error introduced due to this effect is estimated and added in the estimation of errors in determining the height.

The other source of error in determining the height is the limit of accuracy of the x-y coordinate measuring instrument. The stereoscope used for the present purpose could read up to 0.01 cm which is the limit of its accuracy. Any error comparable to the error due to this limitation was considered in estimating the total error in determining the height.

3.6.3. Estimation of error in height determination.

The error in the height determination according to equation (41), due to the possible errors discussed above can be estimated by differentiating equation (41). For example, an error δs in drawing the central line, introduces an error in the values of elevation ($\delta\varphi$) and azimuth ($\delta\theta$) of a vapour cloud point. The error $\delta\varphi$ on the other hand, introduces a partial error Δz in the height of that vapour point.

This partial error is given by

$$\Delta z = \frac{1}{2}\left\{\frac{\partial k_1}{\partial \varphi_1}\cos\gamma_1 + \frac{\partial k_2}{\partial \varphi_1}\cos\gamma_2 + k_1\frac{\partial(\cos\gamma_1)}{\partial \varphi_1} + k_2\frac{\partial(\cos\gamma_2)}{\partial \varphi_1}\right\}d\varphi_1 \qquad (44)$$

where $$k_1 = \frac{(X_2-X_1)(\cos\alpha_1 - p\cos\alpha_2)+(Y_2-Y_1)(\cos\beta_1 - p\cos\beta_2)}{1-p^2}$$

$$k_2 = \frac{(X_2-X_1)(p\cos\alpha_1 - \cos\alpha_2)+(Y_2-Y_1)(p\cos\beta_1 - \cos\beta_2)}{1-p^2}$$

and $$p = \cos\alpha_1\cos\alpha_2 + \cos\beta_1\cos\beta_2 + \cos\gamma_1\cos\gamma_2$$

$(\cos\alpha_1, \cos\beta_1, \cos\gamma_1)$ being direction cosines of the line of sight to the vapour cloud point from the camera sites whose coordinates are (X_1, Y_1) with respect to the origin O'' on the earth's surface below the centre of the trail. The partial errors due to all the probable inaccuracies could be estimated with similar equations and the total error calculated. Table 7 gives the estimate of total error in calculating height at different altitudes.

The partial error in determining the height at an altitude of 175 km, due to an error of 10 minutes of arc in the determination of the latitude or the longitude, is about 0.6 km.

2.6.4. Estimation of error in wind velocity.

The major contribution to the error in determining the

Table 7.

Estimation of total error in calculating the height at different altitudes.

Height in km	Estimation of error in km
100	± 1.33
110	± 1.41
120	± 2.11
130	± 2.46
140	± 2.63
150	± 3.06
170	± 3.19

wind velocity comes from the inaccurate drawing of the central line representing the axis of vapour trail. The exposure times range from 3 seconds to 55 seconds and as the exposure is made, the diameter of the vapour trail expands, partially due to the diffusion of sodium atoms into the surrounding atmosphere but mostly due to the bodily motion of the vapour trail due to winds. These phenomena render the edges of the trail diffuse. The wind velocity at different heights may have any value between 5 m/sec to 150 m/sec and sometimes even more. On the average a wind velocity of about 60 m/sec can be considered. Usually a frame which has an exposure time of 10 seconds or 27 seconds is used in the analysis. Thus in 27 seconds, the vapour particles can be moved through ℓ = 1620 m. As a central line on the vapour trail is drawn representing the average time, the error in x or y may be

$$\Delta x \leq \frac{1620}{2} \quad \text{and} \quad \Delta Y \leq \frac{1620}{2}$$

or $$\Delta x \leq \frac{\ell}{2} \quad \text{and} \quad \Delta Y \leq \frac{\ell}{2}$$

As two such frames separated by time $t_2 - t_1$, are used in determining the positions of vapour points P_1 and P_2 in order to calculate the wind velocity

$$V = \frac{P_1 \; P_2}{t_2 - t_1},$$

the error in $P_1 P_2$ is

$$\Delta P_1 P_2 \leq \frac{\ell_1}{2} + \frac{\ell_2}{2}$$

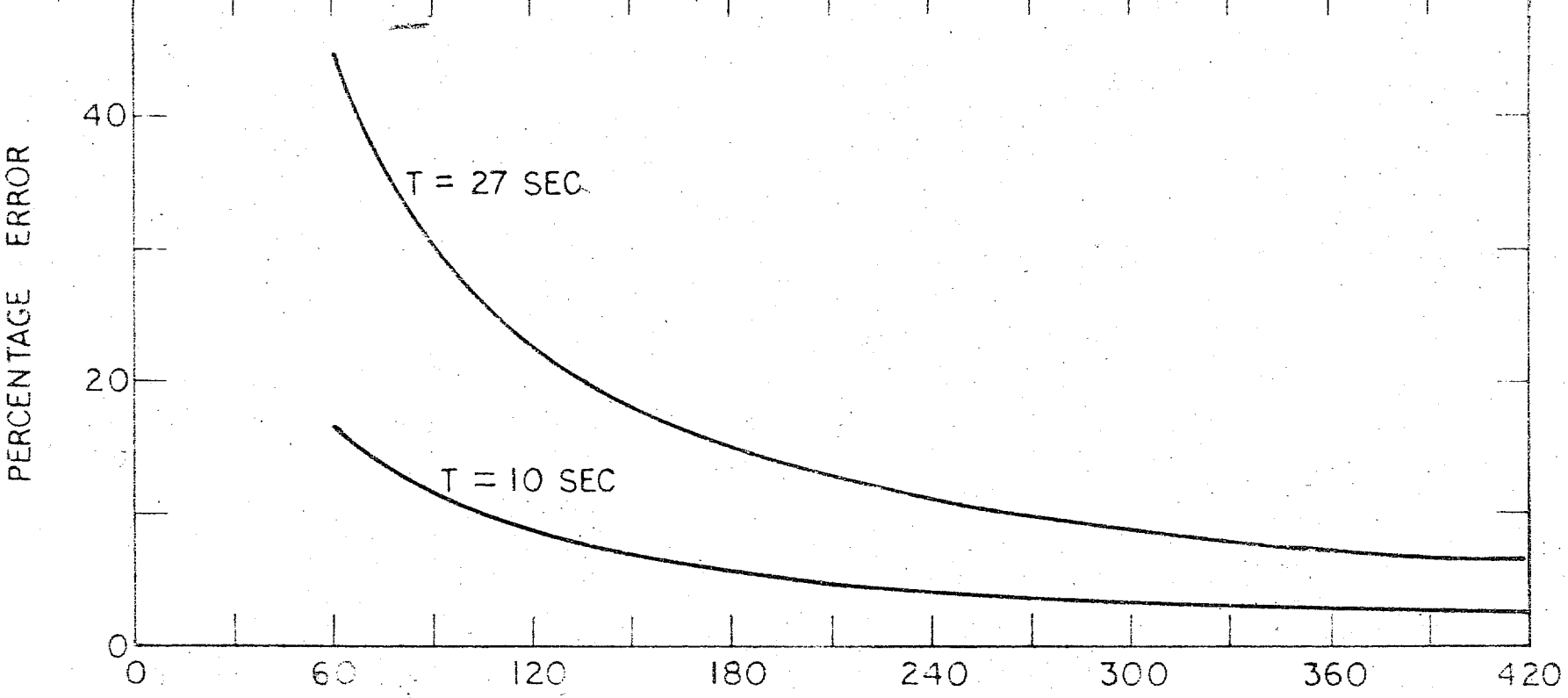

PERCENTAGE ERROR IN WIND SPEED WITH RESPECT TO TIME INTERVAL

FIG.43

PERCENTAGE ERROR IN CALCULATING WIND VELOCITY FROM TWO VAPOUR TRAIL PICTURES TAKEN AT DIFFERENT TIME INTERVALS FOR TWO DIFFERENT EXPOSURE TIMES.

If $l_1 \simeq l_2$, then $\Delta P_1 P_2 \leq l_1$

Now the error in determining the wind velocity is

$$\Delta V = \frac{\Delta P_1 P_2}{t_2 - t_1}$$

or $$\Delta V \leq \frac{l_1}{t_2 - t_1}$$

Thus if two frames separated by 120 seconds are considered to calculate the wind velocity, the error in velocity

$$\Delta V = \frac{1620}{120} \simeq 14 \text{ m/sec}$$

In general the relation for error in the wind velocity is given by

$$\Delta V = \frac{V T}{t_2 - t_1}$$

where T is the time of exposure and V is the velocity. The relative error is then given by

$$\frac{\Delta V}{V} = \frac{T}{t_2 - t_1}$$

Thus the relative error depends only on the time of exposure and the time interval between the frames selected. Fig. 43 gives the percentage error in wind velocity for two exposure times, T = 10 seconds and T = 27 seconds.

CHAPTER III

EXPERIMENTAL RESULTS AND DISCUSSIONS

3.1. EXPERIMENTAL RESULTS

The results obtained from six sodium vapour trail experiments conducted at the Thumba Equatorial Rocket Launching Station (TERLS), India, during 1963 and 1964 are presented in this section. Table 8 gives the particulars of these six rocket launchings.

From the photographic records of the vapour trails, obtained at the camera sites, winds in the upper atmosphere were derived according to the method described in Chapter II. The results of the individual launchings are presented in what follows:

The meridional and zonal components of the winds at each altitude, determined from the vapour trail profiles, are plotted in Fig. 44 to Fig. 49 for individual launchings.

In Fig. 50 to Fig. 55 the wind speeds at different heights, obtained during each launching, are shown separately. These figures are very useful for the study of the speed profiles with height, and give a good idea of the kinetic energy content of the atmosphere at different heights. Fig.56 gives the directions of wind velocity vector at different heights for all the six launchings.

Fig. 57 to Fig. 62 give the wind velocity hodographs

Latitude: 8° 32' Longitude: 76° 52'

Date	Time of launch I.S.T.*	Altitude range in which data are available	Remarks	
1. 21 November 1963	1825	100 to 150 km	First rocket launching from TERLS	
2. 8 January 1964	1845	103 to 190 km		
3. 12 January 1964	0556	107 to 172 km		
4. 6 November 1964	0532	102 to 116 km 146 to 170 km	Data between 116 and 146 km not available due to bad weather and clouds.	These three launchings are part of third series of COSPAR organised synoptic sounding rocket investigations.
5. 9 November 1964	1824	130 to 176 km	Data up to 130 km not available due to cloudy condition of sky.	
6. 10 November 1964	0535	108 to 176 km		

* I.S.T. = 82.5° E meridian time, the Indian Standard Time.

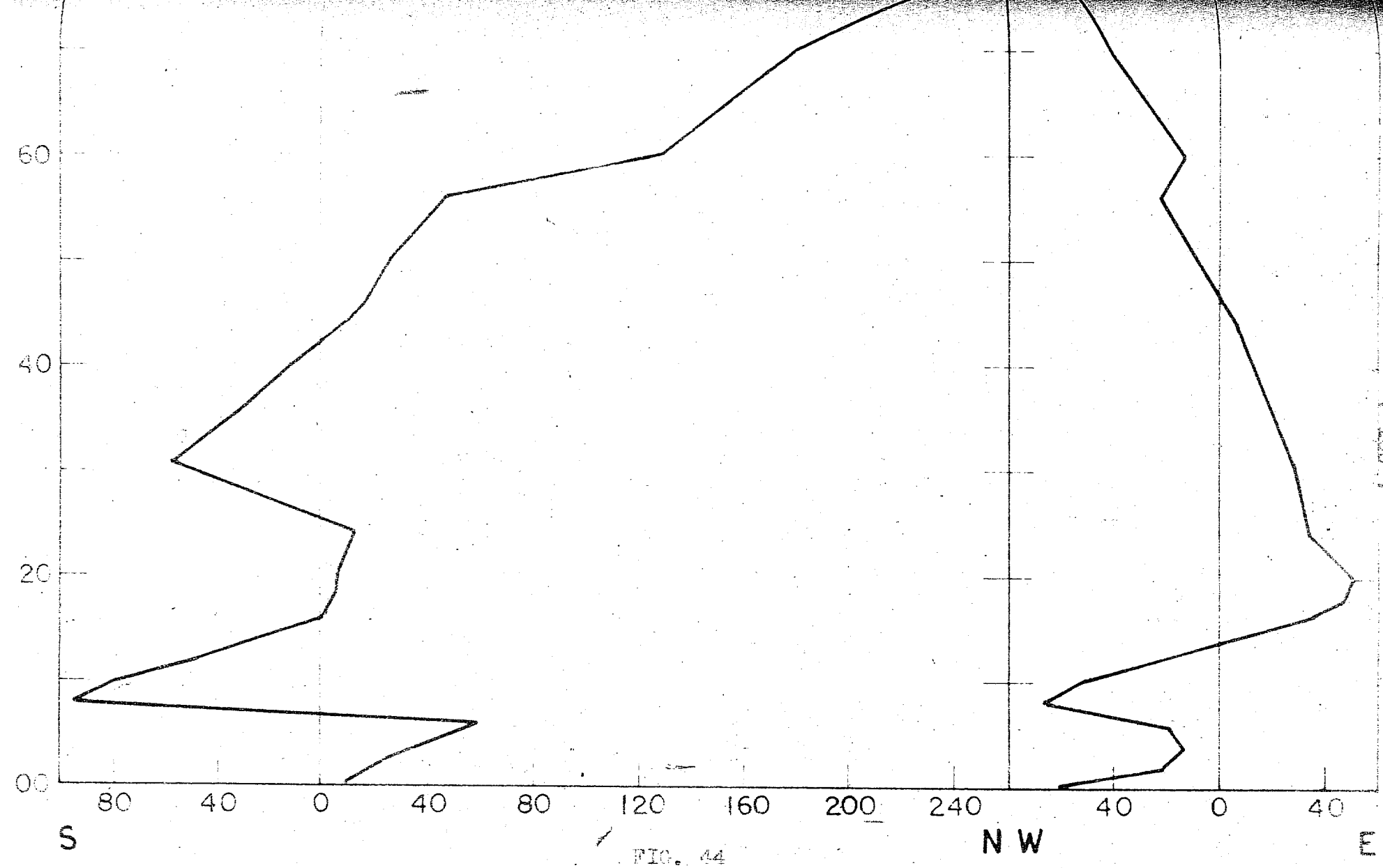

FIG. 44

[illegible] ANALYTICAL COMPUTATIONS OF UTI [illegible] WINDS AT TARLS ON 21 NOVEMBER 1963 [illegible]

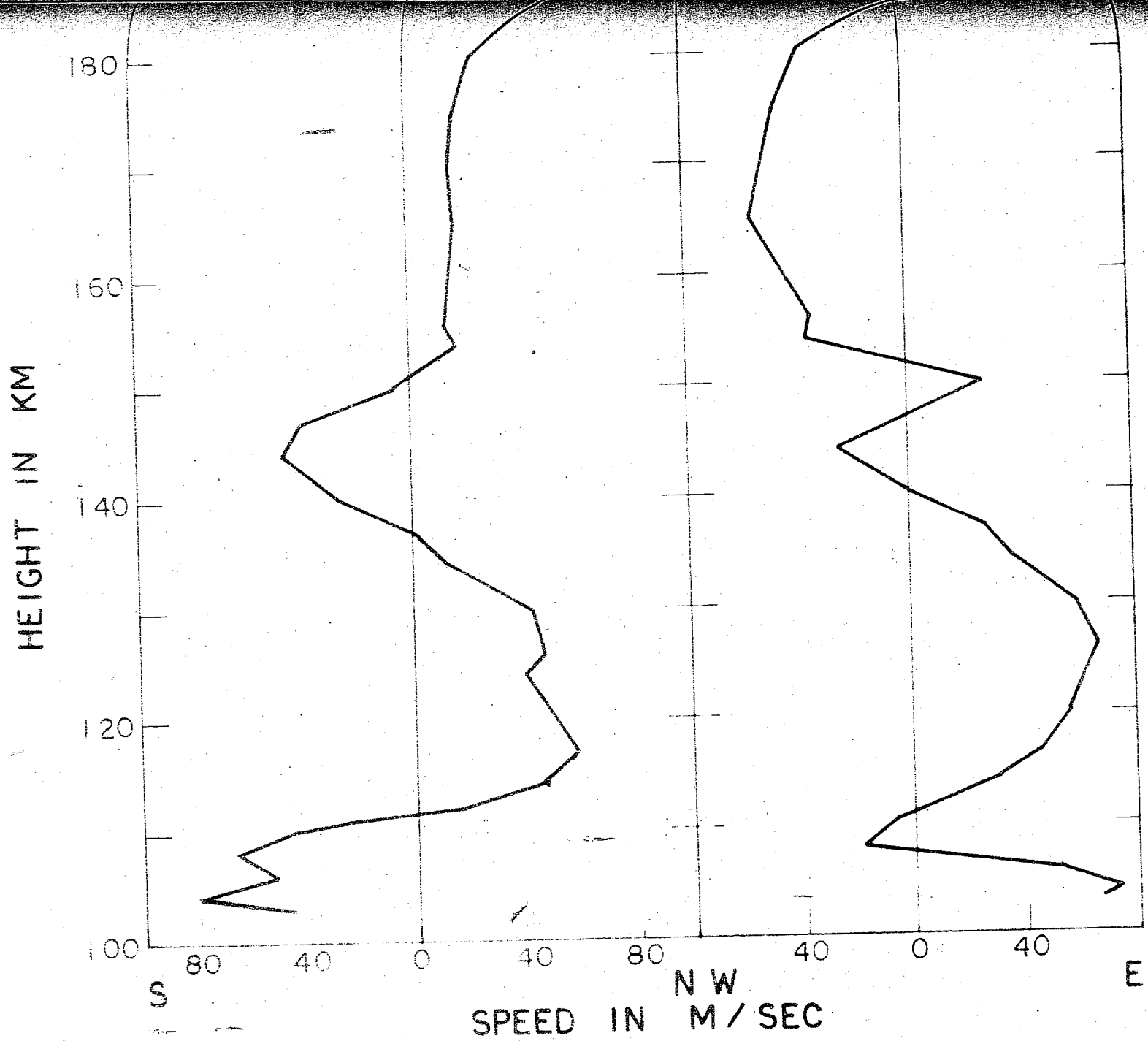

DISTRIBUTION OF UPPER ATMOSPHERE WINDS AT TERLS ON 8 JANUARY 1964 EVENING

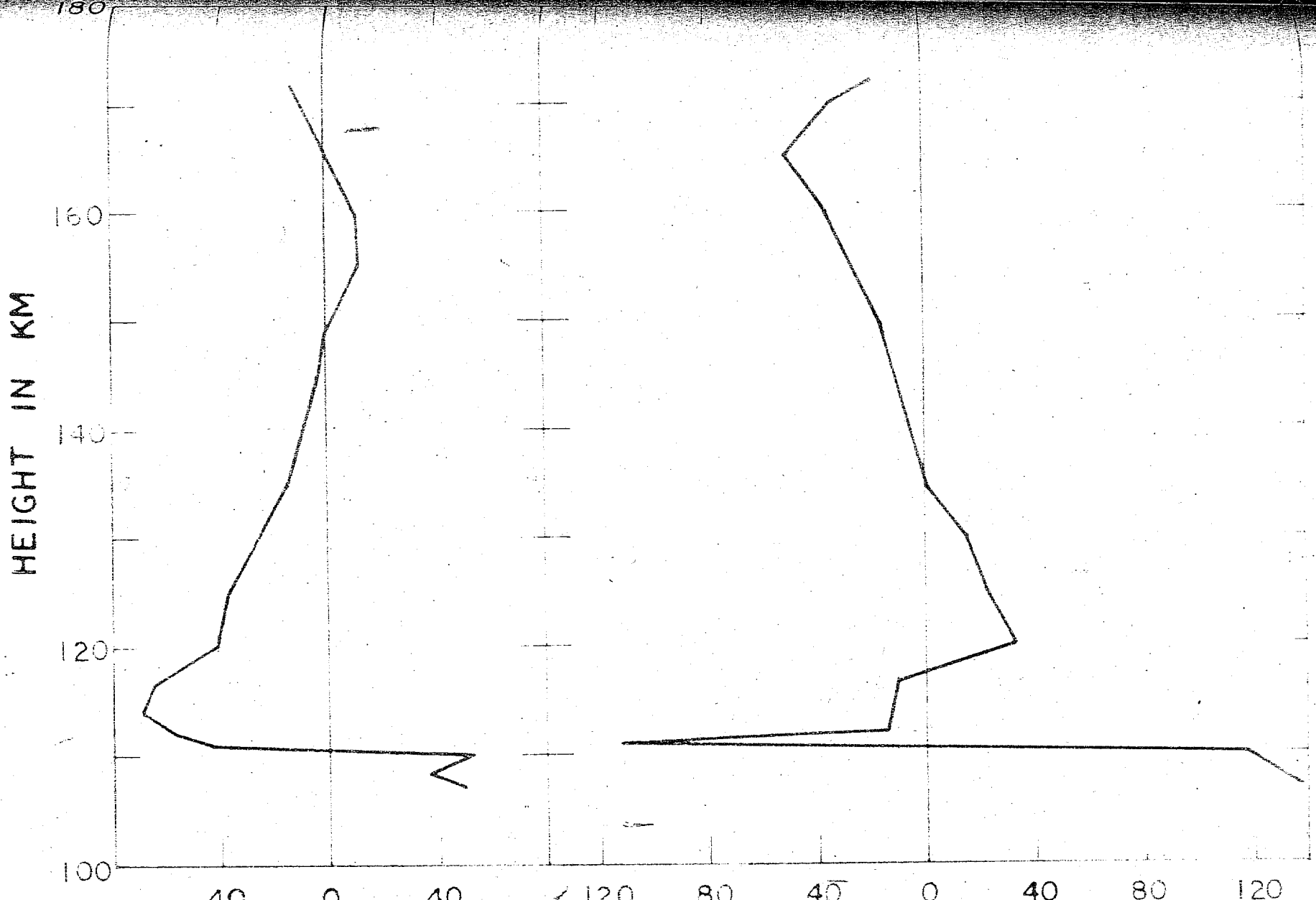

FIG. 46

MERIDIONAL AND ZONAL COMPONENTS OF UP TO 60 KM WINDS AT TERLS ON 12 JANUARY 1964 [illegible]

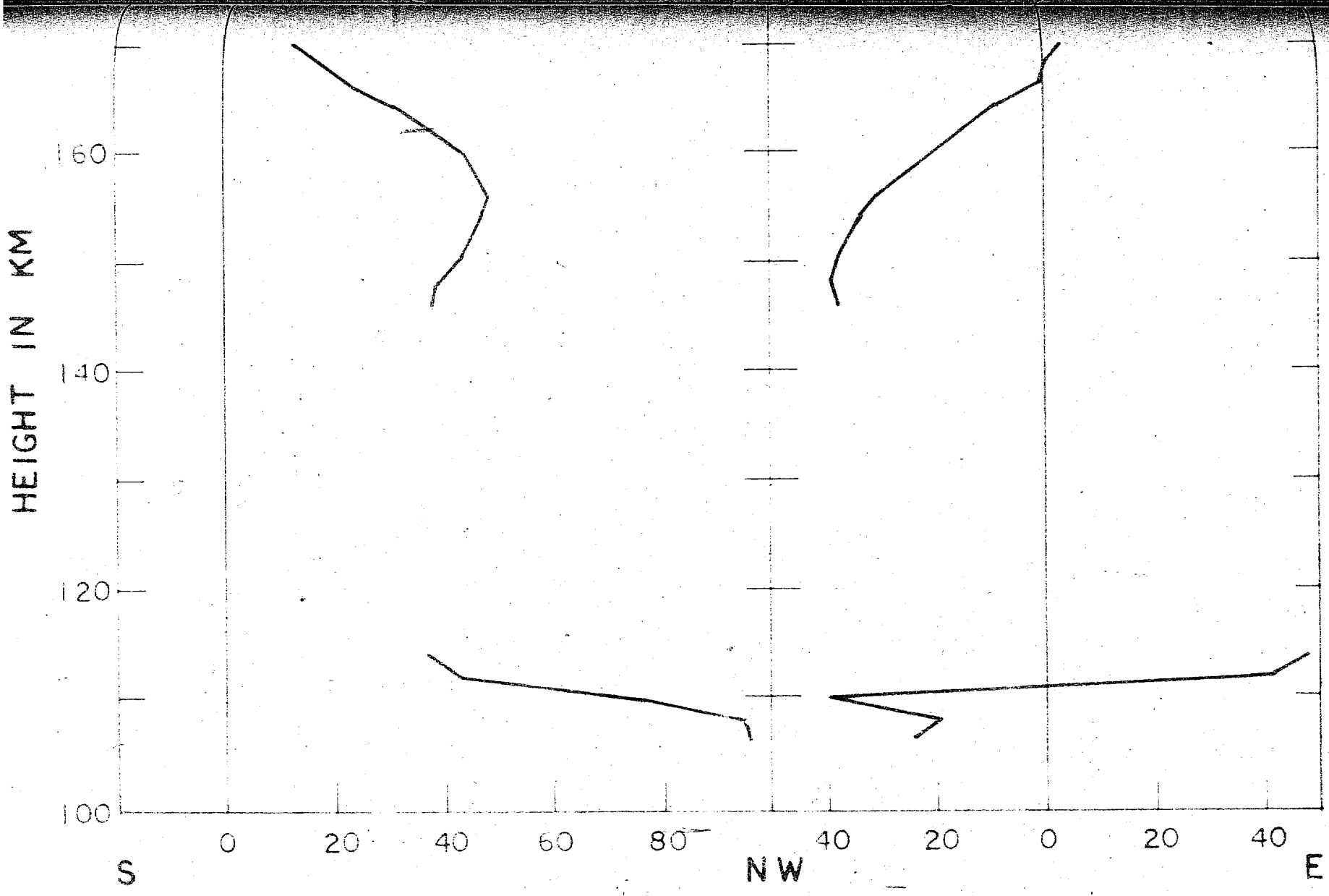

FIG. 47

MERIDIONAL AND ZONAL COMPONENTS OF UPPER ATMOSPHERE WINDS AT TERLS ON 6 NOVEMBER 1964 MORNING

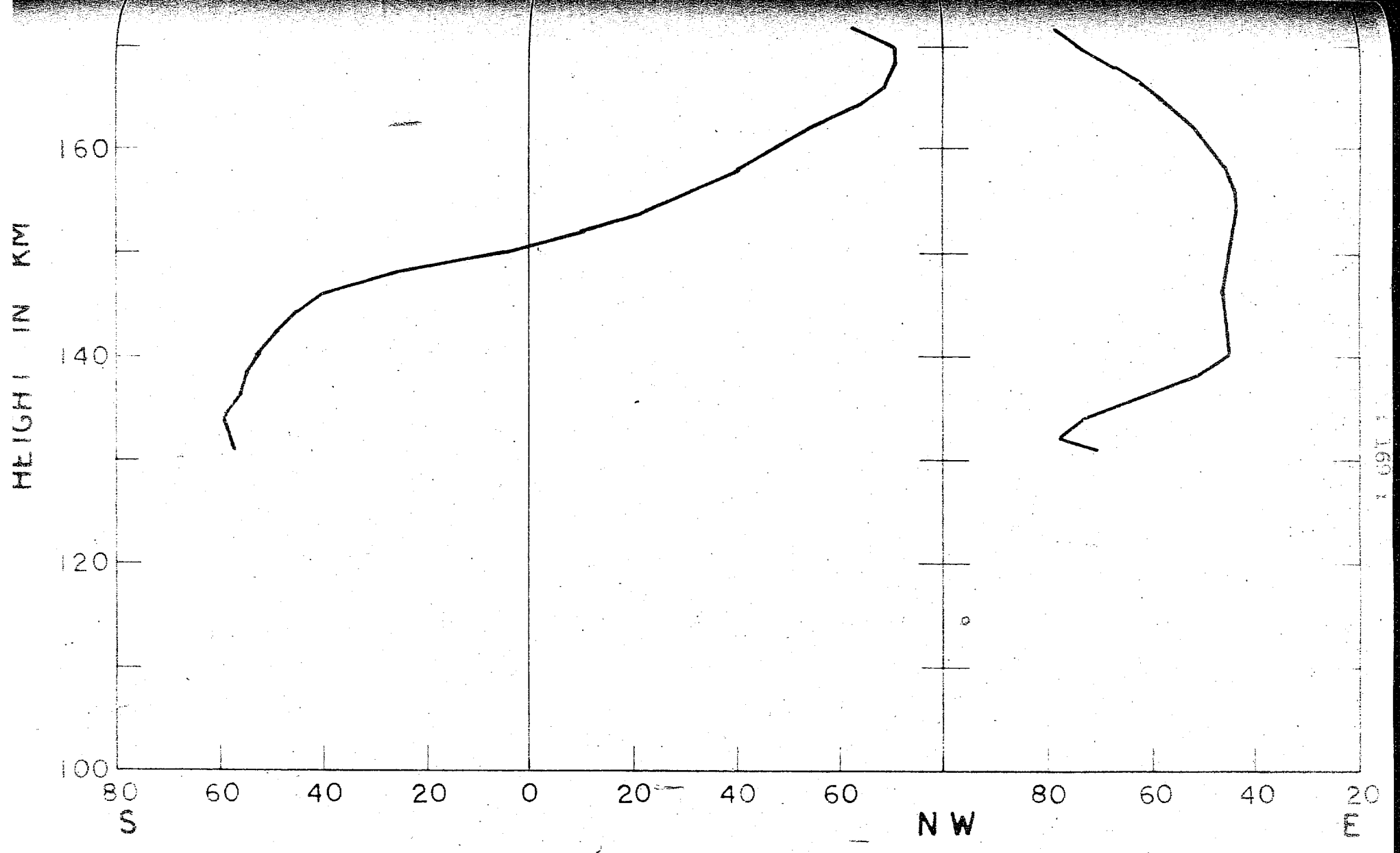

FIG. 48

MERIDIONAL AND ZONAL COMPONENTS OF UPPER ATMOSPHERE WINDS AT TERLS ON 9 NOVEMBER 1964 EVENING

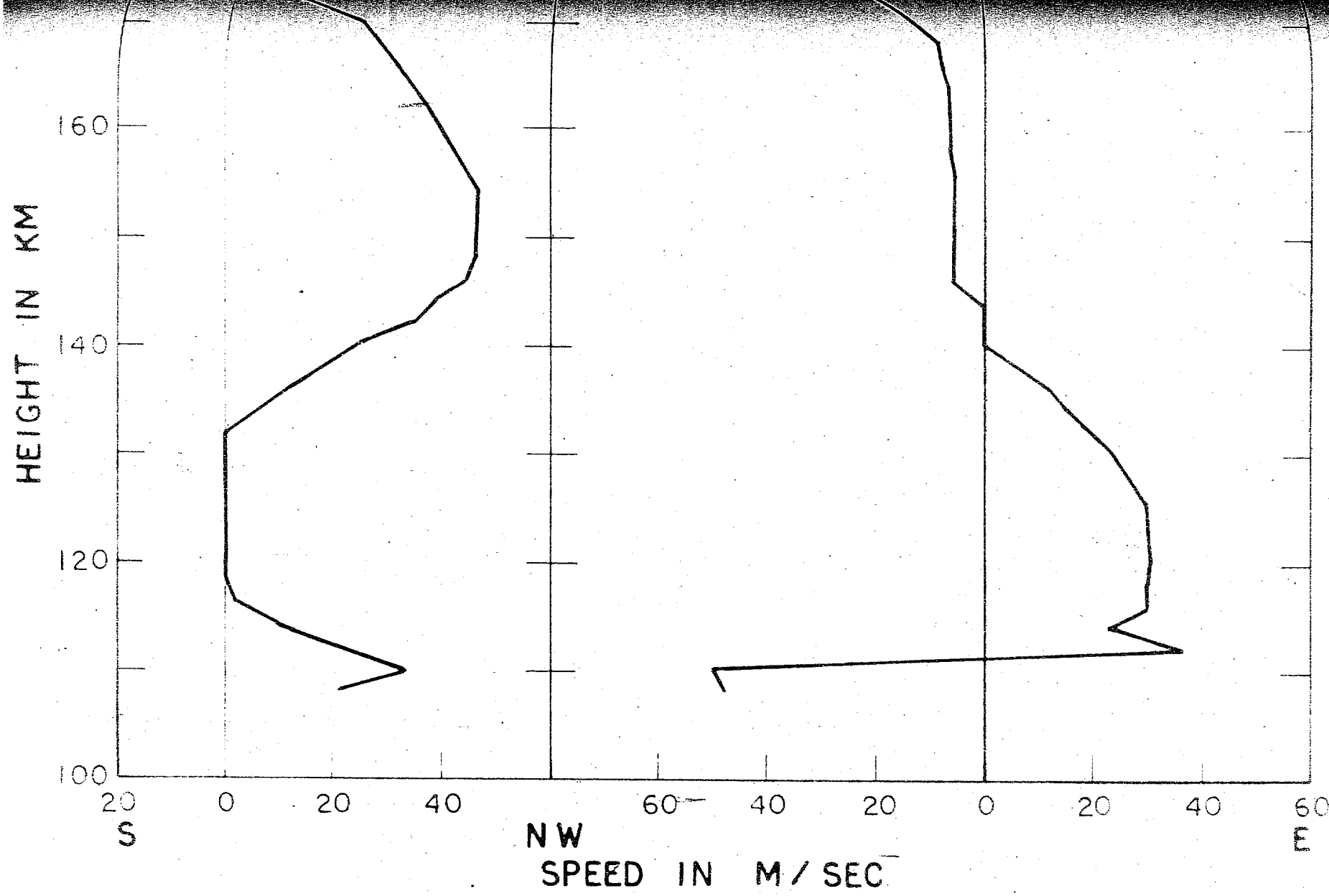

FIG.49

MERIDIONAL AND ZONAL COMPONENTS OF UPPER ATMOSPHERE WINDS AT TERLS ON 10 NOVEMBER 1964 MORNING

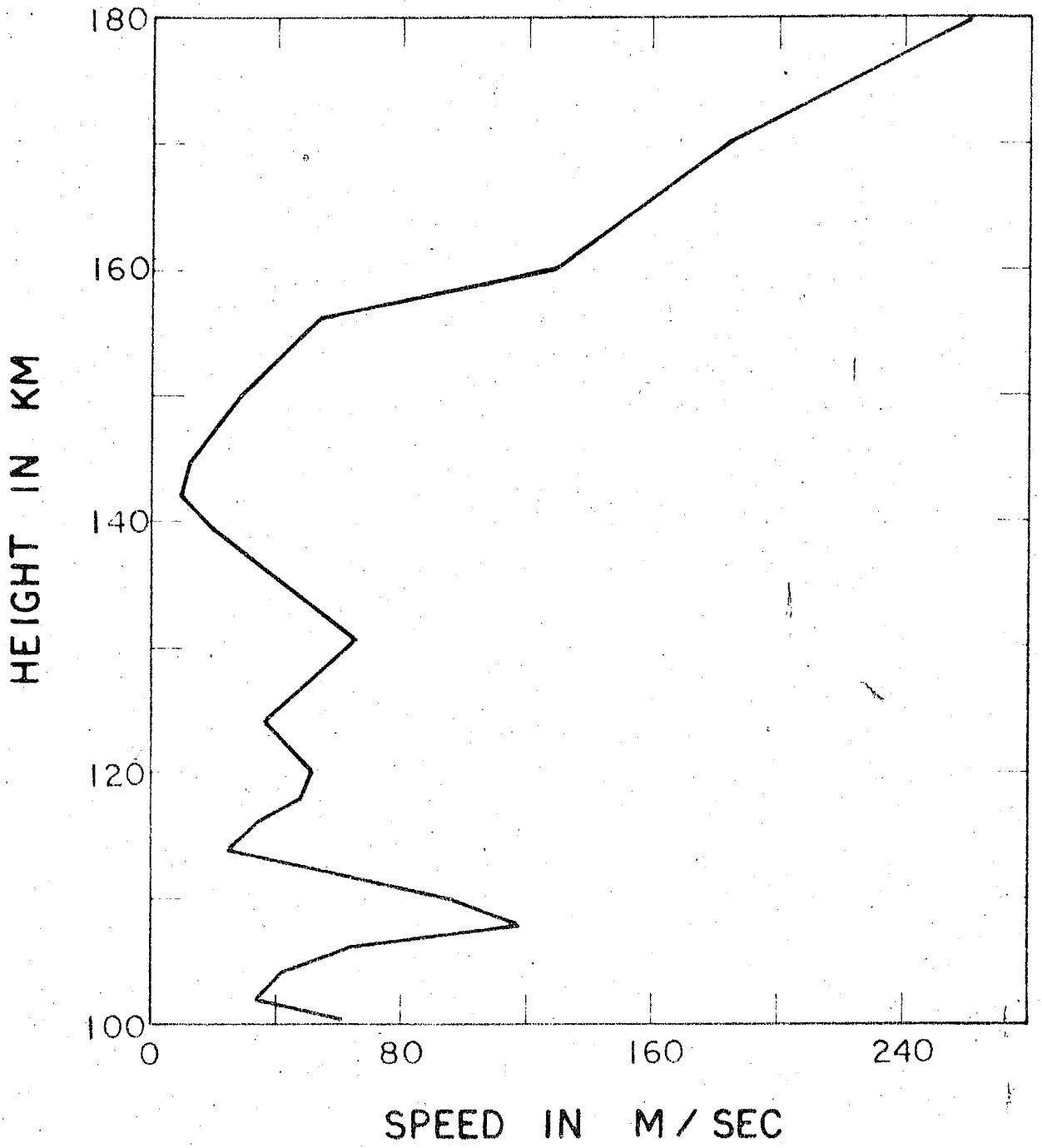

FIG. 50

VARIATION OF NEUTRAL UPPER ATMOSPHERE WIND SPEEDS WITH HEIGHT AT TERLS ON 21 NOVEMBER 1963 EVENING

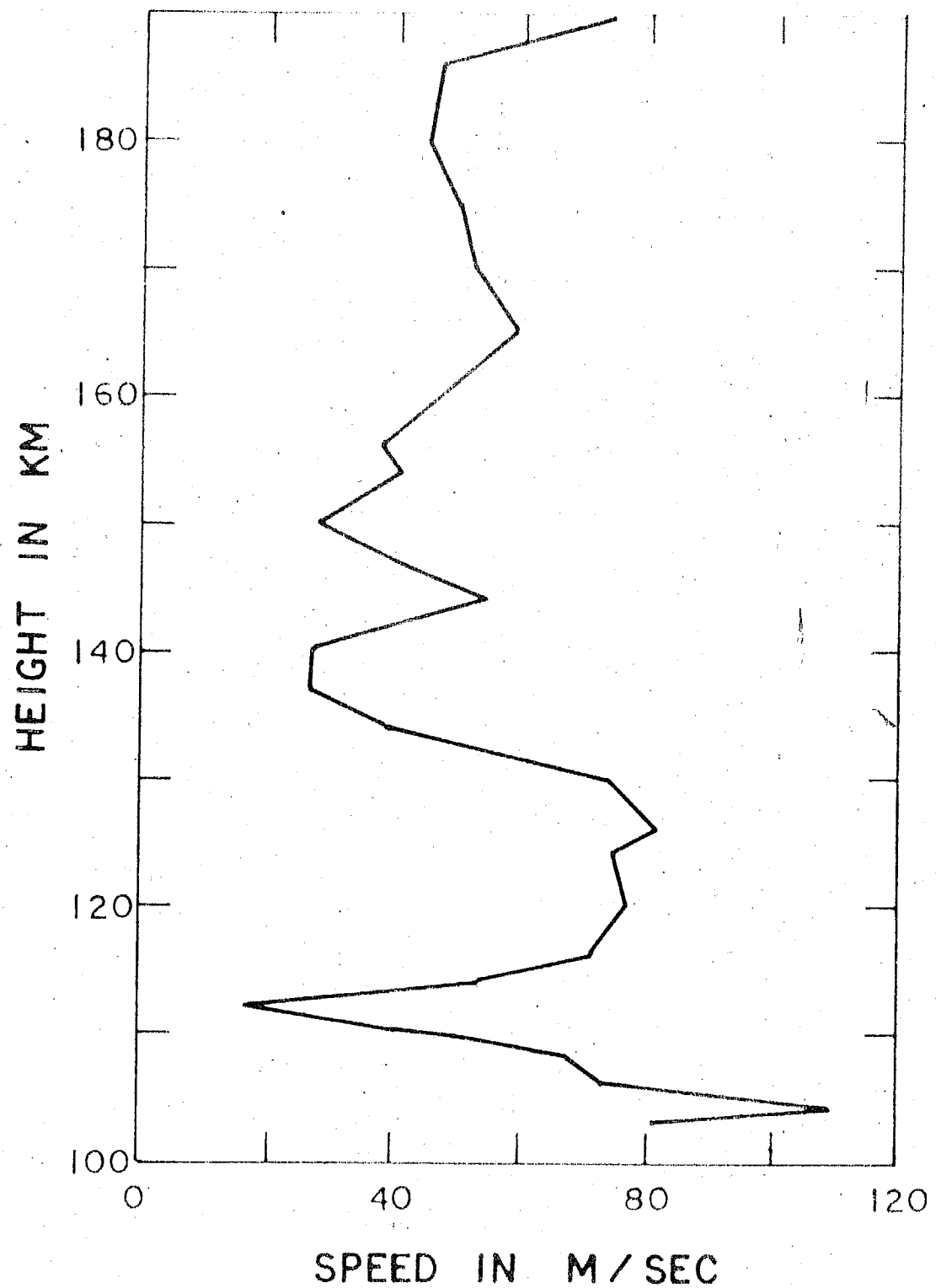

FIG. 51

VARIATION OF NEUTRAL UPPER ATMOSPHERIC WIND SPEEDS WITH HEIGHT AT TERLS ON 6 JANUARY 1964 EVENING

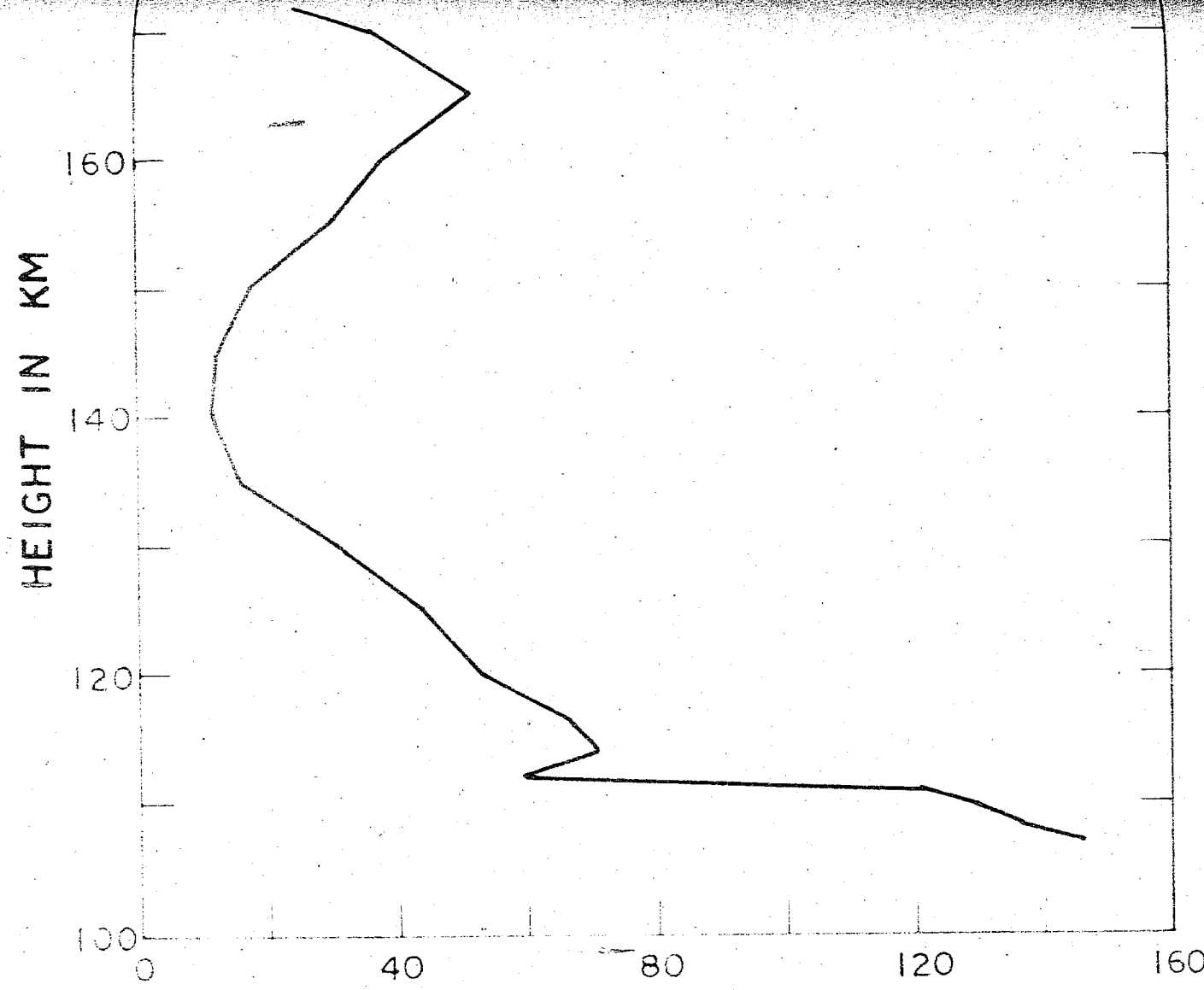

FIG. 52

VARIATION OF NEUTRAL UPPER ATMOSPHERE WIND SPEEDS WITH HEIGHT AT TERLS ON 12 JANUARY 1964 MORNING

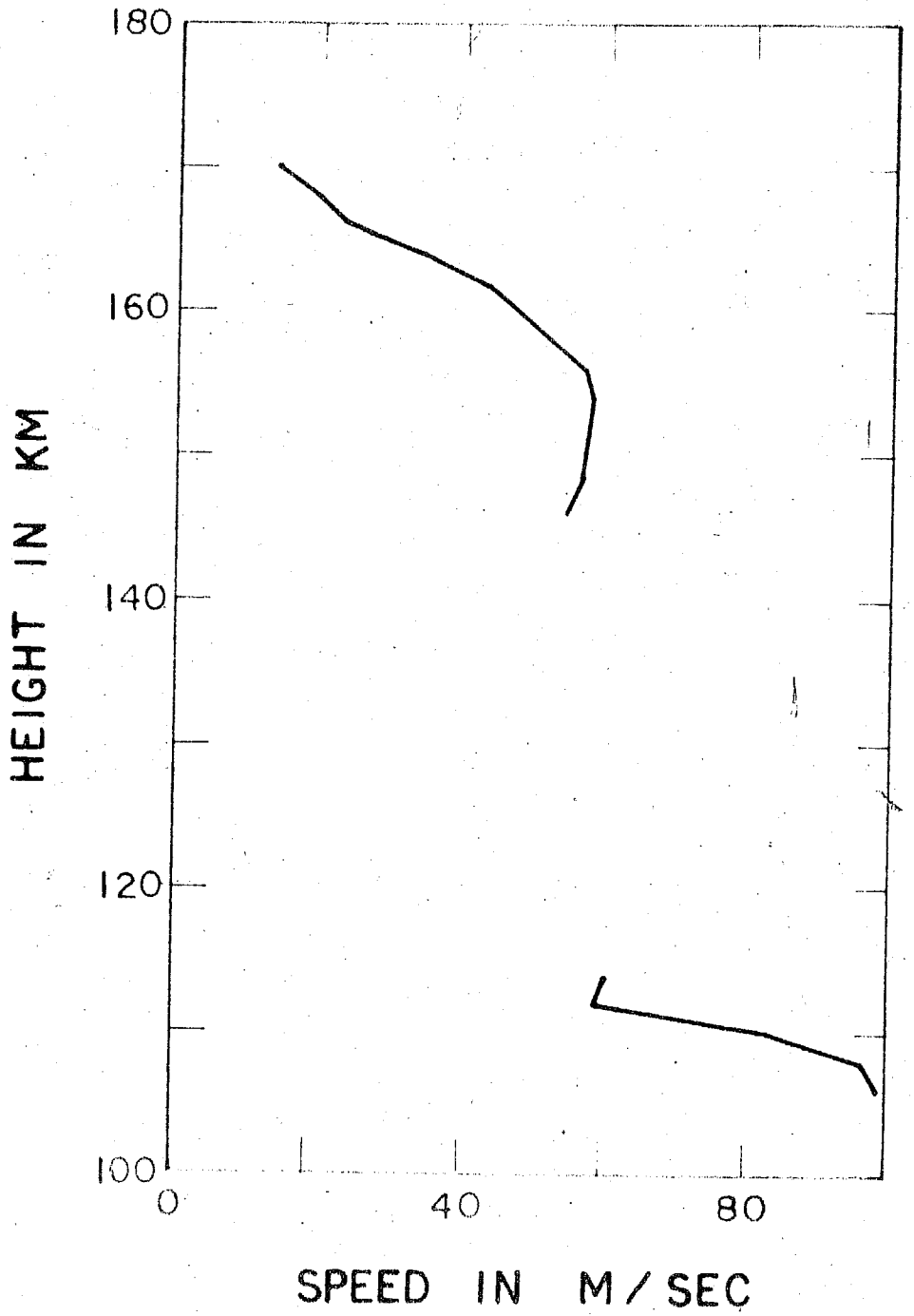

FIG. 53

VARIATION OF NEUTRAL UPPER ATMOSPHERE WIND SPEEDS WITH HEIGHT AT TERLS ON 6 NOVEMBER 1964 MORNING

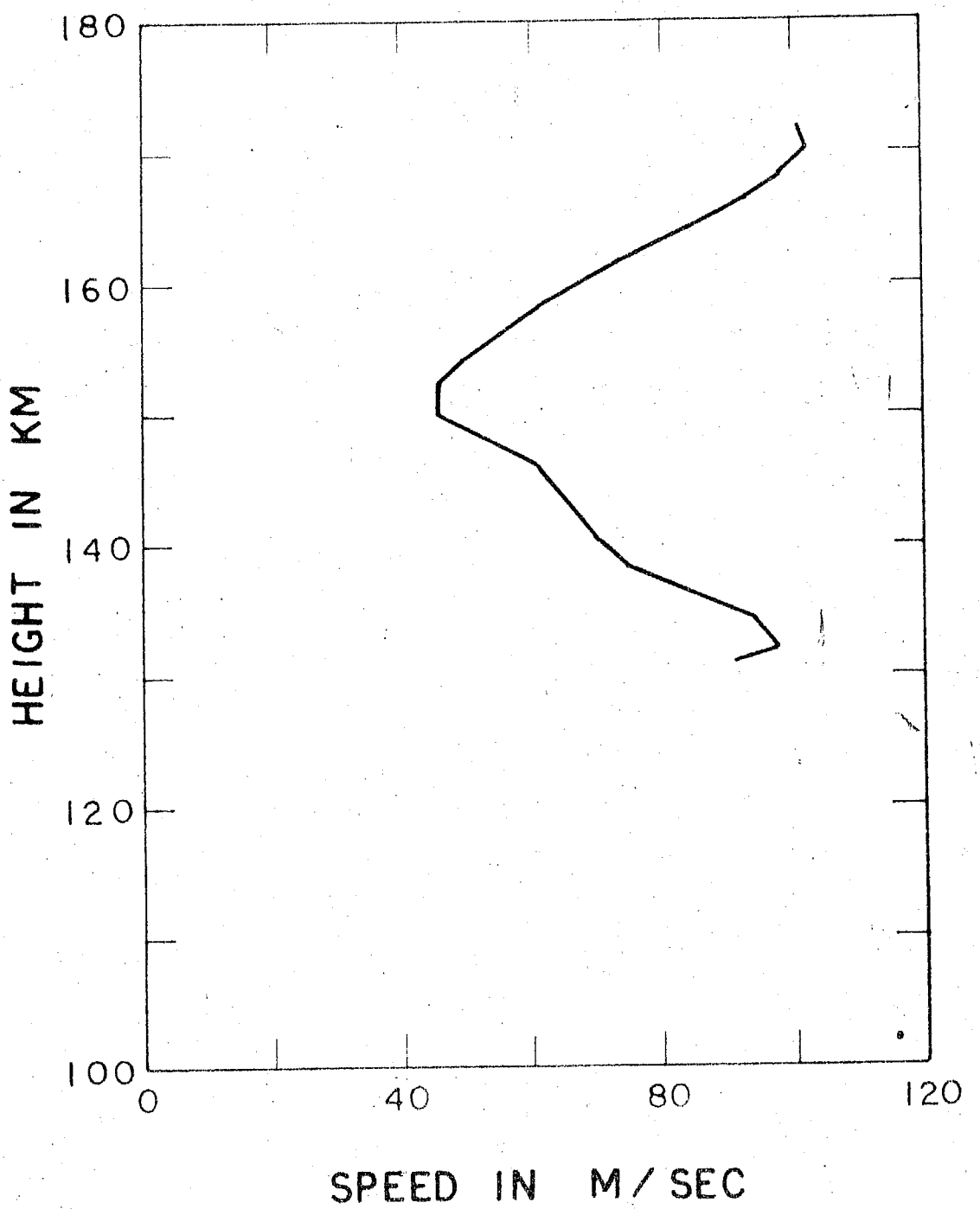

FIG.54

VARIATION OF NEUTRAL UPPER ATMOSPHERE WINDS SPEEDS WITH HEIGHT AT TERLS ON 9 NOVEMBER 1964 EVENING

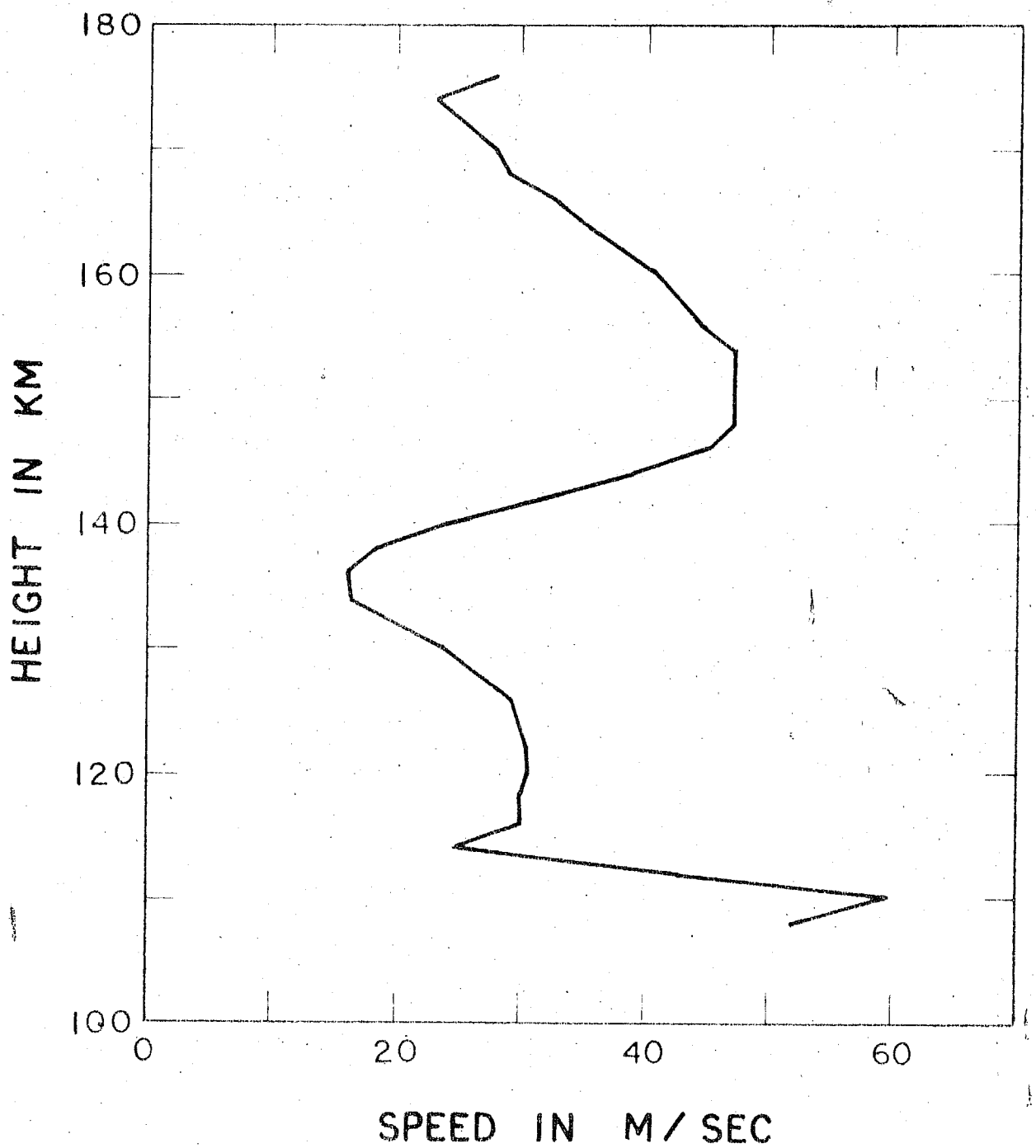

FIG. 55

VARIATION OF NEUTRAL UPPER ATMOSPHERE WIND SPEEDS WITH HEIGHT AT TERLS ON 10 NOVEMBER 1964 MORNING

for each launching separately. In each figure, the wind vectors at different altitudes, at the time of observation, are represented by dots, •, which are the end points of the vectors. The altitude is indicated in each case near the respective dot. A line joining the origin to any one dot gives the magnitude of that vector, and the direction of the wind at that altitude is from the origin towards the dot. The hodographs are obtained by joining these dots (end points) by a smooth line. The wind vectors towards north and towards east are taken as positive. The directions are measured from north through east, that is, the eastward wind has a direction of 90^{o} . The hodograph is very useful in studying the variation of wind vector with height.

Tables 9 to 14 give the magnitude and direction of the wind velocity vector at different heights for individual launchings. The same data are given at 2 km height intervals for comparison in Table 15. Table 16 gives the north and east components at different heights for the six launchings.

3.2. DISCUSSION OF RESULTS

3.2.1 Meridional component of winds.

The north and south components of wind vectors at different heights are given separately for each launching in Fig. 44 to Fig. 49. The same results are plotted on one single diagram in Fig. 63 for comparison with each other.

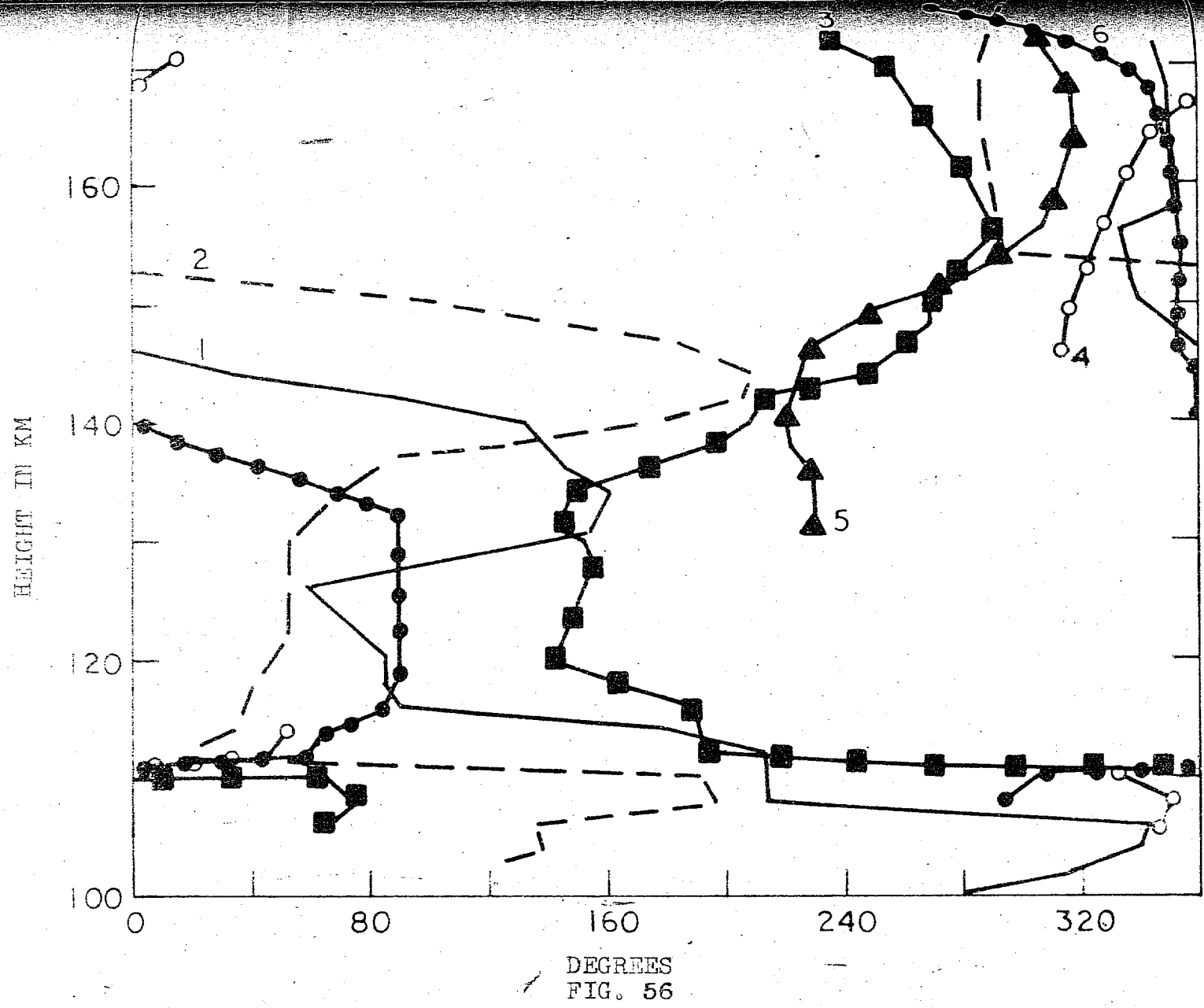

FIG. 56

DIRECTIONS OF THE NEUTRAL UPPER ATMOSPHERIC WIND VECTORS AT DIFFERENT HEIGHTS FOR ALL THE SIX LAUNCHINGS AT TERLS

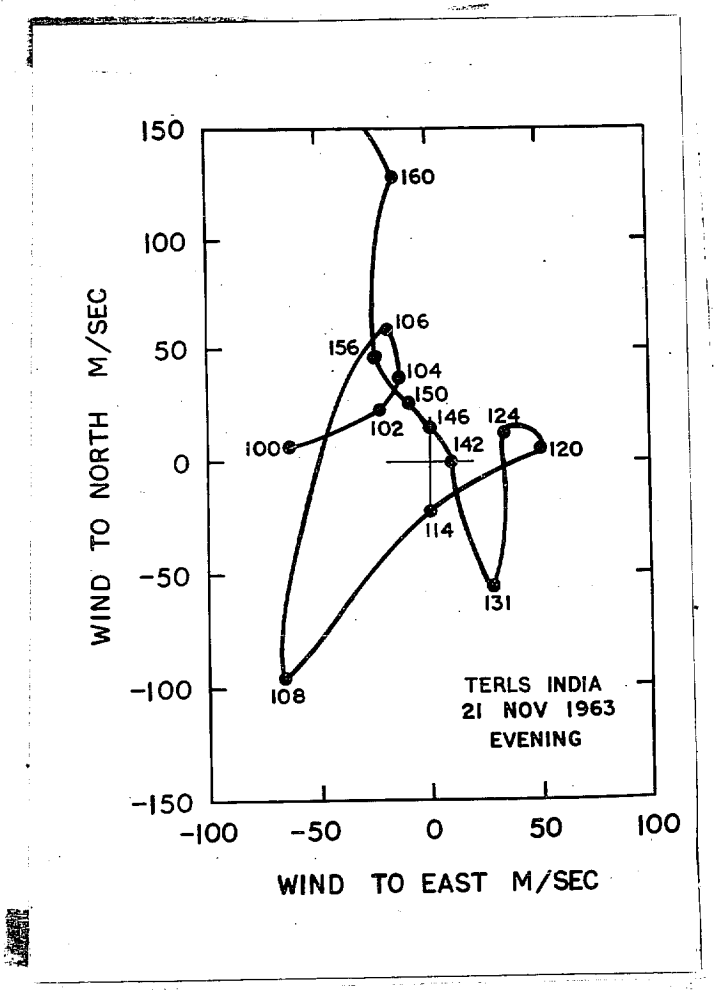

Fig. 67

Hodograph of the neutral upper atmospheric wind vectors at TERLS on 21 November 1963 evening

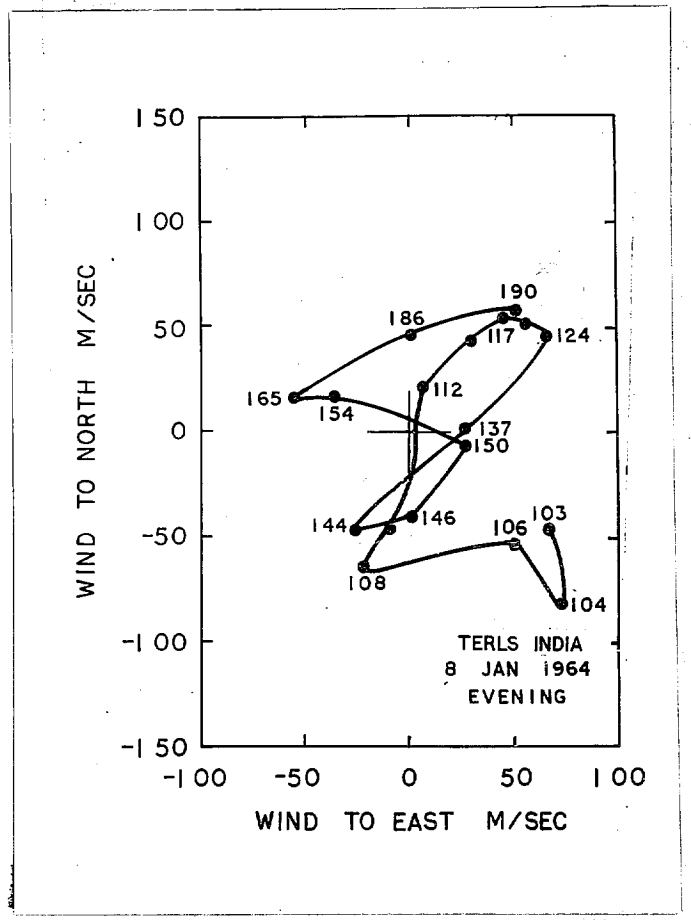

Fig. 68

Hodograph of the neutral upper atmospheric wind vectors at TERLS on 8 January 1964 evening

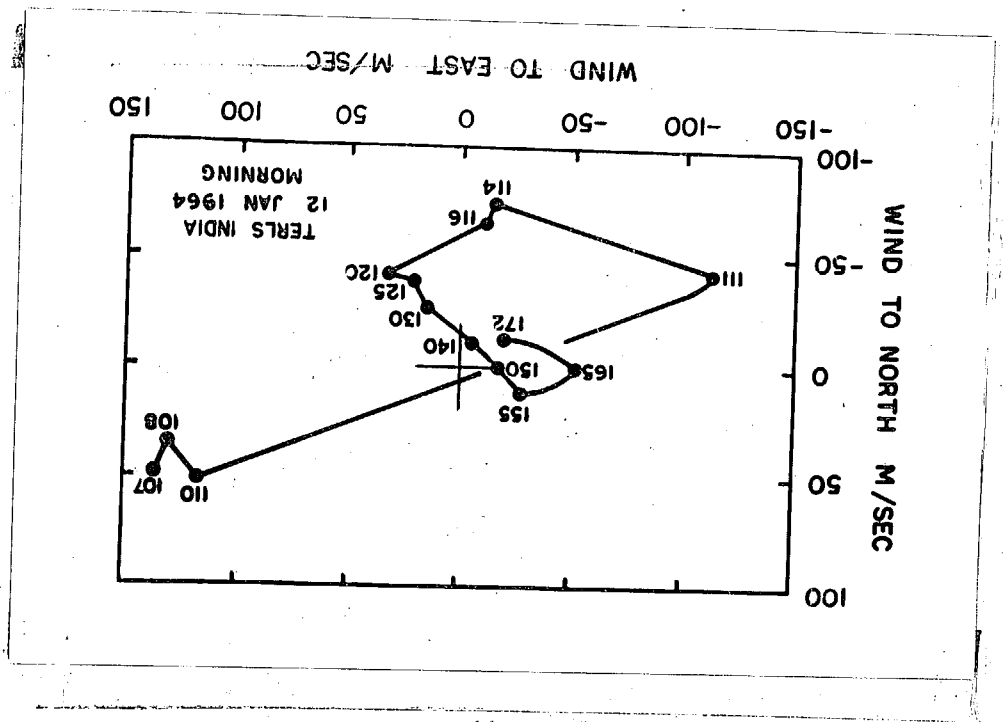

Fig. 59

Hodograph of the neutral upper atmospheric wind vectors on 12 January, 1964 morning

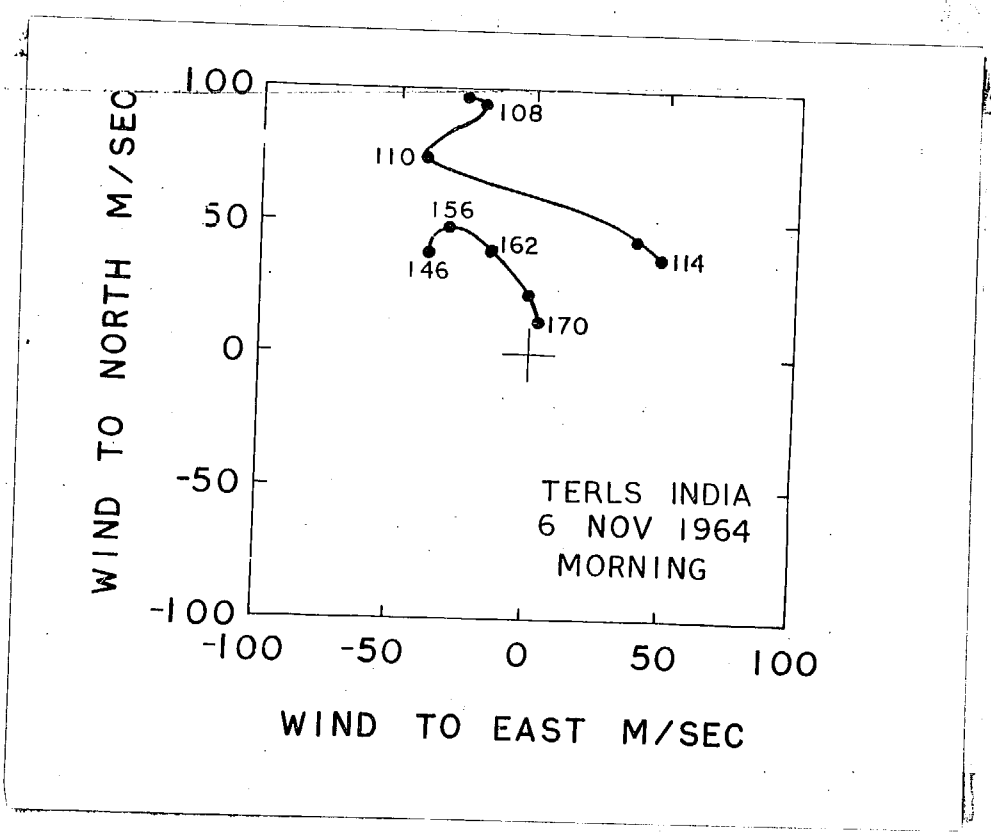

Fig. 60

Hodograph of the neutral upper atmospheric wind vectors on

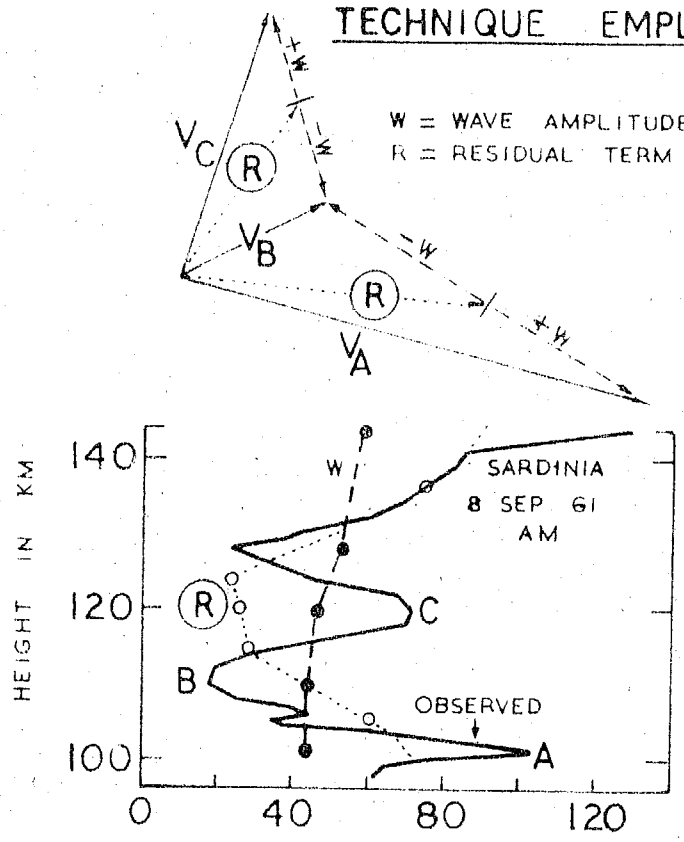

FIG. 75

VECTORIAL RESOLUTION TECHNIQUE TO DETERMINE INTERNAL GRAVITY WAVE COMPONENT AND ITS RESULTS IN THE CASE OF ONE SODIUM WIND PROFILE FROM SARDINA (KOCHANSKI[1])

called the residual term $\vec{R}$. Kochanski[1] analysed data from 64 vapour trails from Eglin, Wallops Island, Sardinia and Fort Churchill and observed that the amplitude of wave motion W increased with height from 80 km onwards and reached a maximum of about 60 m/sec at about 103 km. The amplitude then slowly decreased. The direction of the vector $\vec{W}$ was generally close to the direction of associated velocity maximum of the observed wind. The vector + $\vec{W}$ seemed to have some preferred directions showing that it is polarised. It was also observed that the amplitude of W showed a seasonal variation.

The technique used by Kochanski was applied to the data presented in section 3.1 of this chapter to separate the component due to internal atmospheric gravity wave motion. The average values of W were calculated at different heights for the morning and the evening launchings separately, and also average value for all the six launchings. Fig. 76 shows the variation with height of the amplitude of internal atmospheric gravity waves (W) for the evening, the morning and also the average of both. Below 110 km, the value of W is available only from a single evening launching and therefore it is taken as a representative of the situation up to 110 km with reservations. However, it is seen from the figure that the average value is maximum around 106 km and decreases above this height. This is in good agreement with Kochanski's observations[1]. The value of W reaches a minimum around 125 km and then it increases with increasing height. Such an increase is not observed in middle latitude studies.

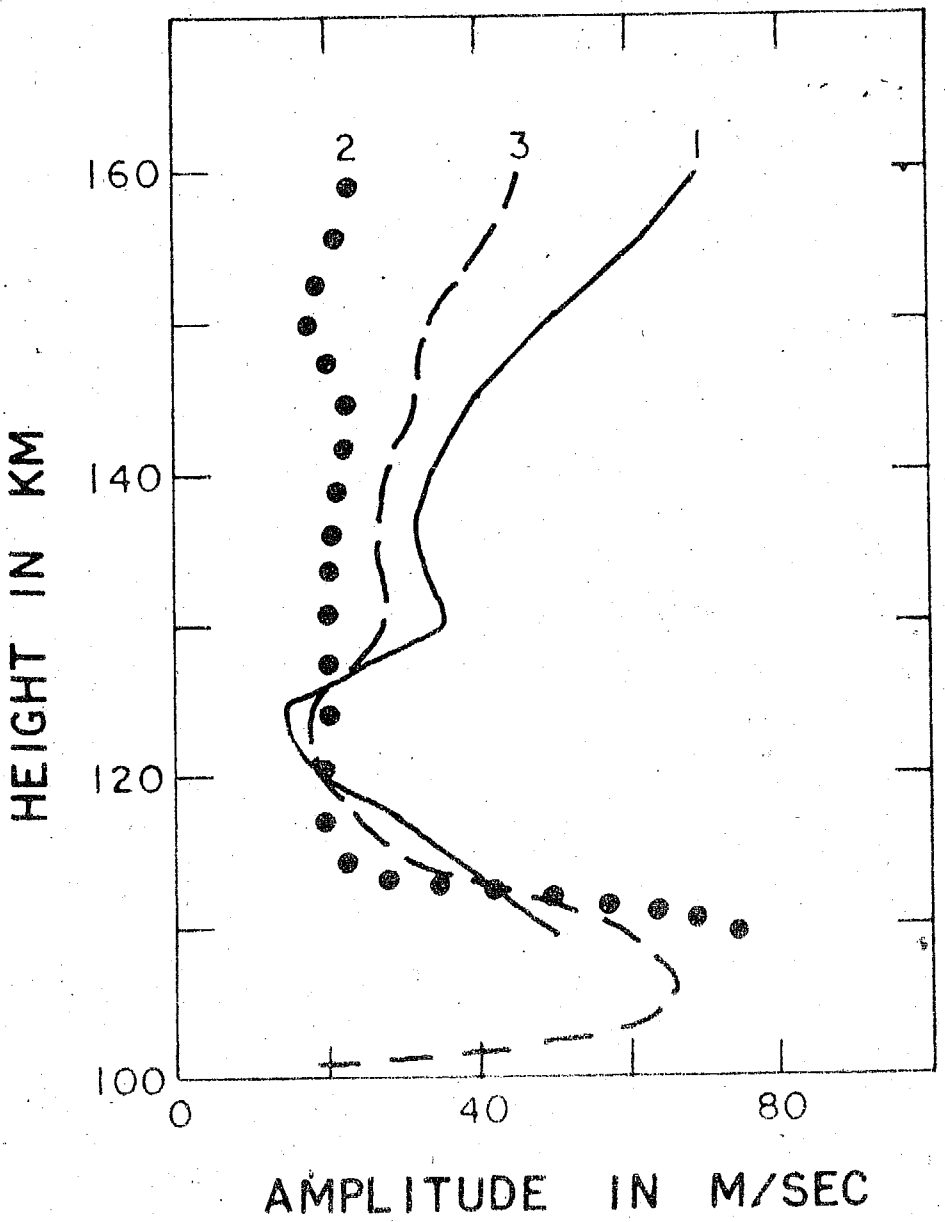

FIG. 76

VARIATION WITH HEIGHT OF MAGNITUDE OF W, WHICH IS ASSUMED TO REPRESENT THE AMPLITUDE OF INTERNAL ATMOSPHERIC GRAVITY WAVES. CURVE 1 FOR THE AVERAGE EVENING OBSERVATIONS; CURVE 2 FOR THE AVERAGE MORNING OBSERVATIONS AND CURVE 3 FOR ALL THE SIX OBSERVATIONS AT TERLS.

Fig. 76 also shows that there is a definite diurnal variation in the value of W i.e., the morning value is less than that for the evening above about 125 km. The amplitude of the internal atmospheric gravity waves, as obtained by Kochanski's method, appears to be constant in the morning, between 115 and 160 km, being about 20 m/sec; while in the evening the amplitude increases from about 15 m/sec at 125 km to about 70 m/sec at 160 km. With this method it is not possible to determine the vector $\vec{W}$ explicitly at any height because the vector varies quasi-sinusoidally over the height interval between the maximum and the minimum winds from $+\vec{W}$ to $-\vec{W}$ through 180^{0}. The vector $\vec{W}$ for intermediate heights is not known.

Kochanski determined the frequency of occurrence of $+\vec{W}$ and $-\vec{W}$ together, in different octants of N+S, NE+SW etc., and found that above 90 km, the most preferred directions, in descending order, were W+E, SE+NW and N+S. A similar analysis with the data presented here showed that the order of preferential direction is reversed, being in descending order, NE+SW, N+S, E+W and SE+NW.

The residual term after removing the effect of internal atmospheric gravity wave consists of the diurnal component, the semi-diurnal component with a possible ter-diurnal component and the component due to prevailing wind. Though it is difficult to separate all these components, the method adopted by

Kochanski[1] to determine the diurnal component, which was similar to the method adopted by Hines, was applied to this residual term in order to get the diurnal component. Here also it is assumed that the diurnal component has the same phase at evening (or morning) on all the days of observation. It is also assumed that all the evening observations are at 1800 hours local time and morning observations at 0600 hours local time. The analysis was carried out in the height range 110 to 160 km where at least two evening and two morning launchings are available. Fig. 77 gives the hodograph of the diurnal component at dawn phase after removing the internal atmospheric gravity wave component. No systematic rotation of the diurnal wind vector is observed in this figure. In Kochanski's analysis of 28 vapour trails it was observed that the diurnal wind vector rotated in clockwise direction from 80 to 120 km, with no or little rotation from 120 to 160 km. The amplitude was large at 106 km as in Hine's analysis. The lack of systematic rotation of vector in the present analysis can be assigned to the lack of data below 110 km, the main region which shows the characteristic rotation at the middle latitudes. Fig. 77 also shows that a systematic rotation of diurnal wind vector in the clockwise direction can be assigned to the hodograph in the height range 110 to 150 km if the origin is properly shifted. This shows, that the assumption that the phase of the diurnal component on all the evenings (or mornings) is same, may not be correct.

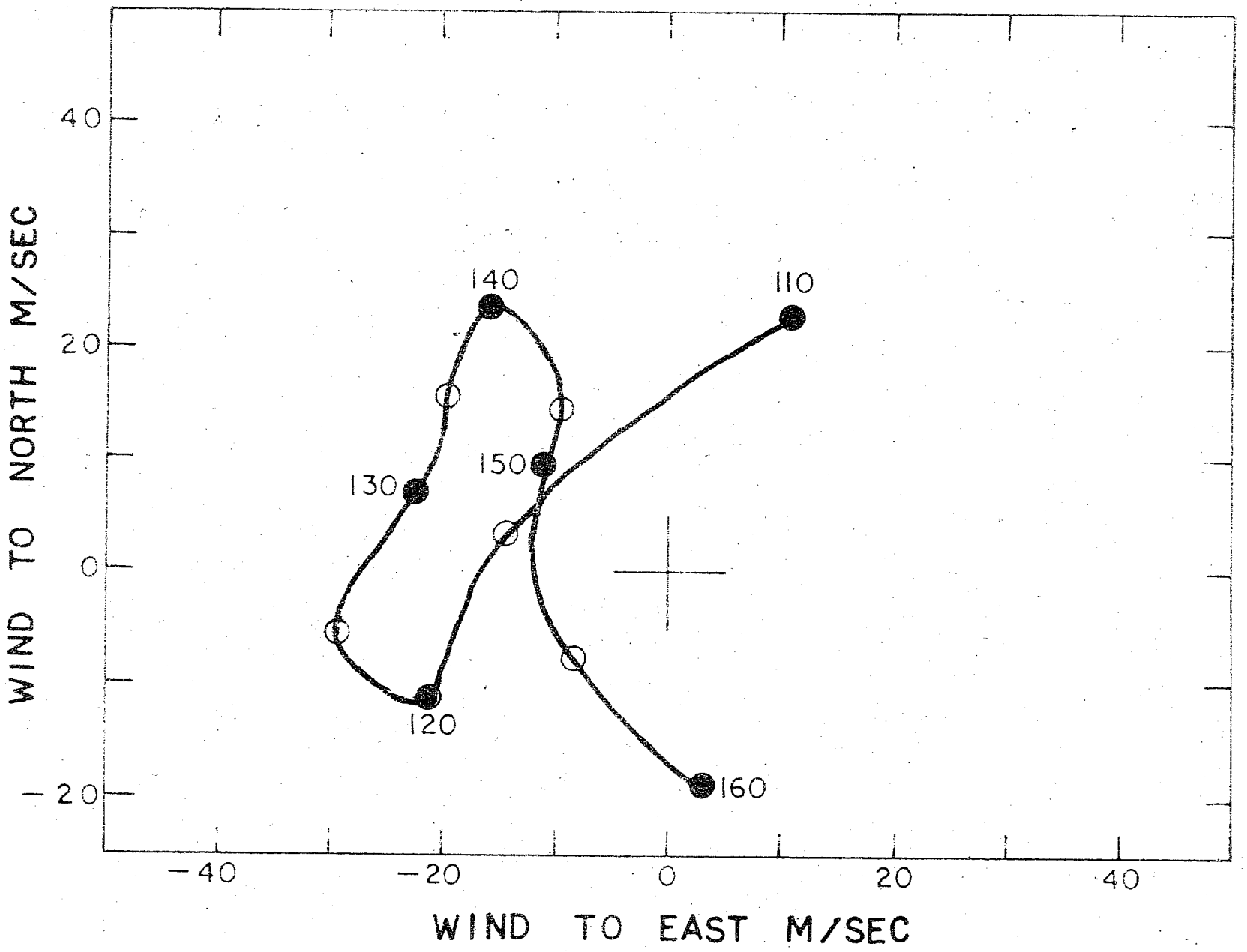

FIG. 77

RESIDUAL-DIURNAL WINDS AT TERLS AFTER THE REMOVAL OF WINDS DUE TO INTERNAL ATMOSPHERIC GRAVITY WAVES (KOCHANSKIXS METHOD)

Fig. 77 can be compared with Fig.73 in which the diurnal component without the removal of the internal atmospheric gravity waves is given. In Fig. 73 the total diurnal component appears to rotate in the clockwise direction from about 110 to 130 km, and in the anticlockwise direction from about 130 to 155 km. It is difficult at this stage to determine the exact effect of the internal atmospheric gravity waves on the rotation of diurnal component, as the vector $\vec{V}$ cannot be precisely determined from the present method of analysis.

Fig. 78 gives the hodograph of the residual term consisting of semi-diurnal component with a possible 8-hour component and the component due to prevailing wind. This figure shows, that this component rotates in anticlockwise direction with height, from about 110 km to about 155 km. The magnitude of vector being small between about 135 and 145 km. It appears that the diurnal component and the sum of semidiurnal component and prevailing wind are of equal importance throughout the observed height range 110 to 160 km.

3.2.9. <u>Comparison of our results with the ionospheric winds derived from S_q variation.</u>

It is known that the quiet day daily variation of the geomagnetic field is related to the solar and lunar day. As mentioned in section 1.2.2. of Chapter I, Stewart [10] suggested that the wind motions in the upper atmosphere, induced by the solar tidal forces, cause the quiet day daily variation

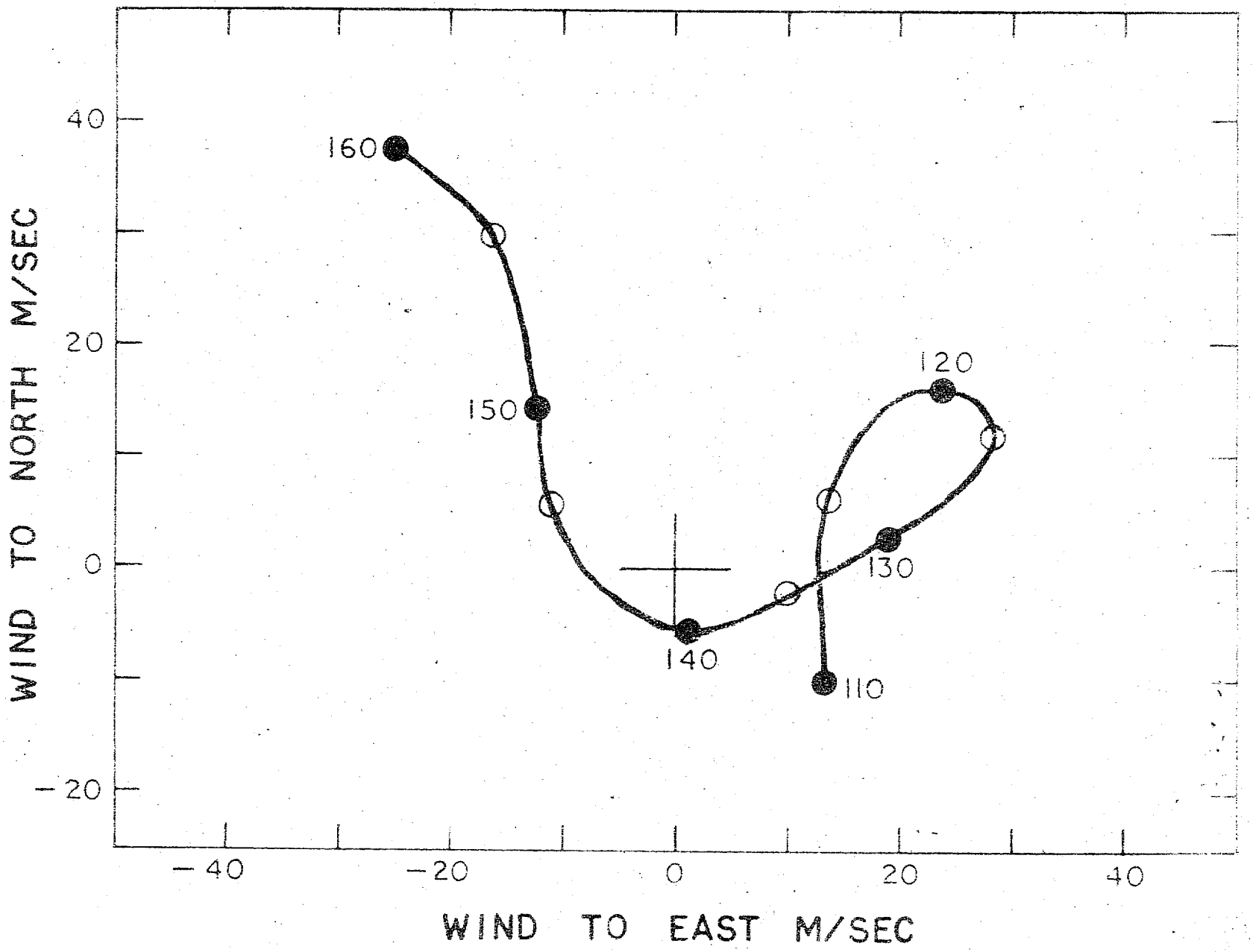

FIG. 78

RESIDUAL SEMI-DIURNAL WINDS AT TEPLS AFTER THE REMOVAL OF GRAVITY WAVES AND THE DIURNAL COMPONENT

of the earth's magnetic field. He assumed a highly conducting air in the upper atmosphere and as a consequence of its motion across the earth's magnetic field, currents are induced in it by the dynamo action. The observed daily magnetic variations on magnetically quiet days can be resolved into solar (S_q) and lunar (L) components. According to the dynamo theory, these variations are supposed to be caused by the magnetic fields produced by the currents in the upper atmosphere. The theory was later revised by several workers[139, 140] to take into account of the anisotropic nature of the ionospheric conductivity. By assuming a particular distribution of conductivity, the current systems that could have caused the S_q and L geomagnetic variations could be deduced. From these current systems, the electric fields and hence the winds required to produce these fields by dynamo action could be derived.

Kato[141] deduced diurnal and semi-diurnal wind systems, from the S_q variation of the earth's magnetic field, assuming the conductivity to be variable with latitude and local time. Wind components thus obtained refer to the dynamo region, which is generally considered to be in the 100-130 km region.

In Table 22, the diurnal and semi-diurnal components at 110 and 115 km, obtained in the present study, after removing the gravity wave term, (section 3.2.8), are compared with the values calculated by Kato for 10° N latitude.

Table 22

Comparison of neutral atmospheric wind components obtained from geomagnetic S_q variations and sodium vapour experiments

Component	Kato's result		Present study			
			110 km		115 km	
	Magnitude m/sec	Direction	Magnitude m/sec	Direction	Magnitude m/sec	Direction
Diurnal (dawn phase)	15	E S E	25	E S E	16.6	W N W
Semi-diurnal	10	E S E	17	E S E	14.5	E N E

It can be seen that the magnitude of the diurnal component obtained by Kato shows better agreement with our results at 115 km, but the directions differ by about 90° at 110 km and 180° at 115 km.

The semi-diurnal component listed as per the present analysis includes the prevailing wind also. This might be the reason for the observed values to be greater than Kato's result of 10 m/sec. The direction of the semi-diurnal component at 110 km agrees quite well with that obtained by Kato. Even at 115 km, the direction is fairly in agreement with the predominantly eastward direction of the semi-diurnal component deduced from S_q variations.

Kato's main conclusion that the diurnal component is greater than the semi-diurnal component at the dynamo region is in good agreement with the observed values, despite the prevailing component having been included in the semi-diurnal component.

The main limitation of the calculation of wind components by Kato is that, he assumed height independent velocity vector in the dynamo region. But the direct observation of winds show quite variable velocity field in this region. Fig.77 shows that the diurnal component changes its direction by about 103° in the height range 110 to 115 km. Fig.78 shows that the direction change in the semi-diurnal component in the same height range is only about 60°. This large change

in the direction of the diurnal component might account for the differences found in the comparison of the two results. It is also to be noted that Kato's derivations are for the equinoxes, while the present results are obtained during the winter months.

3.2.10. Comparison of neutral upper atmosphere winds and drift measurements at TERLS.

The E region drift observations at TERLS, by Mitra's spaced receiver technique[37] were started from 26 January 1964. The frequency used is 2.2 Mc/s. In the initial stages, because of several problems, the drift measurements were infrequent, and therefore we do not have any measurements of these drifts on the same days as our rocket launchings. It is known from the simultaneous observations with a C_4 ionospheric recorder at TERLS that the equatorial sporadic E is quite strong throughout the day time and the drift observations on 2.2 Mc/s could be made without any difficulty. But the critical frequency of E_S abruptly falls below the operating frequency during the night. Between 6 P.M. to 6 A.M. practically no reflections have been observed at 2.2 Mc/s from the sporadic E. Our rocket launchings are only either after 6 P.M. or before 6 A.M. and because of this reason we have no simultaneous observations of neutral upper atmosphere winds with vapour cloud and drift measurements with the spaced receiver method. Nevertheless, a comparison of the drifts that were measured at the earliest hour in the morning and latest hour in the

winter season at the height level of E_s (105-110 Km), with the winds measured just above 100 km show some interesting features.

During the winter months, the average drift speed at TERLS is about 166 m/sec in the morning, and about 134 m/sec in the late afternoon. The drift direction is mostly towards west, with negligible north and south components, and very rarely towards east. As we have seen earlier, the wind measurements have always shown that north-south and east-west components are of equal importance in the height range 100 to 110 km. Though the zonal component of the neutral atmosphere wind is towards west at 110 km on four occasions, its average magnitude is only 38 m/sec. On 12 January 1964, vapour cloud measurements show very strong eastward winds with speeds 132 m/sec at 108 km, and 116 m/sec at 110 km, before 0600 LMT. It is observed that the drifts are invariably towards west on all the days, particularly at early forenoon hours. The percentage of occurrence of eastward drifts being less than 4% in the morning hours and about 15% in the afternoon hours. The observed drift speeds are sometimes as high as 400 m/sec.

These differences between the neutral atmosphere winds obtained from vapour trail experiments and drifts obtained by spaced receivers method show that the drifts do not seem to represent the winds at the magnetic equator. If drifts are assumed to represent winds at the level of reflection of radiowave, it is difficult to understand why the wind velocity

vector which is quite variable around the level of E_s can be directed towards only west at the level of E_s , throughout day time.

Bowles et al[142] showed evidence for the existance of plane acoustic waves travelling with the speed of sound creating irregularities in the equatorial E_s which is closely associated with equatorial electrojet. Farley[74] has theoretically predicted the generation of these waves by a particular plasma instability known as the 'two stream instability'. He has shown that these waves travel mainly perpendicular to the magnetic field towards west during day time. The westward drift velocities observed at TERLS might relate to these acoustic waves as they necessarily generate the irregular electron densities, a requirement for obtaining fading records to measure the drifts.

CHAPTER IV

SUMMARY AND CONCLUSIONS

The thesis is based on the results of sodium vapour cloud experiments conducted from Thumba Equatorial Rocket Launching Station (TERLS), India, which is situated at the magnetic equator, and is only 8° north of the geographic equator. These experiments were conducted for the study of the neutral upper atmospheric winds. The experiments form a part of an extensive research programme, sponsored by the Indian National Committee for Space Research, for the study of the equatorial upper atmosphere.

The experiments were conducted during northern hemispheric winter months in 1963-64. Six launchings were made, three during the morning twilight and three during the evening twilight hours. Winds in the neutral upper atmosphere in the height range 100 to 180 km near the geographic and the geomagnetic equator were obtained for the first time from these experiments. The meridional and the zonal components of the winds were separately studied. The changes in the wind speed and direction with the height and time were also studied, and diurnal and other periodic variations examined. The results were compared with the neutral atmosphere wind observations at the higher latitudes in both the hemispheres. The results were also compared with the ionospheric drift measurements conducted from TERLS.

Following are the conclusions derived from the above study:

1. Meridional winds.

(a) It is observed that in the height range 100 to 150 km the neutral upper atmospheric meridional winds near the equator show equal preference for north and south directions, and changes from one direction to another with height are highly irregular.

(b) Between 150 to 180 km the winds are always towards north, with evening wind speeds always larger than the morning wind speeds.

2. Zonal winds.

(a) Zonal winds also show equal preference for east and west directions in the height range 100 to 115 km.

(b) Between 115-140 km winds are always towards east.

(c) Between 140-180 km winds are towards west.

3. Change in wind speed with height.

(a) All the wind speed profiles show a principal speed maximum between 104 to 110 km with an average height of 107 km. The average maximum wind speed at this height is 106 m/sec and on one occasion it reached as high as 140 m/sec.

(b) All the wind speed profiles show two minima. One is observed around 113 km with an average speed of 36 m/sec. The smallest speed observed at this height is 16 m/sec.

The second minimum is observed between 135-150 km with an average speed of 27 m/sec. The smallest speed observed at this height is 9 m/sec.

4. Wind shears.

Large wind shears have been observed, both in the east-west and north-south directions in the height range 100 to 116 km. At middle and high latitudes also similar shears are observed in the same height range, which shows that the region 100 to 116 km is a high shear region at all latitudes.

5. Diurnal variations.

(a) A definite diurnal effect is observed in the wind speed, the evening speeds being always greater than the morning, particularly between 126 to 138 km and above 160 km.

(b) At the principal speed maximum, mentioned in 3(a) above, the winds are always towards SE or SW in the evenings and towards NE or NW in the mornings.

(c) When the evening and the morning results are separately averaged, a diurnal variation is shown by the meridional winds in the height range 114-150 km. The evening average winds are towards south and the morning average winds are generally towards north.

(d) Above 160 km the diurnal effect is not seen in the direction of the winds.

6. When the heights of the wind maximum and minimum during the evening and the morning are compared, it is found that the morning heights are lower than the corresponding evening heights.

This can be due to the expansion of the atmosphere during day time because of heating and the contraction at nightbecause of cooling. The downward progression of the phase of the tidal and the internal atmospheric gravity wave component may be equally responsible for the above mentioned height changes.

7. Rotation of the wind velocity vector with height.

No regularity is observed in the rotation of the wind velocity vector with height at TERLS.

8. Internal atmospheric gravity waves.

By applying Kochenski's technique, the amplitude W of the internal atmospheric gravity waves was determined at different heights for the evenings and the mornings separately, as well as, for all the six launchings combined. The amplitude shows a definite diurnal effect between 125 to 160 km, W being larger in the evenings. The diurnal effect observed in the wind speeds as stated in 4(a) above may be related to this diurnal effect in the amplitude of the gravity waves.

9. Comparison with the results obtained at other latitudes in both the hemispheres.

(a) When the present results are compared with the results obtained from the middle latitude stations in the northern hemisphere, like Wallops, it is found that speed profiles are in general similar, with a principal maximum around 107 km as mentioned in 3 (a).

(b) When compared with both the northern and the southern hemispheric results, it is found that the meridional winds above 150 km at TERLS are similar to southern hemispheric results, being always towards north at these heights.

(c) Zonal winds are more regular and different from what has been observed in both the hemispheres.

10. Comparison of present results with the neutral atmospheric winds in the dynamo region, deduced by Kato from the S_q variations show fairly good agreement in wind speeds. Directions also agree to some extent. The differences may be due to the fact that Kato's derivations are for the equinoxial period, while the present results were obtained during the winter months.

11. Comparison with the ionospheric drift measurements at TERLS, do not show any agreement between the wind motions and the drifts. This leads us to believe that perhaps the drifts do not represent neutral atmospheric winds.

APPENDIX - I

CAMERA SITE PROGRAMME AND REPORT FORM
Morning Twilight

(Na - K)

Rocket Range
Date of Firing:

Point of Observation
Observer:

Reference time	Operations to be carried out at the reference time	Remarks	Elevation and azimuth
H-t	Adjust the stop watches, check the leveling of the tripods by spirit levels, check the filter. After adjusting azimuth to zero, put on fiducial switch and give two exposures (1 minute & 2 minutes) at the Great bear. Note down and .		= =
H	Theoretical time of Rocket shot		
	Watch closely for sodium trail point camera towards the zone of interest Note down and		= =

Ref.time	Cycle	Sub Cycle	Exposure duration	Operations to be carried out at the ref.time	Remarks	Elevation and azimuth
H+3'	1	A	1"	(0 to 1)		
			3"	(5 to 8)		
			10"	(15 to 25)		
			1"	(20 to 21)		
			3"	(25 to 28)		
			10"	(45 to 55)		
		B	1"			
			3"			
			10"			
			1"	(30 to 31)		
			3"	(35 to 38)		
			10"	(45 to 55)		
		C	1"			
			3"			
			10"			
			1"	(30 to 31)		
			3"	(35 to 38)		
			10"	(45 to 55)		

Ref.time	Cycle	Sub cycle	Exposure duration	Operations to be carried out at the ref.time	Remarks	Elevation and azimuth
H+6'	2	A	3"	(0 to 3)		
			5"	(30 to 35)		
			37"	(24 to 62)		
		B	55"	(0 to 55)		
			3"			
		C	5"			
			37"			
H+9'	3	A	3"			
			5"			
			37"			
		B	3"			
			5"			
			37"			
		C	55"			
H+12'	4	A	3"			
			3"			
			37"			
		B	3"			
			5"			
			37"			
			3"			
			5"			
			37"			
H+15'	6	A	1"	(0 to 1)		
			3"	(5 to 8)		
			10"	(16 to 25)		
			1"	(30 to 31)		
			3"	(35 to 38)		
			10"	(45 to 55)		
		B	1"	(0 to 1)		
			3"	(5 to 8)		
			10"	(15 to 25)		
			1"	(30 to 31)		
			3"	(35 to 38)		
			10"	(45 to 55)		
			1"	(0 to 1)		
			3"	(5 to 8)		
			10"	(16 to 25)		
			1"	(30 to 31)		
			3"	(35 to 38)		
			11"	(45 to 55)		

Ref.time	Cycle	Sub cycle	Exposure duration	Operations to be carried out at the ref.time	Remarks	Elevation and azimuth
H+18'	6	A	1"			
			3"			
			10"			
		B	1"			
			3"			
			10"			
		C	1"			
			3"			
			10"			
H+21'				Answer the telephone call and give information to the Project Director.		

CAMERA SITE PROGRAMME AND REPORT FORM
Evening Twilight

(Na - K)

Rocket Range — Point of Observation
Date of Firing — Observer

Reference	Operations to be carried out at the reference time	Remarks	Elevation and azimuth
H-t	Adjust the stop-watches check the levelling of the tripodes by spirit levels Check the filter		
H	Time of rocket shot (Theoretical) Watch closely for sodium trail point camera towards the zone of interest. Note down and Put on the fiducial lamp switch.		

Ref.	Time Cycle	Sub cycle	Exposure duration	Operations to be carried out at the ref. time	Remarks	Elevation and azimuth
H+3'			1"	(0 to 1)		
			3"	(5 to 8)		
			10"	(15 to 25)		
		A	1"	(30 to 31)		
			3"	(35 to 38)		
			10"	(45 to 55)		
			1"			
			3"			
	1	B	10"			
			1"			
			3"			
			10"			
			1"			
			3"			
		C	10"			
			1"			
			3"			
			10"			
H+6'			1"	(0 to 1)		
		A	3"	(5 to 8)		
			10"	(15 to 25)		
			1"			
	2	B	3"			
			10"			
			1"			
		C	3"			
			10"			

Ref.Time	Cycle	Sub cycle	Exposure duration	Operations to be carried out at the ref.time	Remarks	Elevation and azimuth
H+9'	3	A	1"			
			3"			
			10"			
		B	1"			
			3"			
			10"			
		C	1"			
			3"			
			10"			
H+12'	4	C A	3"	(0 to 3)		
			9"	(5 to 14)		
			27"	(20 to 47)		
		B B	3"			
			9"			
			27"			
		C C	3"			
			9"			
			27"			
H+15'	5	A	3"			
			9"			
			27"			
		B	3"			
			9"			
			27"			
		C	55"	(0 to 55)		
H+18'	6	A	3"	(0 to 3)		
			9"	(5 to 14)		
			27"	(20 to 47)		
		B	3"			
			9"			
			27"			
		C	55"	(0 to 55)		
H+21'	7	A	3"	(0 to 3)		
			9"	(5 to 14)		
			27"	(20 to 47)		
		B	55"			
		C	55"			
H+24'		A	3"			
			9"			
			27"			
		B	55"			
		C	55"			

Ref.Time Cycle	Sub cycle	Exposure duration	Operation to be carried out at the ref.time	Remarks	Elevation and azimuth
H+27'	9	A 55" / B 2'			
H+30'	10	A 66" / B 2'			
H+33'			Point towards the Orion or Belt of Orion Note down and Give 1 minute exposure	=	=
H+36'			Give two minutes exposure on Orion		
H+39'			Answer the Telephone call and give information to the Project Director		

REFERENCES

1. Kochanski, A. Month. Weath. Rev. 94, 199 (1966).
2. Groves, G.V. Report for COSPAR Working Group IV, Warsaw(1963).
3. Champion, K.S.W. Report for COSPAR Working Group IV, Warsaw (1963).
4. Champion, K.S.W. and Minzner, R.A. Rev. Geophys. 1, 67(1963).
5. Chapman, S. Suppl. Il Nuovo Cimen. 4, 1385 (1956)
6. Murgatroyd, R.J. World Meteorol. Organis. Tech. Note 70, 4, (1965).
7. Yamamoto. J.Atm.Sc. 19, 182 (1962).
8. Johnson, F.S. Ann. Geophys. 14, 94 (1958).
9. Craig, R.A. "The Upper Atmosphere Meteorology and Physics" International Geophysics series Vol.8. Academic Press(1965).
10. Stewart, B. Encycl. Britannica, 16, 181 (1882).
11. Schuster, A. Phil.Trans. Roy. Soc.(Lond) A 208, 163(1908).
12. Taylor, G.I. Proc. Roy. Soc. (Lond) A 126, 169 (1929).
13. Taylor, G.I. Proc. Roy. Soc. (Lond) A 156, 318 (1936).
14. Pekeris, C.L. Proc. Roy. Soc.(Lond) A 158, 650 (1937).
15. Wookes, K. and Wilkes, M.V. Proc. Roy. Soc. (Lond) A 192, 80 (1948).
16. White, M.L. J.Geophys. Res. 61, 489 (1956).
17. Lord Kelvin. Proc. Roy. Soc. (Edin) 11, 396 (1882).
18. Mac Donald, G.F. Planet. Space Sc. 10, 79 (1963).
19. Haurwitz, B. World Meteorol. Organis. Tech. Note 66 (1964).
20. Siebert, M. Advances in Geophys. 7, 105 (1961).
21. Sen,H.K. and White, M.L. J.Geophys. Res. 60, 483 (1955)
22. Butler, S.T. and Small, K.A. Proc. Roy. Soc. (Lond) A 274, 91 (1963).
23. Hines, C.O. "Physics of the Upper Atmosphere" ed. Hines et.al. Prentice Hall, (1965).
24. Hines, C.O. J.Geophys. Res. 70, 177 (1965).

25. Greenhow, J.S. and Neufeld, E.L. J.Geophys. Res. 64, 2129 (1959).

26. Booker, H.G. J.Geophys. Res. 61, 347 (1956).

27. Hines, C.O. Can. J. Phys. 38, 1440 (1960).

28. Hines, C.O. Quart. J. Roy. Met. Soc. 89, 1, (1963)

29. NASA. "Special Publication on the significant achievement in Planetary Atmosphere 1958-1964 (1966).

30. Jastrow, R. J.Geophys. Res. 64, 1799 (1959).

31. Greenhow, J.S. J.Geophys. Res. 64, 2306 (1959).

32. Jesse. Astr. Nachr. Bl. 140, 161 (1896).

33. Murgatroyd, R.J. Quart. J.Royd. Met. Soc. 83, 417 (1957).

34. Wilkes, M.V. "Oscillations of the Earth's Atmosphere" Cambridge Monograph (1949).

35. Greenhow, J.S. and Neufeld, E.L. Phil Mag. 1, 1157 (1956).

36. Blamont, J.E. and de Jager, C. Ann. Geophys. 17, 134 (1961).

37. Mitra, S.N. Proc. Instn. Elect. Engrs. Part III 96, 441 (1949).

38. Ratcliff, J.A. J.Geophys. Res. 64, 2102 (1959).

39. Rosenberg, N.W., Edwards. H.D. and Wright, J.W. Space Research Vol.IV, ed. Muller, F.(North-Holland Publ.Co., Amsterdam) 171 (1964).

40. Hines, C.O. Rev. in Geophys. Vol. I, 239, (1964).

41. Deshpande, M.R. Ph.D. Thesis, Gujarat University (1966).

42. Phillips, G.J. J. Atmos. Terr. Phys. 2, 141 (1952).

43. Salzberg, C.D. and Greenstone, R. J.Geophys.Res. 66, 521 (1961).

44. Chapman, J.H. Can. J.Phys. 31, 130 (1953).

45. Briggs, B.H. and Spencer, M. Rep. Prog. Phys. 17, 245 (1954).

46. Koster,J.R. Report on Equatorial Aeronomy, ed. Mendonca,F. 285 (1965).

47. Kelleher, D.F. and Miall, F. Report on Equatorial Aeronomy, ed. Mendonca, F. 283 (1965).

48. Morris, R.M. and Lyon, A.J. Report on Equatorial Aeronomy, ed. Mendonca, P. 294 (1966).

49. Munro, G.H. Aust. J. Phys. 11, 91 (1958).

50. Martyn, D.F. Proc. Roy. Soc. (Lond) A 201, 216 (1950).

51. Martyn, D.F. "The Physics of Ionosphere", (The Physical Society, Lond.) 168, (1955).

52. Dungey, J.W. J. Atm. Terr. Phys. 8, 39 (1956).

53. Cowling, T.G. Proc. Roy. Soc. (Lond) A 183, 453 (1945).

54. Rishbeth, H., Megill, L.R., and Cahn, J.H. Ann. Geophys. 21, No.2 (1965).

55. Dokuchayev "News of Institutes of Higher Learning, USSR", 4, 5 (1961).

56. Hines, C.O. Proc. IRE 47, 176 (1958).

57. Axford, W.I. J.Geophys. Res. 68, 769 (1963).

58. Axford, W.I., and Cunnold, D.M. Radio Res. 1, 191 (1964).

59. Heisler, L.H. and Whitehead, J.D. Nature, 191, 157 (1961).

60. Whitehead, J.D. J. Atm. Terr. Phys. 20, 49 (1961)

61. Kato, S. Radio Res. 1, 326 (1956).

62. Layzer, D. J. Geophys. Res. 69, 1953 (1964).

63. Layzer, D. J. Geophys. Res. 69, 5099 (1964).

64. Tauda, T., Sato, T., and Maeda, K. Radio Res. 1, 212 (1956).

65. Matsushita, S. Rep. Ionos. Res. Japan, 6, 118 (1952).

66. Matsushita, S. Rep. Ionos, Res. Japan, 7, 72 (1953).

67. Whitehead, J.D. J.Geophys. Res. 69, 5091 (1964).

68. Smith, L.G. Geophy. Corp. Am. Rept. NASw-469 (1963).

69. Manring, E., Bedinger, J.F., and Knaflich, H. Geophy. Corp. Am. Rept. NASw-396 (1963).

70. Bowen, P.J., Norman, K., Willmore, A.P., Baguette, J.M., Martin, F., and Storey, L.R.O. Planet. Space Sci. 12, 1173 (1964).

71. Groves, G.V. Space Research V ed. King-Hele et. al. (North-Holland Publ. Co. Amsterdam) 1012 (1965).

72. Mac Leod, M.A. Air Force Cambridge Res. Lab. Rept. MITSE, I.

73. Cohen, R., Bowles, K.L., and Calvert, W. J.Geophys. Res. 67, 966 (1962).

74. Farley, D.T. Phy. Rev. Lett. 10, 279 (1963).

75. Ludlam, F.H. Tellus 9, 341 (1957).

76. Pogle, R. Nature 204, 14 (1964).

77. Paton, J. Nature 168, 467 (1951).

78. Soberman. Scient. Amer. 208, No.6, 61 (1963).

79. Paton, J. Met. Mag. 93, 161 (1964).

80. Sales, G.H. Ionos. Res. Scient. Rept. No. 131 (Penn Uni.).

81. Elford, W.G., and Robertson D.S. J.Atmos. Terr. Phys. 4, 271 (1953).

82. Greenhow, J.S., and Neufeld, E.L. Quart.J. Roy. Met.Soc. 87, 472 (1961).

83. Whipple, F.L. Rev. Mod. Phys. 15, 246 (1943).

84. Millman, P.M. J. Geophys. Res. 64, 2132 (1959).

85. Katasev, L.A. "Photographic Methods in Meteor Astronomy" Translation from Russian by NASA, Jerusalem (1964).

86. Lovell, A.C.B. Rep. Progr. Phys. 11, 415 (1948).

87. Manning, L.A. J. Appl. Phy. 19, 659 (1948).

88. Hurihata. Pub. Ast. Soc. Japan 1, 39 (1949).

89. Bates, D.R. J. Geophys. Res. 55, 347 (1950).

90. Edwards,H.D., Bedinger, J.F., Manring, E.R., and Cooper,C.D. "The Air-glow and Aurora" ed. Armstrong, E.B. and Dalgarno, A.D. (Pergamon Press, Lond.) 122, (1956).

91. Bedinger, J.F., Manring, E., and Ghosh, S.N. J.Geophys. Res. 63, 19 (1958).

92. Smith, M., Katchen, L., Sacher, P., Swartz, P. and Theon, J. NASA Technical Report X-651-64-106 (1964).

93. Stroud, W.G., Nordberg, W., Bandeen, W.R., Bartman, F.L. and Titus, P. Space Research I ed. Kallmann Bijl, H. (North-Holland Publ.Co. Amsterdam), 117 (1960).

94. Groves, G.V. Proceedings of the First International Symposium on Rocket and Satellite Meteorology, 1962 (North-Holland Publ. Co. Amsterdam), 42 (1963).

95. Groves, G.V. Space Research I ed. Kallmann Bijl, H. (North-Holland Publ.Co. Amsterdam), 144 (1960).

96. Rosenberg, N.W. J.Geophys. Res. 68, 3329 (1963).

97. Bedinger, J.F. "Compendium of Wind data from the Vapour Trail Technique" GCA Tech. Rept. No. 66-7-N.

98. Elford, W.G., and Murray, E.L. Space Research I ed. Kallmann Bijl, H. (North-Holland Publ. Co. Amsterdam), 168 (1960).

99. Störmer, C. Astrophy. Norvegica, Oslo, 1, 67 (1935).

100. Witt, G. Tellus, 2, 365 (1957).

101. Hamilton, R.A. Met. Mag. 93, 201 (1964).

102. Groves, G.V. Space Research IV ed. Muller, P. (North-Holland Publ. Co. Amsterdam), 155 (1964).

103. Greenhow, J.S. and Neufeld, E.L. Phil Mag. 46 549 (1955).

104. Bedinger, J.F. and Knaflich, H.B. Radio Res. 1, 166 (1960).

105. Manring, E., Bedinger, J., Knaflich, H., and Leyser, D. "An Experimentally determined Model for the Periodic Character of Winds from 85 to 135 km) NASA Report, NASA CR-36 (1964).

106. Kochanski, A. J.Geophys. Res. 69, 3651 (1964).

107. Kochanski, A. World Meteorol. Organiz. Tech. Note No.70, 140 (1965).

108. Hines, C.O. J.Geophys. Res. 71, 1453 (1966).

109. Hines, C.O. J.Geophys. Res. 71, 1461 (1966).

110. Rosenberg, N.W., Golomb, D., Allen, Jr. E.F. J.Geophys. Res. 68, 5695 (1963).

111. Rosenberg, N.W. and Edwards, H.D. J.Geophys. Res. 69, 2819 (1964).

112. Kellogg, W.W. and Shilling, G.F. J.Meteor. 8, 222 (1951).

113. Batten, E.S. J. Meteor. 18, 283 (1961).

114. Kochanski, A. J.Geophys. Res. 68, 213 (1963).

115. Kantor, A.J. and Cole, A.E. J. Geophys. Res. 69 5131 (1964).

116. Pant, D. J. Geophys. Res. 61, 459 (1956).

117. Deb, S. J. Atmos. Terr. Phys. 4, 28 (1953).

118. Murgatroyd, R.J. World Meteorol. Organiz. Tech. Note 70, 170, (1966).

119. Ragsdale, G.C., and Wanko, P.E. NASA Tech. Note D-1573, (1963).

120. Greenhow, J.S. Phil. Mag. 45 471 (1954).

121. Berg, D. J. Meteor. 8, 244 (1951).

122. Broglio, L. Space Research II ed. van de Hulst, H.C.,et.al. (North-Holland Publ. Co. Amsterdam) 1125 (1961).

123. Smith, F.J. Planet. Space Sc. 11, 1311 (1963).

124. CCA. "Final Report for the period February 11, 1959 to February 11, 1960.

125. Cooper, C.D. "Spectrographic Observations of the May, September and October, 1959 Firefly Series". Project Firefly Part I (GRD Publication), 1959.

126. Levy, R.J., and Manring, E.R. CCA Tech.Report 61-4-N (1961)

127. Dubin, M. "A guide to Rocket Luminous Vapour Trail Experiments". Published by COSPAR Working Group II for the IQSY (1964).

128. Gulatee. "Gravity data in India". Tech. Paper No.10, Survey of India, (1956).

129. Groves, G.V. Project Firefly Vol. IV ed. Golomb,D. AFCRL-62-826, 15 (1962).

130. Manring, E., Bedinger, J.F., Pettit, H.B. and Moore, C.B. J. Geophys. Res. 64, 697 (1959).

131. Jarrat, A.H., Mc Grattan, G.J., Rees, J.A. Planet Space Sc. 11, 1309 (1963).

132. Baguett, J.M. Thesis submitted to the University of Paris. (1961).

133. Justus, C.G., Edwards, H.D., and Fuller, R.N. "Study of Photochemistry, Physical State and Motion of the Upper Atmosphere". Final Report Georgia Tech. No.A-434. ed. Edwards, H.D., 52 (1963).

134. Norton, A.P. A star Atlas, Gall and Inglis, Lond. (1950).

135. Todhunter. "Spherical Trignometry".

136. Bell, R.J.T. "Elementary Treatise on Coordinate Geometry of Three Dimensions". Macmillan Lond. (1931).

137. Chauvenet, W. "A Manual of Spherical and Practical Astronomy". Vol.II. Dover Publ. (1960).

138. Rosenberg, N.W., and Justus, C.G. Radio Sci. 1, 149 (1966).

139. Hirono, M. J.Geomag. Geoel. 5, 22 (1953).

140. Maeda, K. Rep. Ionos. Res. Japan 9, 71 (1955).

141. Kato, S. J. Geomag. Geoel. 8, 24 (1956).

142. Bowles, K.L., Balsley, B.B., and Cohen, R. J. Geophys. Res. 68, 2485 (1963).

143. Rosenberg, N.W. Project Firefly Vol. IV ed. Golomb, D. AFCRL-62-526, 1 (1962).

144. Jachia, L.G. Report by COSPAR Working Group IV, Warsaw (1963).

145. Elford, W.G. Planet Space Sc. 1, 94 (1959).

146. Manning, L.A., Willard, O.G., Peterson, A.M. Proc. IRE 38, 877 (1950).

147. Greenhow, J.S. J. Atmos. Terr Phys. 2, 282 (1952).

148. Diamont, J.E. and Lory, M.L. Proceedings of the First International Symposium on Rocket and Satellite Meteorology 71 (1962).

149. Vegard, L. Terr. Magn. 37, 389 (1932).